ISTANBUL TECHNICAL UNIVERSITY ★ GRADUATE SCHOOL

DEEP FEATURE TRANSFER FROM DEEP LEARNING MODELS INTO MACHINE LEARNING ALGORITHMS TO CLASSIFY COVID-19 FROM CHEST X-RAY IMAGES

M.Sc. THESIS

Ozan GÜLDALİ

Department of Mathematical Engineering

Mathematical Engineering Programme

AUGUST 2021

ISTANBUL TECHNICAL UNIVERSITY ★ GRADUATE SCHOOL

DEEP FEATURE TRANSFER FROM DEEP LEARNING MODELS INTO MACHINE LEARNING ALGORITHMS TO CLASSIFY COVID-19 FROM CHEST X-RAY IMAGES

M.Sc. THESIS

Ozan GÜLDALİ
(509191238)

Department of Mathematical Engineering

Mathematical Engineering Programme

Thesis Advisor: Assist. Prof. Dr. Gül İNAN

AUGUST 2021

İSTANBUL TEKNİK ÜNİVERSİTESİ ★ LİSANSÜSTÜ EĞİTİM ENSTİTÜSÜ

GÖĞÜS RÖNTGENİ GÖRÜNTÜLERİNDEN COVID-19 SINIFLANDIRMASI YAPMAK AMACIYLA DERİN ÖĞRENME MODELLERİNDEN MAKİNE ÖĞRENMESİ ALGORİTMALARINA DERİN ÖZNİTELİK AKTARIMI

YÜKSEK LİSANS TEZİ

Ozan GÜLDALİ
(509191238)

Matematik Mühendisliği Anabilim Dalı

Matematik Mühendisliği Programı

Tez Danışmanı: Assist. Prof. Dr. Gül İNAN

AĞUSTOS 2021

Ozan GÜLDALİ, a M.Sc. student of ITU Graduate School student ID 509191238 successfully defended the thesis entitled "DEEP FEATURE TRANSFER FROM DEEP LEARNING MODELS INTO MACHINE LEARNING ALGORITHMS TO CLASSIFY COVID-19 FROM CHEST X-RAY IMAGES", which he/she prepared after fulfilling the requirements specified in the associated legislations, before the jury whose signatures are below.

Thesis Advisor :	**Assist. Prof. Dr. Gül İNAN** Istanbul Technical University	.....
Jury Members :	**Prof. Dr. Name SURNAME** Yıldız Technical University	.....
	Prof. Dr. Name SURNAME Boğaziçi University	.....
	Prof. Dr. Name SURNAME Gebze Institute of Technology	.....

Date of Submission : **22 September 2009**
Date of Defense : **21 December 2009**

To my family,

FOREWORD

I would like to express my deepest sincere gratitude to my thesis advisor Assist. Prof. Dr. Gül İNAN for supporting and encouraging me with her immense knowledge during the writing process of my thesis. From the day I enrolled in the master's program, regardless of time and place, she was with me every step of the way and became more than an lecturer for me.

Last but not least, I would like to express my endless thanks to my beloved mother, father, Kübra Özcan, and my managers Mehmet Oğuz Bici and Kemal Uğur, who have never lost their support from me. They have never lost their faith in me and have always been full of love and understanding.

August 2021 Ozan GÜLDALİ

TABLE OF CONTENTS

Page

ABBREVIATIONS

AI	**:** Artificial Intelligence
NN	**:** Neural Network
DL	**:** Deep Learning
CNN	**:** Convolutional Neural Network
TL	**:** Transfer Learning
DTL	**:** Deep Transfer Learning
ML	**:** Machine Learning
CV	**:** Cross-Validation
LOO	**:** Leave-One-Out
SVM	**:** Support Vector Machines
LR	**:** Logistic Regression
KNN	**:** K-Nearest Neighbor
LDA	**:** Linear Discriminant Analysis
TP	**:** True Positive
TN	**:** True Negative
FP	**:** False Positive
FN	**:** False Negative
TPR	**:** True Positive Rate
TNR	**:** True Negative Rate
PPV	**:** Positive Prediction Value
ACC	**:** Accuracy
AUC	**:** Area Under the Curve

LIST OF TABLES

Page

LIST OF FIGURES

Page

DEEP FEATURE TRANSFER FROM DEEP LEARNING MODELS INTO MACHINE LEARNING ALGORITHMS TO CLASSIFY COVID-19 FROM CHEST X-RAY IMAGES

SUMMARY

Coronavirus disease 2019 (COVID-19) is a contagious disease caused by SARS-CoV-2. It was first reported on December 2019 in Wuhan, China, and declared as a pandemic on 11 March, 2020. Even though the disease is a severe acute respiratory illness, it effects various organs and causes several symptoms such as fever, dry cough, tiredness, the loss of taste or smell, diarrhoea, headache, aches and pains, sore throat, and conjunctivitis. As of the end of April 2021, over 145 million people has been infected and more than 3 million people died because of COVID-19. That is why, one of the most important issues is the diagnosis of COVID-19. Although the most basic method to diagnose COVID-19 is Polymerase Chain Reaction (PCR) test, different techniques have been being experimented and developed. Since COVID-19 has a huge effect on lungs, diagnosis methods based on lung characteristics and images are emphasized. However, there are various illnesses affecting lungs. Thus, it has been an important challenge and problem to find a procedure to classify COVID-19 having high success rate.

In this thesis, we suggest deep feature transform method from deep learning models to machine learning algorithms to classify patients COVID-19 infected via chest X-Rays. In addition to image data, we also use the demographic information of patients during machine learning process to contribute the information coming from deep features. Chapter 1 includes the the introduction about our problem, the purpose of this study, the related literature search and the structure of this thesis. The basic information about our image data, chest X-Rays, are given in Chapter 2.

The problem we focus on is the binary classification between COVID-19 patients and other people. In order to solve this problem, we used dataset containing 131 COVID-19 and 123 non-COVID-19 labeled data. Then, we divided the data set into train and test sets so that 80% of the total data is in the train set, and augmented the train set with horizontal flip, vertical flip, 90 degrees of rotation, 180 degrees of rotation and 270 degrees of rotation. Thus, at the end, we yielded 630 COVID-19 and 588 non-COVID-19 labeled data in train set, and 26 COVID-19 and 25 non-COVID-19 labeled data in test set. The augmented data only used on CNN experiments. At the begin of Chapter 5, the dataset and augmentation technique was detailed.

The deep learning models we used are Convolutional Neural Network (CNN) models such that AlexNet, ResNet-18, ResNet-34, ResNet-50, VGG16 and VGG19. We particularly experimented three different optimization methods for each CNN models such that SGD with momentum, Adam and Adam with decoupled weight decay. The objective loss function to minimize was common for each model as cross-entropy loss function. Each image sample was resized to 227 x 227, center cropped, converted to gray-scale and normalized. Chapter 3 consists of the introduction to deep learning, basic information about CNNs and how to perform transfer learning. Two types of

transfer learning were used in this study, which are transferring pre-trained model weights into CNN models and transferring deep features extracted from CNN models into machine learning algorithms. Pre-trained CNN models are the models that previously trained on ImageNet dataset on the record, and we performed re-train after initializing the models with these recorded weights. Deep feature transfer learning is extracting the features of CNN model from the fully-connected block of model, and using it as feature matrix in another artificial intelligence technique such as ML algorithms.

The machine learning algorithms we used are supervised learning algorithms such that Support Vector Machines (SVM), Logistic Regression (LR), K-Nearest Neighbor (KNN) and Linear Discriminant Analysis (LDA). We experimented different regularization techniques, which are Lasso known as L1 norm and Ridge known as L2 norm, on stated ML algorithms. Chapter 4 consists of the introduction to machine learning, basic information about algorithms and regularizers, and cross-validation technique. We performed 10-Fold cross-validation on train set to obtain the generalized hyper-parameter choices besides hyper-parameters specific to our initially split test set. The algorithms and experiments were applied to the feature set of demographic information, the deep transferred feature set, and the combination of transferred features and demographic information separately. The demographic information feature matrix clearly consists of two feature columns such that age and sex information. The length of transferred deep features for each sample is thousand. Hence, the combined feature matrix contains thousand two columns.

All experiments for CNN and ML are detailed under Chapter 5, including data pre-processing and hyper-parameter tuning techniques for ML specifically. Grid search was used to find optimal parameters for each feature matrix and algorithm. The source code for experiments is mainly in Python programming language, and a small part is in R programming language. The CNN models were applied using PyTorch library in Python, and the ML algorithms were applied using Sklearn library in Python. Only regularized LDA algorithm was coded in R programming language using TULIP library. We performed our CNN experiments on GPU to have faster and parallel processes. Since we did not have an opportunity to reach a physical computer including GPU that we can use during our experiments, we performed the experiments on the Google Colaboratory platform. It is a partially-free platform for Gmail users to implement CUDA to use its provided GPU. After collecting CNN results and *.pth files containing the best model weights, the ML experiments were performed locally on CPU.

We explained the performance measurement techniques in Chapter 6 together with experiment results for CNN and ML processes. The best result was achieved by using ResNet-50 model with Adam optimizer. The metrics on this result are 92.16%, 0.9216, 0.9215, 0.9216, 0.9216, 0.9215 for the accuracy, sensitivity, specificity, precision, F1 score and AUC score respectively. Since we experimented obtaining optimal hyper-parameters for both generalized and specific to our test data, the results for both were reported too. For the feature matrix of demographic information, the best results for both generalized and chosen test set hyper-parameters are the same, and achieved with KNN algorithm. The metrics on this result are the accuracy of 56.86%, the sensitivity of 0.56863, the specificity of 0.58368 the precision of 0.6863, the F1 score of 0.49545, and the AUC score of 0.5745. For the deep feature matrix obtained

from ResNet-50 model weights, SVM with Ridge regularizer, LR, LR with Ridge, and KNN algorithms had the same results according to generalized hyper-parameters. The metrics on this results are the accuracy, sensitivity, specificity, precision, F1 score and AUC score of 92.16%, 0.9216, 0.9230, 0.9243, 0.9215, 0.9223 respectively. Finally, for the combined feature matrix of demographic information and extracted deep features obtained from ResNet-50 model weights, SVM with Ridge regularizer, LR, LR with Ridge, and KNN algorithms had the same results as well according to generalized hyper-parameters. The metrics on this results are the accuracy, sensitivity, specificity, precision, F1 score and AUC score of 92.16%, 0.9216, 0.9230, 0.9243, 0.9215, 0.9223 respectively.

In conclusion, according to stated results, we yielded an improvement of using regularization with linear discriminant analysis and Lasso regularizer. We did not have an improvement by combining demographic information with deep features. However, we anticipate an improvement with this image and non-image data combining technique by using more data samples and more information about patients such as doctors report, tobacco product use, associated genetic diseases, respiratory test information, etc. Finally, even though we could not see an improvement from CNN testing results to ML testing results in terms of the accuracy, sensitivity and F1 score, the specificity and precision improved. As we discussed in Chapter 7, a dataset with more samples and these samples inspected by subject matter experts, such as specialist radiologists for our X-Rays, would allow the study to have better metric results and better comparison opportunities between experimental phases.

Keywords: COVID-19, Chest X-Ray, Data augmentation, Binary classification, Demographic information, Deep learning, Convolutional Neural Networks, Pre-trained CNN models, Transfer learning, Deep feature extraction, Deep feature transfer, Machine learning, Supervised learning, Regularization, Lasso, Ridge, Grid search.

GÖĞÜS RÖNTGENİ GÖRÜNTÜLERİNDEN COVID-19 SINIFLANDIRMASI YAPMAK AMACIYLA DERİN ÖĞRENME MODELLERİNDEN MAKİNE ÖĞRENMESİ ALGORİTMALARINA DERİN ÖZNİTELİK AKTARIMI

ÖZET

Koronavirus hastalığı 2019 (COVID-19), SARS-CoV-2'nin neden olduğu bulaşıcı bir hastalıktır. İlk vakalar Aralık 2019'da Çin'in Wuhan kentinden bildirilmiş olup, 11 Mart 2020'de dünya genelini saran bir pandemi olarak ilan edilmiştir. Hastalık şiddetli bir akut solunum yolu hastalığı olmasına rağmen, çeşitli organları etkiler ve ateş, kuru öksürük, yorgunluk başta olmak üzere, tat veya koku kaybı, ishal, baş ağrısı, ağrı ve sızılar, boğaz ağrısı ve konjonktivit gibi çeşitli semptomlara neden olur. Nisan 2021 sonu itibariyle 145 milyondan fazla insan COVID-19 hastalığına yakalanmış ve 3 milyondan fazla insan hayatını kaybetmiştir. Bu nedenle en önemli konulardan biri COVID-19'un hızlı ve erken tanısıdır. COVID-19'u teşhis etmenin en temel yöntemi Polimeraz Zincir Reaksiyonu (PCR) testi olsa da farklı teknikler denenmekte ve geliştirilmektedir. COVID-19'un akciğerler üzerinde bıraktığı etki çok büyük olduğu için, hastanın akciğerindeki duruma ve akciğer görüntülerine dayalı tanı yöntemleri üzerinde durulmaktadır. Ancak akciğerleri etkileyen çeşitli hastalıklar da vardır. Bu nedenle, COVID-19'u sınıflandırmak için yüksek başarı oranına sahip bir yöntem bulmak önemli bir zorluk ve problem haline gelmiştir.

Bu tezde, göğüs röntgen görüntüleri aracılığıyla COVID-19 hastalığına sahip hastaları sınıflandırmak için, derin öğrenme modellerinden makine öğrenmesi algoritmalarına derin öznitelik aktarımı yöntemini önermekteyiz. Görüntü verilerine ek olarak, derin özniteliklerden gelen bilgileri desteklemek için, makine öğrenimi sürecinde hastaların demografik bilgilerini de kullanıyoruz. Bölüm 1, problemimiz hakkında giriş, bu çalışmanın amacı, ilgili literatür taraması ve bu tezin yapısını içermektedir. Görüntü verilerimiz olan göğüs röntgenleri ile ilgili temel bilgiler Bölüm 2'de verilmiştir.

Odaklandığımız sorun, COVID-19 hastaları ve diğer insanlar arasındaki ikili sınıflandırmadır. Bu sorunu çözmek için 131 COVID-19 ve 123 COVID-19 olmayan etiketli veri içeren veri kümesi kullandık. Daha sonra veri kümesini, toplam verinin %80'i öğrenme kümesinde olacak şekilde, öğrenme ve test kümelerine böldük. Ayrıca öğrenme kümesi verilerine yatay çevirme, dikey çevirme, 90 derece döndürme, 180 derece döndürme ve 270 derece döndürme ile çoğaltma uyguladık. Böylece öğrenme kümesinde 630 COVID-19 ve 588 COVID-19 olmayan etiketli veri, test setinde 26 COVID-19 ve 25 COVID-19 olmayan etiketli veri elde ettik. Belirtilen çoğaltılma işlemi sadece Evrişimsel Sinir Ağı deneyleri sırasında kullanılmıştır. Bölüm 5'in başlarında, veri seti ve çoğaltma işlemi tekniği detaylandırılmıştır.

Kullandığımız derin öğrenme modelleri AlexNet, ResNet-18, ResNet-34, ResNet-50, VGG16 ve VGG19 Evrişimsel Sinir Ağı (ESA) modelleridir. Her ESA modeli için özellikle üç farklı optimizasyon yöntemi uyguladık, ve bunlar SGD momentum, Adam ve ayrıştırılmış ağırlık düşüşüne sahip Adam'dır. Her model için ortak olarak kayıp fonksiyonununu çözebilmek adına cross-entropy kayıp fonksiyonunu kullandık.

Her bir görüntü 227 x 227 olarak yeniden boyutlandırıldı, merkezsel olarak kırpıldı, gri tonlamaya dönüştürüldü ve normalleştirildi. Bölüm 3, derin öğrenmeye giriş, ESA'lar hakkında temel bilgiler ve transfer öğreniminin nasıl gerçekleştirileceğinden oluşmaktadır. Bu çalışmada, önceden eğitilmiş modellerin ağırlıklarının mevcut ESA modellerine aktarılması, ve ESA modellerinden çıkarılan derin özniteliklerin makine öğrenimi algoritmalarına aktarılması olarak iki tür aktarımlı öğrenme kullanılmıştır. Ön-eğitimli ESA modelleri, resmi olarak ImageNet veri kümesi üzerinde daha önceden eğitilmiş modeller olup, kaydedilen bu ağırlıklarla modeller başlatılmış ve sonrasında yeniden öğrenim gerçekleştirilmiştir. Derin öznitelik aktarımlı öğrenme ise, ESA modelinin özelliklerini tam bağlı model bloğundan çıkartarak makine öğrenmesi algoritmaları gibi başka bir yapay zeka tekniğinde öznitelik matrisi olarak kullanmaktır.

Kullandığımız makine öğrenmesi (MÖ) algoritmaları, Destek Vektör Makineleri (SVM), Lojistik Regresyon (LR), K-En Yakın Komşu (KNN) ve Doğrusal Ayırma Analizi (LDA) olan gözetimli öğrenme algoritmalarıdır. Belirtilen makine öğrenmesi algoritmaları üzerinde L1 normu olarak bilinen Lasso ve L2 normu olarak bilinen Ridge olarak farklı düzenlileştirme tekniklerini uyguladık. 4. Bölüm, makine öğrenmesine giriş, makine öğrenmesi algoritmaları ve düzenlileştirciler hakkında temel bilgiler ve çapraz doğrulama tekniğini içermektedir. Başlangıçtaki bölünmüş test kümemize özgü hiper parametrelerin yanı sıra, genelleştirilmiş hiper parametre seçeneklerini elde etmek için öğrenme kümesi üzerinde 10-Katlı çapraz doğrulama gerçekleştirdik. Algoritmalar ve tüm deneyler, demografik bilgilerden oluşan öznitelik kümesine, aktırılmış derin özniteliklerden oluşan öznitelik matrisine ve aktarılan derin öznitelikler ile demografik bilgilerin birleşiminden oluşan öznitelik matrisine ayrı ayrı uygulanmıştır. Demografik bilgi özellik matrisi, bilindiği üzere yaş ve cinsiyet bilgisi olmak üzere iki özellik sütunundan oluşmaktadır. Her örnek için aktarılan derin özniteliklerin uzunluğu bindir. Dolayısıyla, birleşik öznitelik matrisi bin iki sütun içermektedir.

ESA ve MÖ için tüm deneyler, MÖ için veri ön işleme ve hiper parametre seçimi teknikleri dahil olmak üzere, Bölüm 5'te ayrıntılı olarak açıklanmıştır. Her bir öznitelik matrisi ve algoritma için en uygun parametreleri bulmak amacıyla Izgara araması yöntemi kullandık. Deneylerin kaynak kodu ağırlıklı olarak Python programlama dilinde, küçük bir kısmı ise R programlama dilinde yazılmıştır. ESA modelleri Python'da PyTorch kütüphanesi kullanılarak, MÖ algoritmaları ise Python'da Sklearn kütüphanesi kullanılarak uygulanmıştır. Yalnızca düzenlileştirilmiş LDA algoritması, TULIP kütüphanesi kullanılarak R programlama dilinde kodlanmıştır. Daha hızlı ve paralelleştirilmiş işlemler için ESA deneylerimizi GPU üzerinde gerçekleştirdik. Deneylerimiz sırasında kullanabileceğimiz GPU içeren fiziksel bir bilgisayara sahip olma fırsatımız olmadığından, deneyleri Google Colaboratory platformunda gerçekleştirdik. Google Colaboratory, Gmail kullanıcılarına, içermiş olduğu GPU'yu CUDA eklentisi teknolojisi ile kullanma imkanı sağlayan kısmen ücretsiz bir platformdur. ESA sonuçlarını ve en iyi model ağırlıklarını içeren *.pth dosyalarını toplandıktan sonra, MÖ deneyleri lokal olarak CPU üzerinde gerçekleştirilmiştir.

Bölüm 6'da performans ölçüm tekniklerini ESA ve MÖ süreçleri için deney sonuçlarıyla birlikte açıkladık. En iyi sonuca Adam optimizasyon yöntemi ile ResNet-50 modeli kullanılarak ulaşılmıştır. Bu sonuca ilişkin metrikler, doğruluk,

duyarlılık, özgüllük, kesinlik, F1 skoru ve AUC skoru için sırasıyla %92.16, 0.9216, 0.9215, 0.9216, 0.9216, 0.9215'tir. Hem genelleştirilmiş hem de test verilerimize özel optimum hiper parametreleri elde etmeyi amaçladığımızdan, her ikisi için de sonuçlar rapor edilmiştir. Demografik bilgilerin öznitelik matrisi için hem genelleştirilmiş hem de seçilmiş test kümesi hiper parametreleri için en iyi sonuçlar aynıdır, ve KNN algoritması ile elde edilir. Bu sonuca ilişkin metrikler, %56.86 doğruluk, 0.56863 duyarlılık, 0.58368 özgüllük, 0.6863 kesinlik, 0.49545 F1 skoru ve 0.5745 AUC skorudur. ResNet-50 model ağırlıklarından elde edilen derin öznitelik matrisi için, Ridge düzenleyicili SVM, Ridge düzenleyicili LR, LR ve KNN algoritmaları genelleştirilmiş hiper parametrelere göre aynı sonuçları vermiştir. Bu sonuçlara ilişkin metrikler sırasıyla %92.16, 0.9216, 0.9230, 0.9243, 0.9215, 0.9223 olmak üzere doğruluk, duyarlılık, özgüllük, kesinlik, F1 skoru ve AUC skorudur. Son olarak, demografik bilgiler ve ResNet-50 model ağırlıklarından elde edilerek çıkarılan derin özniteliklerin birleştirilmesiyle oluşan öznitelik matrisi için, Ridge düzenleyicili SVM, Ridge düzenleyicili LR, LR ve KNN algoritmaları da genelleştirilmiş hiper parametrelere göre aynı sonuçları vermiştir. Bu sonuçlara ilişkin metrikler sırasıyla %92.16, 0.9216, 0.9230, 0.9243, 0.9215, 0.9223 olmak üzere doğruluk, duyarlılık, özgüllük, kesinlik, F1 skoru ve AUC skorudur.

En nihayetinde, belirtilen sonuçlara bakılacak olursa, doğrusal ayırma analizi ve Lasso düzenleyicisini kullanarak, düzenleyicinin kullanımının bir gelişme sağlayabilmiş olduğunu gördük. Demografik bilgileri derin özniteliklerle birleştirerek bir iyileştirme elde edemedik. Ancak, sayı olarak daha fazla veri ve doktor raporu, tütün ürünü kullanımı, ilişkili genetik hastalık, solunum testi vb. gibi daha fazla hasta bilgileri kullanıldığı takdirde, görüntü ve görüntü olmayan bilgilerin birleştirilmesi tekniğinin gelişme sağlayacığını ön görüyoruz. ESA test sonuçlarından MÖ test sonuçlarına geçişte, doğruluk, duyarlılık ve F1 skoru açısından bir gelişme göremesek de, özgüllük ve kesinlik metriklerinde bir artış yakaladık. Bölüm 7'de söz ettiğmiz gibi, daha fazla numune içeren bir veri kümesi kullanılır ve bu numuneler, bizim kullandığımız röntgenler için uzman radyologlardan yardım alınabilecek olması gibi, konu uzmanları tarafından incelenerek seçilirse, bu durum çalışmanın daha iyi metrik sonuçlarına ve deneysel aşamalar arasında daha iyi karşılaştırma fırsatlarına sahip olmasını sağlayacaktır.

Anahtar Kelimeler: COVID-19, Göğüs Röntgeni, Veri çoğaltma, İkili sınıflandırma, Demografik bilgi, Derin öğrenme, Evrişimsel Sinir Ağları, Ön-eğitimli ESA modelleri, Öğrenme aktarımı, Derin öznitelik çıkarma, Derin öznitelik aktarımı, Makine öğrenmesi, Gözetimli öğrenme, Düzenleme, Lasso, Ridge, Izgara araması.

1. INTRODUCTION

Coronaviruses are first named in early 1960s. Disease reports caused by this family of viruses had been reported about chickens since lately 1920s; however, human coronaviruses could be detected after 40 years. Then, because of their the distinctive morphological appearance, they were accepted as a new group of viruses and named as coronaviruses in 1968. First two human coronaviruses studied were named as coronavirus 229E and coronavirus OC43 [8]. In following years, more coronaviruses have been discovered including SARS-CoV in 2003, HCoV NL63 in 2003, HCoV HKU1 in 2004, MERS-CoV in 2013, and SARS-CoV-2 in 2019. SARS-CoV-2 and most other coronaviruses cause serious respiratory infections on humans.

Coronavirus disease 2019 (COVID-19) is caused by severe acute respiratory syndrome coronavirus 2 (SARS-CoV-2) [9]. It was reported in December 2019 in Wuhan, China as a pneumonia outbreak. In January 2020, the transmission of virus from human to human was confirmed, and the first quarantine was applied by Chinese Government in lately January 2020. On February 2020, the new coronavirus was named officially as SARS-CoV-2, and the World Health Organization (WHO) declared a pandemic on 11 March, 2020 [10].

The most common symptoms of COVID-19 is known as fever, dry cough and tiredness. The loss of taste or smell, diarrhoea, headache, aches and pains, sore throat, and conjunctivitis are also agreed to strong high probability symptoms. Since the symptoms are very common with most other diseases, and they are not still precise, it is significant to find a highly accurate distinctive method to detect COVID-19. Moreover, infected people begin to show symptoms within an average of 5-6 days; however, this period can take up to 14 days [11]. Furthermore, the demographic information of a patient, i.e. the age and sex information, has a major role on how the patient is effected on COVID-19.

As of April 24, 2021, COVID-19 has caused more than 145 million people to be infected and more than 3 million deaths worldwide, and continues to spread rapidly

[12]. As stated above, the demographic information has a huge effect on death ratios. Anyways, early and rapid diagnosis plays a very important role in the treatment of the disease. That is why, WHO published protocols on diagnostic detection for COVID-19 on 13 and 17 January, 2020. Polymerase Chain Reaction (PCR) test [13] is the most basic method of COVID-19 diagnosis; however, the sensitivity is not high enough for the low viral load. Moreover, laboratory errors present in test samples. Because of it, all symptoms, test result and other reports must be considered on diagnostic process.

COVID-19, a respiratory disease, also plays a major role in the increase of pneumonia. Therefore, the diseases most confused with COVID-19 are those that cause pneumonia. One way to distinguish them is to examine the most damaged organ, lungs. Chest X-Rays are one of the fastest, the most accessible and the most reliable way to make observations on human lungs. However, the diagnosis of pneumonia from chest X-Rays may be a difficult task even for expert radiologists. The most important part of detecting COVID-19 by chest X-Rays is to distinguish the cause of pneumonia [14]. Therefore, computerized support systems are needed to help radiologists diagnose pneumonia from chest X-Ray images.

Thanks to large data sets, rapid progress is being made in artificial intelligence-based computer vision problems. It has been observed that deep learning gives better results compared to manual diagnosis in problems such as object recognition, perception and segmentation. On the other hand, machine learning has various strong classification algorithms on categorical data including either small or large information.

1.1 Purpose of Thesis

The scope of this study is two fold: 1) to show the capability of deep features transfer learning from deep learning to machine learning, and 2) to apply this knowledge onto an ongoing global public health problem. Deep learning is performed for feature extraction with methodologies which are AlexNet, RestNet-18, Resnet-50, VGG16 and VGG19, and machine learning is performed for final classifications with algorithms including their original and regularized versions which are Support Vector Machines, Logistic Regression, K-Nearest Neighborhoods and Linear Discriminant Analysis. Moreover, the demographic information of patients in thesis dataset is

also studied to make conclusions on their effect to machine learning classification algorithms.

For this purpose, chest X-Ray images shared on GitHub platform were used. In this dataset, there are data with and without demographic information, non-diseased, virus-induced pneumonia, bacterial-induced pneumonia, fungal-induced pneumonia, and lipoid-induced pneumonia. Moreover, samples with pneumonia finding have detailed causes such as COVID-19, Influenza, Escherichia coli, Aspergillosis spp., etc. Hence, data extraction on this dataset was applied to obtain two classes as non-COVID-19-diseased and COVID-19-diseased of data having demographic information.

By applying the stated scope to the mentioned dataset, the main aim of this thesis is to explain how to prepare data for study, how to perform deep learning algorithms, machine learning algorithms and transfer learning from deep learning to machine learning, how to use demographic information together with chest X-Ray image data, and to show how demographic information affects and what are the effects of regularization on machine learning algorithms by various performance measures.

1.2 Literature Review

With the increase in information about COVID-19 and the formation of data that can be used during this period, artificial intelligence researchers had started to work on this disease. Since both the effectiveness and the limitations of machine learning and deep learning, which are the sub-branches of artificial intelligence, had been already experienced and known by the previous numerous studies, researchers could started new studies without wasting time and achieved satisfying results rapidly.

Ali Abbasian Ardakani et al. [15] worked on chest computed tomography (CT) images to detect whether a person has COVID-19 disease or not. They studied on 10 different convolutional neural network (CNN) models, and compared them. The CNN models they compared are AlexNet, VGG-16, VGG-19, SqueezeNet, GoogleNet, MobileNet-V2, ResNet-18, ResNet-50, ResNet-101, and Xception. They achieved to the best results with ResNet-101 CNN model as the AUC score of 0.994, the sensitivity of 100%, the specificity of 99.02%, the accuracy of 99.51%, the precision

of 99.03%, and the negative predictive value of 100%. Moreover, the results of other CNN architectures can be found on the original paper.

Y. Pathak et al. [16] used a deep transfer learning technique on chest computed tomography (CT) images to classify non-COVID-19 and COVID-19 people. They used pre-trained ResNet-50 CNN architecture on ImageNet [17] dataset to train their classification problem, and 10-Fold cross-validation to prevent overfitting. Then, they obtained the testing accuracy as 93.02%.

Tulin Ozturk et al. [18] developed a new CNN architecture, named as DarkCovidNet, to classify chest X-Ray images among COVID-19 and no-finding, and among COVID-19, no-findings and pneumonia not caused by COVID-19. They inspired by the DarkNet architecture [19] and constructed theirs as consisting of seventeen convolution layers and one fully-connected layer. The final test result were achieved as the accuracy of 87.02% for 3-class classification problem, while it was 98.08 for binary classification problem.

Yujin Oh et al. [20] solved COVID-19, normal and pneumonia not caused by COVID-19 classification problem with first segmenting the chest X-Ray images and yielding extracted lung areas. Then, segmented images were classified patch-by-patch in ResNet-18 CNN architecture based model. For the final decision among patches, the majority voting method was used, and the results were obtained as the accuracy of 88.9%, the sensitivity of 85.9%, and the specificity of 96.4%.

Elshennawy and Ibrahim [21] proposed four different deep learning models to solve 3-class classification problem. The dataset consist of chest X-Ray images and the three classes are no finding, bacterial pneumonia and COVID-19. A CNN model containing 4 convolutional layers and 3 fully-connected layers is proposed and trained from stretch, and the validation loss and accuracy were obtained as 0.3020 and 92.19% respectively. A LSTM-CNN model containing one LSTM layer, 4 convolutional layers and 2 fully-connected layers were developed, and the final results were yielded as the loss of 0.5771 and the accuracy of 91.80%. Furthermore, two CNN models, ResNet152V2 and MobileNetV2, were used as pre-trained. The test results for ResNet152V2 and MobileNetV2, were achieved as the loss of 0.0523 and the accuracy of 99.22%, and as the loss of 0.1665 and the accuracy of 96.48% respectively.

Ruaa Adeeb Al-Falluji et al. [22] were used a modified ResNet-18 CNN model to classify X-Ray images among COVID-19, no-findings and pneumonia not caused by COVID-19. The original ResNet-18 architecture was modified as changing the kernel size of conv1 convolution layer from 7 to 3, and adding two new convolution layers after the global average pooling layer. The final test result obtained with this technique was the accuracy of 96.73%.

Majid Noue et al. [4] was developed a novel CNN architecture, and solved the 3-class, COVID-19, normal and viral pneumonia other than SARS-CoV-2, based on Deep Features and Bayesian Optimization. The developed CNN architecture includes 5 convolution layers, 3 fully-connected layers and Softmax activation layer at the end. Deep features extracted from fc1 and fc2 layers are used to feed machine learning algorithm, which are support vector machine, decision tree and k-nearest neighbor, for final classification. The result achieved for features extracted from fc2 are obtained by SVM classifier as the sensitivity of 89.39%, the specificity of 99.75%, the F-score of 96.72, and the accuracy of 98.97%.

The results of studies stated in this section can be viewed as merged in the Table 1.1.

Table 1.1 : Reviewed works in the literature and their stated results.

Authors	Technique	Dataset	The Number of Classes	Accuracy (%)	Sensitivity (%)	Specificity (%)
Ali Abbasian Ardakani et al. (2020)	ResNet-101 CNN model	Chest CT images	3	99.51	100.00	99.02
Y. Pathak et al. (2020)	Deep transfer learning on ResNet-50 CNN model	Chest CT images	3	93.02	91.46	94.78
Tulin Ozturk et al. (2020)	DarkCovidNet CNN model	Chest X-Ray images	3	87.02	92.18	89.96
Tulin Ozturk et al. (2020)	DarkCovidNet CNN model	Chest X-Ray images	2	98.08	95.13	95.30
Yujin Oh et al. (2020)	Patch-by-patch classification in ResNet-18 CNN based model after segmentation	Chest X-Ray images	2	88.90	85.90	96.40
Elshennawy and Ibrahim (2020)	Pre-trained ResNet152V2 CNN model	Chest X-Ray images	2	99.22	99.44	99.45
Ruaa Adeeb Al-Falluji et al. (2020)	Deep transfer learning on the modified ResNet-18 CNN model	Chest X-Ray images	2	96.73	94.00	100.00
Majid Noue et al. (2020)	SVM classifier fed with deep features obtained from the novel proposed CNN model	Chest X-Ray images	2	98.97	89.39	99.75

1.3 Structure

This thesis consists of seven chapters. Chapter 1 presents an overview of the study including the history of COVID-19 disease, the scope and aim of thesis, the literature survey on related works, and this structure.

In Chapter 2, the information about chest X-Rays are given.

Chapter 3 introduces the basics of deep learning, loss functions and optimization methods, the basics of convolutional neural networks, transfer learning, and the CNN models experimented in this study such that AlexNet, ResNet-18, ResNet-34, ResNet-50, VGG16 and VGG19.

Chapter 4 introduces the basics of machine learning, the method of cross-validation, the regularization, and the ML algorithms experimented in this study such that SVM, LR, KNN and LDA.

In Chapter 5, all experiments on convolutional neural networks and machine learning carried out in this study take place together with how the dataset was constructed, data augmentation, deep feature extraction, how the feature matrices were formed, and the methods for hyper-parameter tuning on ML.

In Chapter 6, all results of experiments are given together with how we measure the performance by confusion matrices.

Finally, in Chapter 7, the conclusions of our study are presented with interpretations and suggestions for further researches.

2. CHEST X-RAY

X-radiations (X-rays) are electromagnetic waves which is actually a type of radiation. German physicist Wilhelm Konrad Röntgen discovered these specific type of photons while investigating cathode rays in Crookes tubes at 1895. Röntgen named these rays as X-radiations to signify an unknown type of radiation.

The first use of X-rays for chest imaging dates back to 1896. Nowadays, X-rays are mostly used in medical industry for medical and radiological imaging, and at public areas in purpose of security.

The least photons are absorbed by air while the most photons are absorbed by the calcium in bones. That is why bones are visible as white. Fat and other soft tissues absorbs X-rays in middle level, so they are seen as gray. Because of the absorption properties of X-rays, stated above, the lungs are observed in blackish color.

Figure 2.1 : Hand mit Ringen (Hand with Rings): print of Wilhelm Röntgen's first "medical" X-ray, of his wife's hand [1].

Chest X-rays can be taken in 3 main projection methods. The projection method may vary from country to country or even from hospital to hospital. However, the most preferred projection method is Postero-Anterior (PA) view in which X-rays go through from patient's posterior to anterior. The patient has to be stand during the operation.

Second most used method is Antero-Posterior (AP) erect view. On the contrary of frontal view, beams traverse from anterior to posterior in AP projection. When the PA or AP view is not possible due to the health issue of patient, such that the patient is not able to stay erect, supine position is applied as AP-Supine projection method. The other most used view type is Lateral (L) projection. It is performed from the left lateral of patient while the patient is standing. There are another various projection methods to film the chest of patient by X-rays.

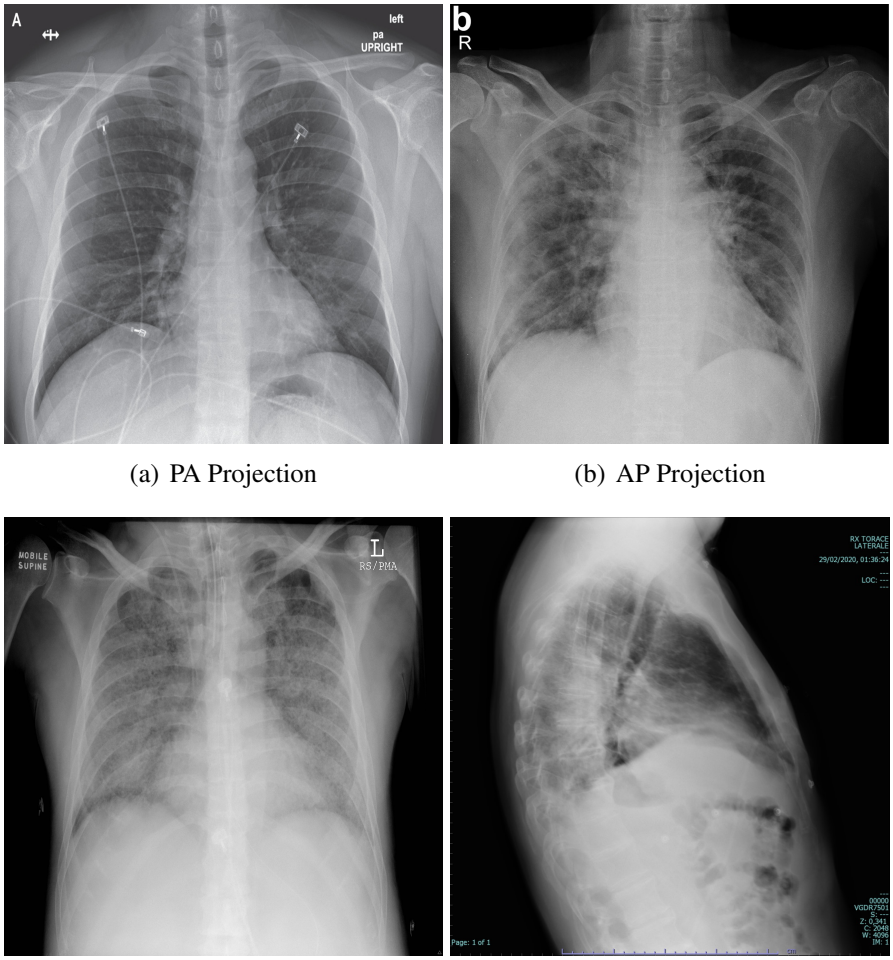

(a) PA Projection (b) AP Projection

(c) AP Supine Projection (d) L Projection

Figure 2.2 : Chest X-Ray Projections.[1]

Chest X-ray imaging has very significant role on detecting serious disease such as pneumonia and its causes, pneumothorax, heart failures, emphysema, lung cancer, broken ribs for years, and COVID-19 recently. Thanks to the accessibility and the ease of use of chest X-rays, various artificial intelligence problems can be formed and accomplished for the benefit of medical use, computer science and mathematics.

[1]Retrieved from GitHub: `https://github.com/ieee8023/covid-chestxray-dataset/tree/master/images` on March 25, 2021.

3. INTRODUCTION TO DEEP LEARNING

In this section, we start with the basics of deep learning. Then we mention the loss function used in the thesis, and the optimization of it. Finally, we end the section with the basics of convolutional neural networks, the CNN models used in the thesis, and the transfer learning concept.

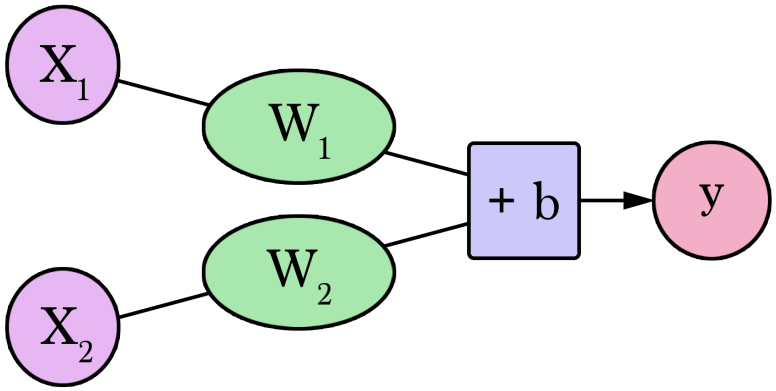

(a) Neuron with two variables

$$y = W_1 x_1 + W_2 x_2 + b$$

(b) Formula for the output of neuron on (a)

Figure 3.1 : Sample Neuron.[1]

3.1 The Basics of Deep Learning

Let us take a look at basic deep learning terminologies.

- **Neural Network**: A neural network is a learning framework for machines using a collection of functions to understand and translate a data input into a desired output. The main inspiration is the human brain structure.

[1]Retrieved from GitHub: `https://jalammar.github.io/visual-interactive-guide-basics-neural-networks/` on March 28, 2021.

- **Nodes (Neurons)**: Neural networks are made of nodes (neurons). A node is a set of weights for that node and its associated nodes. Each node has an input data, a weight and a bias value.
- **Weight and Bias**: Weight transforms input data to the hidden layers of neural network. Some sources includes the bias into the weight. Both of them are learnable parameters, but bias is used and optimized to tune the distance between the predicted value and the intended value.
- **Batch**: A batch of data is a group selected from the whole data. The number of data in a batch are mostly chosen as a power of 2, such as $2^4, 2^5, 2^6$ etc ...
- **Epoch**: An epoch is an iteration to learn through all train data. If batches are used, it is recommended to shuffle data order in each epoch before creating new batches on train data.
- **Train Data and Training**: The data group reserved to be used in learning process is called as train data. The ratio of the number of train data is generally determined as 80% or 70%, and the rest is placed into test data group. The train data must be strictly separated from validation and test data, and only used on training process. Training process is consisting of multiple epochs. In each epoch, the train data go into the model as input, the neural network works on learning from data, the losses and accuracy (if desired) are computed and the losses are optimized. If batching is used, this process is applied on each batch, and the average and final losses and accuracy (if desired) are calculated over all batches at the end of each epoch.
- **Validation Data and Validating**: If there exists enough train data for the problem and learning process, one may need to have validation data to validate the learning process periodically. The validation data group is strictly separated from train data such that generally the 80% or 70% of number of train data. During the validation process, the weights and biases are stable and no optimization process is applied, that is only the losses and other desired metrics, such as accuracy, are computed.
- **Test Data and Testing**: The data group reserved to be used in testing process is called as test data. The ratio of the number of test data is generally determined as 20% or 30%. The test data must be strictly separated from train data, and only used on testing process. The training process should not see any of test data. Testing

process is usually only applied on the end of all epochs. However, when the train data is not feasible to be divided into validation data, at the end of each epoch testing process may be applied on test data. This method is also used to determine the overfitting and stop point.

- **Underfitting and Overfitting**: A learning algorithm is appeared to have underfitting when it cannot capture or fit the data well. On the other hand, when the model fits on the train data perfectly, it may be started actually to memorize the train data, not learn from the data. Therefor, the testing metrics are seen in the opposite direction of what is desired. This situation is called as overfitting.

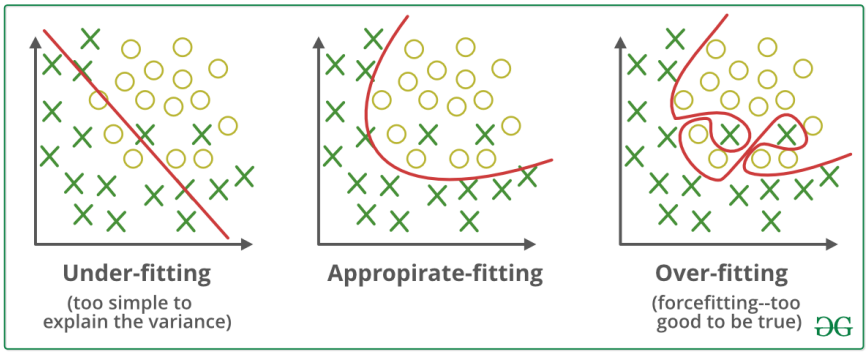

Figure 3.2 : Underfitting - Well Fitting - Overfitting.[2]

3.2 The Cross-Entropy Loss Function

The loss function is the function that represents the error between predicted and true values, which can be called as the cost, of the problem to be optimized.

The cross-entropy loss function is one of the most used loss functions to measure the performance of corresponding classifier. The function maps the probability values between 0 and 1 to the cost value. Here the loss value increases together with the divergence between the true label and the predicted probability.

The cross-entropy loss function is as in the equation (3.1).

$$L_{cross-entropy} = -\sum_{i=1}^{n} y_i \log(p_i)\,, \tag{3.1}$$

[2]Retrieved from GeeksforGeeks: `https://www.geeksforgeeks.org/underfitting-and-overfitting-in-machine-learning/` on March 28, 2021.

where n is the number of classes, and y_i and p_i are the truth label and Softmax probability respectively for the i^{th} class. Thus, for a binary classification problem, the cross-entropy loss function can be taken as in the equation (3.2).

$$L = -\left(y \log(p) + (1-y) \log(1-p)\right), \tag{3.2}$$

where y and p are the binary indicator (0 or 1) depends on the correctness of observed class label and the probability of observation respectively.

3.3 The Basics of Optimization Methods

To reduce the losses and to reach the more accurate possible predictions, various optimization methods can be used. The weights are initialized and updated on each training epoch. The initialization strategies may vary depending on the neural network. It is aim to achieve the most satisfying results by using some algorithms called as optimizers.

3.3.1 Stochastic Gradient Descent with Momentum (SGD) Optimization Algorithm

Stochastic gradient descent is an iterative method for optimizing an objective function with suitable smoothness properties. It can be regarded as a stochastic approximation of gradient descent optimization. Momentum remembers the weight update at each iteration, and determines the next update as a linear combination of the gradient and the previous update [23].

Algorithm 1 SGD with momentum

given learning rate $\alpha_t \in \mathbb{R}$, momentum factor $\beta_1 \in \mathbb{R}$, weight decay factor $w \in \mathbb{R}$
initialize time step $t \leftarrow 0$, parameter vector $\boldsymbol{x}_{t=0} \in \mathbb{R}^n$, first moment vector $\boldsymbol{m}_{t=0} \leftarrow \boldsymbol{0}$
repeat
  $t \leftarrow t+1$
  $\nabla f_t(\boldsymbol{x}_{t-1}) \leftarrow SelectBatch(\boldsymbol{x}_{t-1})$ ▷ select batch and return the corresponding gradient
  $\boldsymbol{g}_t \leftarrow \nabla f_t(\boldsymbol{x}_{t-1}) + w_t \boldsymbol{x}_{t-1}$
  $\eta_t \leftarrow SetScheduleMultiplier(t)$ ▷ can be fixed, decay, be used for warm restarts
  $\boldsymbol{m}_t \leftarrow \beta_1 \boldsymbol{m}_{t-1} + \eta_t \alpha_t \boldsymbol{g}_t$
  $\boldsymbol{x}_t \leftarrow \boldsymbol{x}_{t-1} - \boldsymbol{m}_t$
until *stopping criterion is met*
return optimized parameters $\boldsymbol{x}_t$

Figure 3.3 : Pseudocode for SGD with Momentum [2].

3.3.2 Adam Optimization Algorithm

Adaptive moment estimation is an optimization algorithm that uses the running averages of both the gradients and the second moments of the gradients. Before each step, the gradient of loss function is calculated and a step in the opposite direction is taken with corresponding rate. This process is also called as Adam with L2 regularization [24].

3.3.3 Adam with Decoupled Decay (AdamW) Optimization Algorithm

Adam with decoupled weight decay does not use the regularization as the normalized by square root of second moment vector. Thus, it is only proportional to the weight itself [24].

Algorithm 2 Adam and AdamW

given $\alpha_t = 0.001, \beta_1 = 0.9, \beta_2 = 0.999, \epsilon = 10^{-8}, w \in \mathbb{R}$
initialize time step $t \leftarrow 0$, parameter vector $\boldsymbol{x}_{t=0} \in \mathbb{R}^n$, first moment vector $\boldsymbol{m}_{t=0} \leftarrow \boldsymbol{0}$, second moment vector $\boldsymbol{v}_{t=0} \leftarrow \boldsymbol{0}$, schedule multiplier $\eta_{t=0} \in \mathbb{R}$
repeat
  $t \leftarrow t + 1$
  $\nabla f_t(\boldsymbol{x}_{t-1}) \leftarrow SelectBatch(\boldsymbol{x}_{t-1})$ ▷ select batch and return the corresponding gradient
  $\boldsymbol{g}_t \leftarrow \nabla f_t(\boldsymbol{x}_{t-1}) + w_t \boldsymbol{x}_{t-1}$
  $\boldsymbol{m}_t \leftarrow \beta_1 \boldsymbol{m}_{t-1} + (1 - \beta_1)\boldsymbol{g}_t$ ▷ here and below all operations are element-wise
  $\boldsymbol{v}_t \leftarrow \beta_2 \boldsymbol{v}_{t-1} + (1 - \beta_2)\boldsymbol{g}_t^2$
  $\hat{\boldsymbol{m}}_t \leftarrow \boldsymbol{m}_t / (1 - \beta_1^t)$ ▷ here, β_1 is taken to the power of t
  $\hat{\boldsymbol{v}}_t \leftarrow \boldsymbol{v}_t / (1 - \beta_2^t)$ ▷ here, β_2 is taken to the power of t
  $\eta_t \leftarrow SetScheduleMultiplier(t)$ ▷ can be fixed, decay, be used for warm restarts
  $\boldsymbol{x}_t \leftarrow \boldsymbol{x}_{t-1} - \eta_t \left(\alpha_t \hat{\boldsymbol{m}}_t / (\sqrt{\hat{\boldsymbol{v}}_t} + \epsilon) + w_t \boldsymbol{x}_{t-1} \right)$
until *stopping criterion is met*
return optimized parameters $\boldsymbol{x}_t$

Figure 3.4 : Pseudocode for Adam and AdamW [2].

3.4 The Basics of Convolutional Neural Networks

The convolutional neural networks (CNNs) are the special study and research area of deep neural networks. They are mostly used in visual problem analyzing and solving. In this section and its subsections we study on the fundamental layers and elements of CNN architectures.

Basically, a CNN model consists of three parts such that an input layer, hidden layers and an output layers. The structure of CNNs comports with the feed-forward networks. That is, the information only goes through in one direction, forward. To feed and

train a feed-forward network, backpropagation algorithm is commonly used. The algorithm orders to compute the gradients in weight space of a feed-forward network, with respect to a loss function. Then the weight space is updated with these gradients by the method of corresponding optimizer. The gradient of objective loss function $f(\theta)$ at a weight vector θ_t is computed via directional derivatives and chain rule, and represented by $\nabla f(\theta_t)$.

An example of using directional derivatives and chain rule can be found in Figure 3.5. Assume there exist m number of x_i nodes feeding y where $\mathbf{x} = (x_1, \ldots, x_m)$ is m-dimensional vector. Then the gradient of y at $\mathbf{x}$ is constructed as $\nabla y(\mathbf{x}) = \begin{bmatrix} \frac{\partial y}{\partial x_1}(\mathbf{x}) \\ \vdots \\ \frac{\partial y}{\partial x_m}(\mathbf{x}) \end{bmatrix}$.

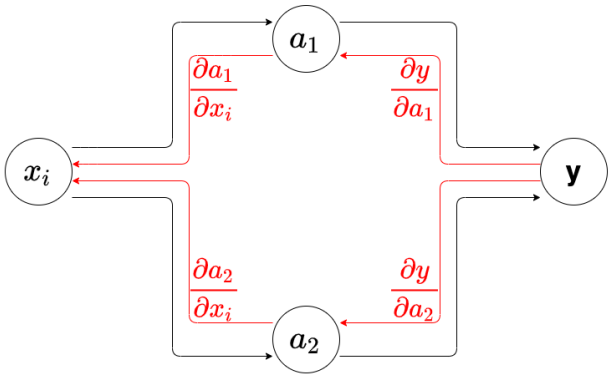

$$\frac{\partial y}{\partial x_i} = \frac{\partial y}{\partial a_1}\frac{\partial a_1}{\partial x_i} + \frac{\partial y}{\partial a_2}\frac{\partial a_2}{\partial x_i}$$

Figure 3.5 : The usage example of directional derivatives and chain rule.

Assume the simple CNN sample in Figure 3.6. Let us name the output layer vector as $\mathbf{y} = \mathbf{a}_6 = (a_{6,1}, a_{6,2})$, and each i^{th} layer vector as $\mathbf{a}_i$. For instance, $\mathbf{a}_3 = (a_{3,1}, a_{3,2}, a_{3,3}, a_{3,4})$ and $\mathbf{a}_5 = (a_{5,1}, a_{5,2}, a_{5,3})$. The gray nodes appearing above each layer are real valued bias terms. Assume that the objective loss function is least squares loss, i.e. $l(\mathbf{y}, \mathbf{y}^{GT}) = \frac{(\mathbf{y}^{GT} - \mathbf{y})^2}{2}$ where $\mathbf{y}^{GT}$ is the grand-truth labels of our dataset. Assume that our hypothesis function to create CNN architecture is in the form $f : \mathbb{R}^k \to \mathbb{R}^t$ where k and t vary according to corresponding layers. Then define $\mathbf{a}_i = f_i(W^i \mathbf{a}^{i-1} + b^i)$ for each i^{th} layer where $W \in \mathbb{R}^{t \times k}$ is weight matrix. We obtain the backward pass of our loss function with respect to the first weight matrix and bias term by chain rule:

$$\frac{\partial l(\mathbf{y},\mathbf{y}^{GT})}{\partial W^1} = \frac{\partial l}{\partial \mathbf{a}_6} \times \frac{\partial \mathbf{a}_6}{\partial \mathbf{a}_5} \times \frac{\partial \mathbf{a}_5}{\partial \mathbf{a}_4} \times \frac{\partial \mathbf{a}_4}{\partial \mathbf{a}_3} \times \frac{\partial \mathbf{a}_3}{\partial \mathbf{a}_2} \times \frac{\partial \mathbf{a}_2}{\partial \mathbf{W}^1}, \text{ and} \tag{3.3}$$

$$\frac{\partial l(\mathbf{y},\mathbf{y}^{GT})}{\partial b^1} = \frac{\partial l}{\partial \mathbf{a}_6} \times \frac{\partial \mathbf{a}_6}{\partial \mathbf{a}_5} \times \frac{\partial \mathbf{a}_5}{\partial \mathbf{a}_4} \times \frac{\partial \mathbf{a}_4}{\partial \mathbf{a}_3} \times \frac{\partial \mathbf{a}_3}{\partial \mathbf{a}_2} \times \frac{\partial \mathbf{a}_2}{\partial b^1}. \tag{3.4}$$

Here, each partial derivative is computed as shown in Figure 3.5. For instance, if the forward pass connection between $\mathbf{a}_{4,2}$ and $\mathbf{a}_{5,1}$ is $W^4_{2,1}$, we use the directional derivative rule while computing $\frac{\partial l}{\partial \mathbf{a}_6}$ for the backward pass gradient to update $W^4_{2,1}$ value as:

$$\frac{\partial l}{\partial W^4_{2,1}} = \frac{\partial l}{\partial \mathbf{a}_6} \times \frac{\partial \mathbf{a}_6}{\partial \mathbf{a}_{5,1}} \times \frac{\partial \mathbf{a}_{5,1}}{\partial W^4_{2,1}} = \left(\frac{\partial l}{\partial \mathbf{a}_{6,1}} \times \frac{\partial \mathbf{a}_{6,1}}{\partial \mathbf{a}_{5,1}} + \frac{\partial l}{\partial \mathbf{a}_{6,2}} \times \frac{\partial \mathbf{a}_{6,2}}{\partial \mathbf{a}_{5,1}} \right) \times \frac{\partial \mathbf{a}_{5,1}}{\partial W^4_{2,1}}. \tag{3.5}$$

In the same way, the gradient for b^5 can be computed as:

$$\frac{\partial l}{\partial b^5} = \frac{\partial l}{\partial \mathbf{a}_6} \times \frac{\partial \mathbf{a}_6}{\partial b^5} = \frac{\partial l}{\partial \mathbf{a}_{6,1}} \times \frac{\partial \mathbf{a}_{6,1}}{\partial b^5} + \frac{\partial l}{\partial \mathbf{a}_{6,2}} \times \frac{\partial \mathbf{a}_{6,2}}{\partial b^5}. \tag{3.6}$$

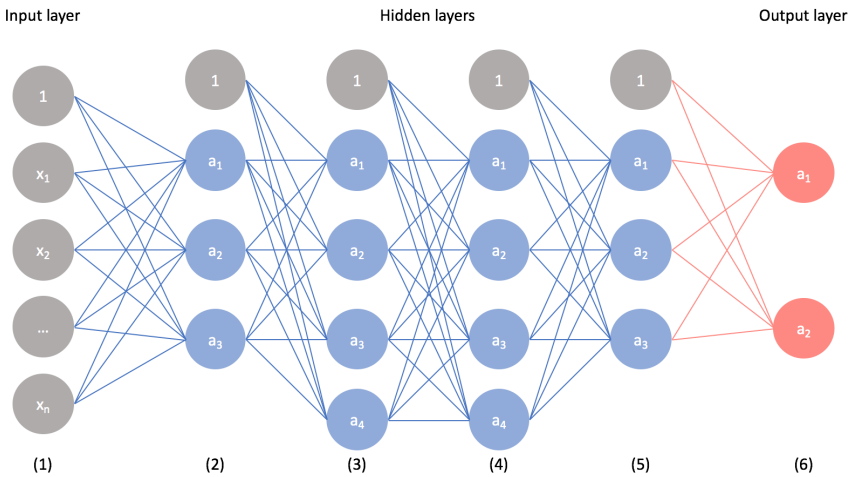

Figure 3.6 : Sample CNN Architecture.[3]

3.4.1 Convolutional Layer

Convolutional layer is the building block of CNN architectures and is used to reveal the distinctive features of input data. The various filters are applied to the data to reveal low and high-level feature map. After convolution, the size of the input data changes

[3]Retrieved from: `https://www.jeremyjordan.me/convolutional-neural-networks/` on March 31, 2021.

depending on the filter (or kernel), stride and padding choices. The outputs of the convolution layers are called activation maps.

A convolution layer includes a window named as filter or kernel that can be of different sizes as $2x2$, $3x3$, etc.. The coefficients that filters include change on each iteration during the training of a CNN. This coefficients and their updates are used to detect the significant and learnable parts of the data.

Filter is started to be applied from the upper left corner, and continues moving towards the right. When there are no cells left to be scanned on the right, it continues from the lower cells as before. On each step, the filter and the corresponding area of input matrix are multiplied by element-wise. The step length of scanning process is called as stride. The default stride value is 1; however, different stride values may be used depends on the data and CNN architecture. If the stride is set as s, then the kernel window move by jumping s cells.

On some situations, such as a size inconsistency or paying attention to the information on the edges and corners of the image, the edges of input matrix may be filled by zeros. These process is calling as padding. If the padding value is set as p, the p cells with zero values are added to the edges of input matrix.

The Figure 3.7 gives a summary about how activation map is constructed for a given input matrix and a filter. Let us give a detailed example to about it. Assume that the input data is a three layered, which are red, green and blue, image in the shape of 223 x 223 x 3, and the padding size is 1. Let choose two filter windows in the size of 5 x 5 and the step size (stride) as 2. Let denote the input size with $W_{input}xH_{input}xD_{input}$, the padding with P, the number of filters with K, the size of a filter window with FxF and the stride with S. Here, we have:

- $W_{input} = 223$, $H_{input} = 223$, $D_{input} = 3$,
- $K = 2$, $F = 5$,
- $P = 1$, and $S = 2$.

The size of activation map is calculated as:

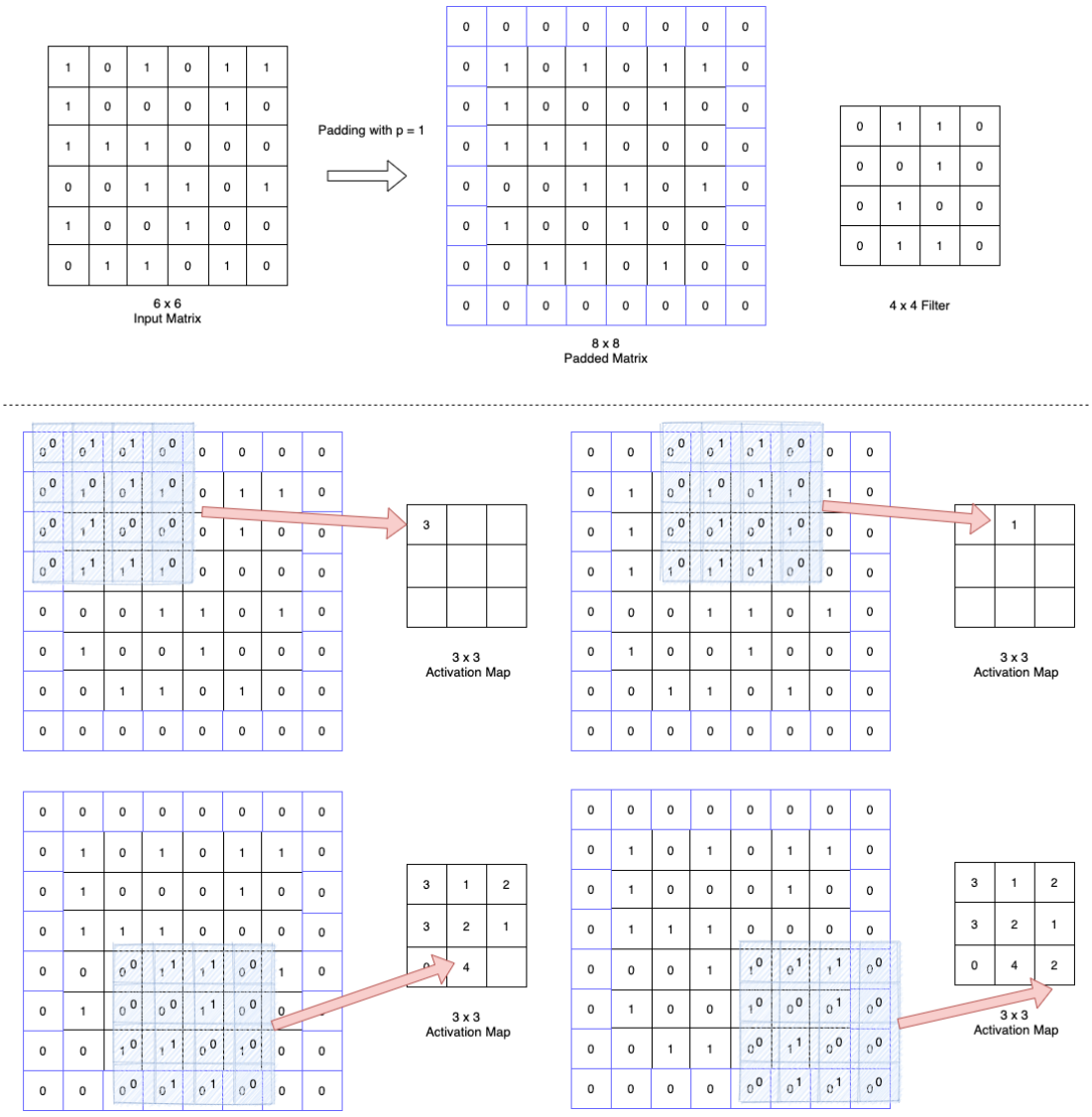

Figure 3.7 : Activation map construction by 4 x 4 filter window with stride as 2.

$$W_{output} = (W_{input} - F + 2P)/S + 1\,, \tag{3.7}$$

$$H_{output} = (H_{input} - F + 2P)/S + 1\,, \quad \text{and} \tag{3.8}$$

$$D_{output} = K\,. \tag{3.9}$$

Consequently, the activation map is yielded in the size of 112 x 112 x 2 by the equations (3.7), (3.8) and (3.9) respectively.

3.4.2 Activation Function (Rectified Linear Units - ReLU)

The activation function forms the output of the node for a given input or input set. Rectifier activation function maps the input to non-negative values. A unit form of the

rectifier activation function, which is given in equation (3.10), is called as Rectified Linear Units (ReLU) which is the most common used in neural networks.

$$\text{ReLU is defined as:} \quad f(x) = \max(0, x)\,. \tag{3.10}$$

3.4.3 Pooling Layer

Pooling layers are commonly used in between the convolutional layers, especially after activation functions. A pooling layer outputs a a new feature map with the lower size than the size of input feature map. The characteristics of output feature map is depends on the type of pooling layer. The pooling layers have a stride parameter to control the step size of the movement of pooling window. The most common pooling functions are given below.

- **Average Pooling:** The average of corresponding window is computed and inserted into output feature map.
- **Maximum Pooling:** The maximum value of corresponding window is inserted into output feature map.

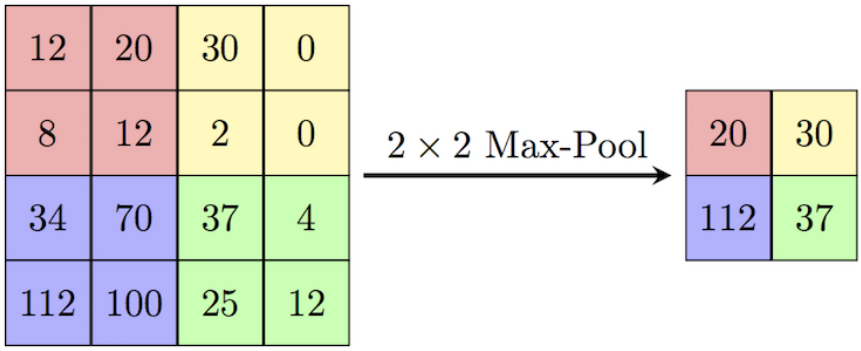

Figure 3.8 : Maximum pooling operation sample with 2 x 2 window and stride as 2.[4]

3.4.4 Batch Normalization

Batch normalization is a technique for training the deep neural networks that standardize the inputs to one layer for each mini batch. This has the effect of stabilizing the learning process and significantly reducing the number of training epochs required [4].

[4]Retrieved from: `https://computersciencewiki.org/index.php/Max-pooling_/_Pooling` on April 3, 2021.

3.4.5 Dropout

Dropout is the removing operation of the nodes below certain threshold value in the network at each training iteration. In other words, it is aimed not to use weak information and memorize the network. Dropout can be in any layer and its threshold value, which can differ in different layers, is between [0,1].

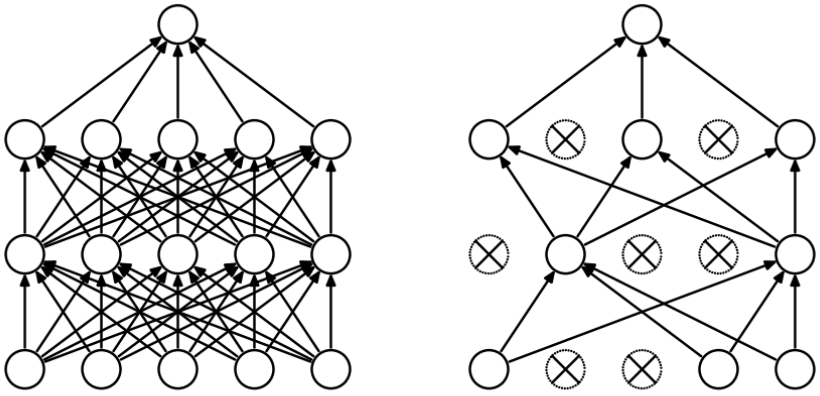

(a) Standard Neural Net (b) After applying dropout.

Figure 3.9 : (a) A standard neural network, (b) A neural network after applying dropout [3].

3.4.6 Flattening

Flatten operation reshapes the input into the one-dimension. It is used before passing to the fully-connected layers.

3.4.7 Fully-Connected Layer

This structure is used to combine the information in the previous layers. It pre requires the flatten operation before itself. The fully-connected layers are used to classify data in different categories, or construct feature maps to be used in another artificial network methods.

3.5 Transfer Learning

Transfer learning is transferring the features, weights, etc. in pre-trained model to another artificial learning model. This can be between two deep learning models or across a machine learning and deep learning model. In this thesis, the weight transfer

[5]Retrieved from: `https://www.superdatascience.com/blogs/convolutional-neural-networks-cnn-step-4-full-connection` on April 3, 2021.

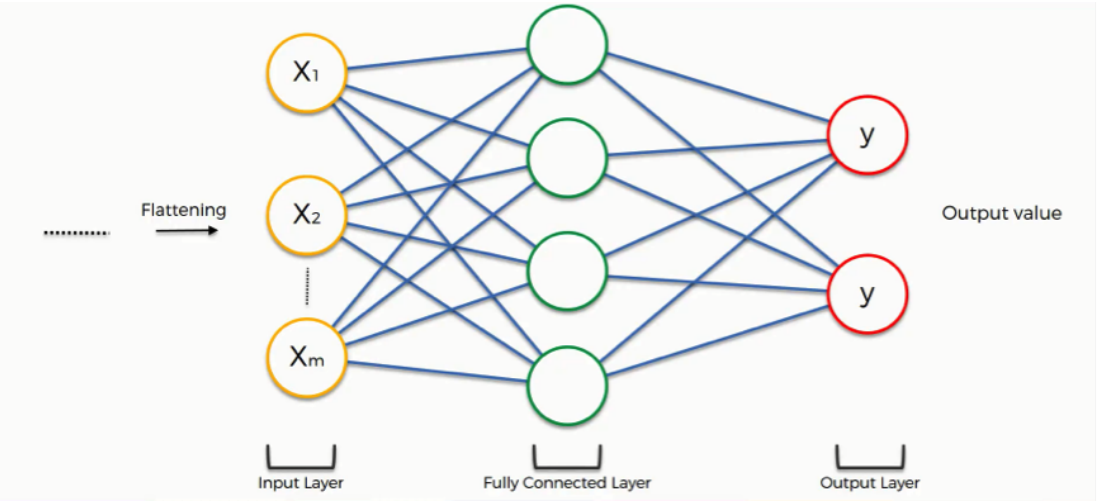

Figure 3.10 : The usage of full-connected layer for a binary classifier.[5]

from pre-trained CNN models to CNN models and feature transfer from CNN models to machine learning models are used.

Transfer earning is used to shorten the training time if the data set is insufficient and to achieve high performance with less data. If the data on each class is less than 1000, the dataset may be considered as small.

To prepare a pre-trained CNN model for visual artificial intelligence problems, ILSVRC 2012 ImageNet [17] dataset, including 1000 class with large data, is commonly used. The weights after the training process is saved and shared to use in transfer learning afterwards. On transfer learning, the pre-trained model is called with its pre-computed weights, and the weights are transferred into the same empty neural network. There exist different approaches to train this new neural network; such that, training the all layers on the convolutional block, training a part of the layers on the convolutional block and freezing the other, or freezing all layers on the convolutional block. The choice of strategy, which is called as fine-tuning operation, depends on the size of dataset and the similarity between the dataset used in pre-training process and the dataset to be used in current task. Then the last fully-connected layer is adapted to the current task by updating itself or adding new fully-connected layers.

To prepare a deep feature set to be used in another artificial learning model, such as machine learning models, the features on a fully-connected layer, mostly the first or

[6]Retrieved from: `https://towardsdatascience.com/transfer-learning-from-pre-trained-models-f2393f124751` on April 3, 2021.

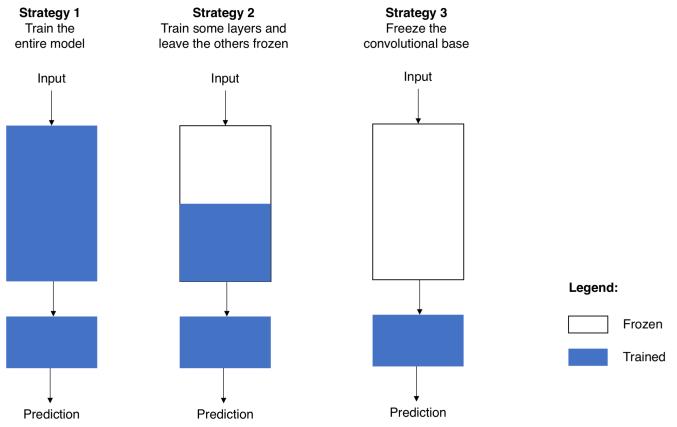

Figure 3.11 : Different fine-tuning strategies on pre-trained model.[6]

second, are extracted and saved. Then the saved deep features are used in the target artificial learning model as the feature map of dataset.

3.6 CNN Models

There are too many similar and different CNN architectures which can be simply called as models. These models consist of various combinations of input layer, hidden layers and an output layer such that some basics of them are explained in Section 3.4.

In this section, the state-of-the-art CNN models used in the thesis are introduced and detailed.

3.6.1 AlexNet

The AlexNet architecture was developed by Krizhevsky et al. [5] for the object recognition problem. This model was trained with the ILSVRC 2012 ImageNet [17] dataset, and achieved high performance results and won first place in the ImageNet competition in 2012. There are 8 layers in total in the AlexNet architecture. The first five are convolution, which uses 11x11 size filters with the stride as 4, and some are supported by the maximum pooling layer, the remaining three are the fully-connected layers. The ReLU activation function is used after each convolution and fully-connected layer. The size of the input image is $224 \times 224 \times 3$, and the number of filters used increases as going deeper into the model.

3.6.2 Residual Neural Network (ResNet)

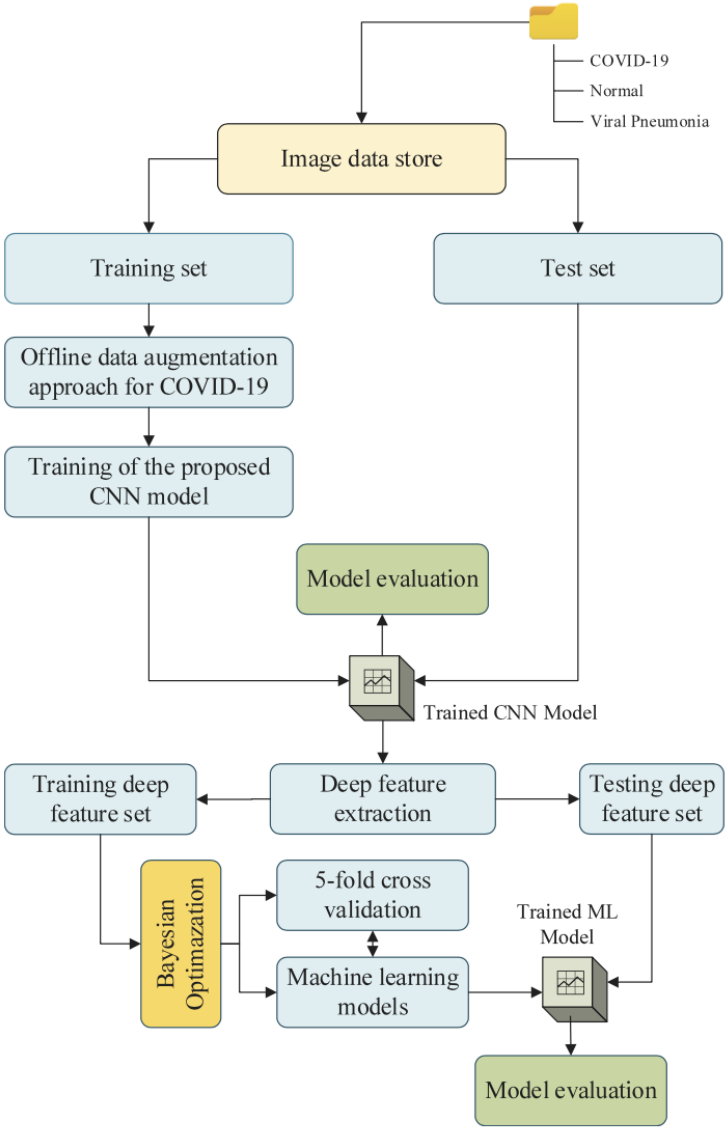

Figure 3.12 : Deep feature extraction from CNN models and using them in machine learning models [4].

The residual neural network architectures was announced by He et al. [6] to avoid the vanishing and exploding gradient problems by using residual blocks. A residual block is simply a connection which allows to take the activation from one layer and feed it to another layer in much deeper. This model achieved high performance results on ILSVRC 2015 ImageNet [17] dataset, and won the 1st place on the corresponding task.

ResNet-18

The first convolution layer includes a 7 x 7 filter and scans with stride as 2, then maximum pooling is applied with 2 x 2 window and stride as 2. Afterwards, 8 residual

[7]Retrieved from: `http://datahacker.rs/deep-learning-residual-networks/` on April 4, 2021.

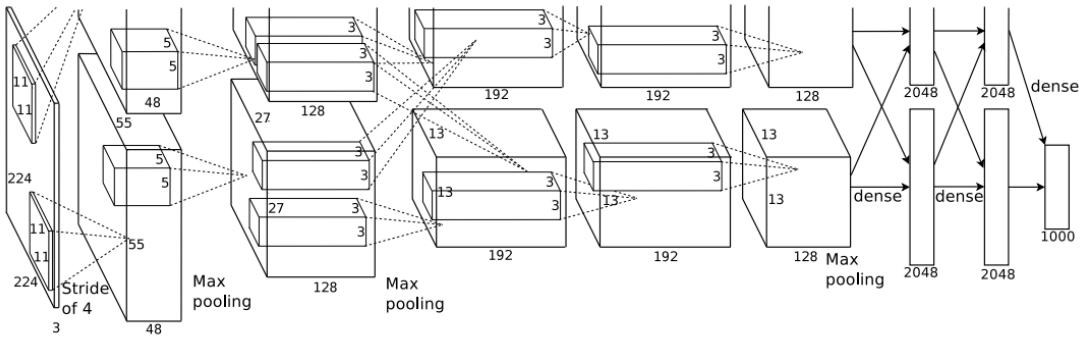

Figure 3.13 : An illustration of AlexNet architecture with input image in the size of $224 \times 224 \times 3$ [5].

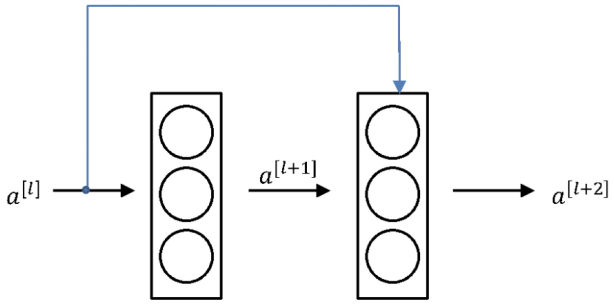

Figure 3.14 : An illustration for residual block. Here, $a^{[l]}$ is the starting activation layer and $a^{[l+2]}$ is the fed activation layer.[7]

blocks, such that each of them includes 2 convolutional layers with 3 x 3 filters, come. That is, there exist 16 convolutional layers inside of residual blocks. After the residual blocks, there is an average pooling following with a fully-connected layer with 1000 neurons, which represents the class number.

ResNet-34

The first convolution layer includes a 7 x 7 filter and scans with stride as 2, then maximum pooling is applied with 2 x 2 window and stride as 2. Afterwards, 16 residual blocks, such that each of them includes 2 convolutional layers with 3 x 3 filters, come. That is, there exist 32 convolutional layers inside of residual blocks. After the residual blocks, there is an average pooling following with a fully-connected layer with 1000 neurons, which represents the class number.

ResNet-50

The first convolution layer includes a 7 x 7 filter and scans with stride as 2, then maximum pooling is applied with 2 x 2 window and stride as 2. Afterwards, 16 residual blocks, such that each of them includes 3 convolutional layers with 1 x 1,

layer name	output size	18-layer	34-layer	50-layer	101-layer	152-layer
conv1	112×112	7×7, 64, stride 2				
conv2_x	56×56	3×3 max pool, stride 2				
		$\begin{bmatrix} 3\times3, 64 \\ 3\times3, 64 \end{bmatrix}\times2$	$\begin{bmatrix} 3\times3, 64 \\ 3\times3, 64 \end{bmatrix}\times3$	$\begin{bmatrix} 1\times1, 64 \\ 3\times3, 64 \\ 1\times1, 256 \end{bmatrix}\times3$	$\begin{bmatrix} 1\times1, 64 \\ 3\times3, 64 \\ 1\times1, 256 \end{bmatrix}\times3$	$\begin{bmatrix} 1\times1, 64 \\ 3\times3, 64 \\ 1\times1, 256 \end{bmatrix}\times3$
conv3_x	28×28	$\begin{bmatrix} 3\times3, 128 \\ 3\times3, 128 \end{bmatrix}\times2$	$\begin{bmatrix} 3\times3, 128 \\ 3\times3, 128 \end{bmatrix}\times4$	$\begin{bmatrix} 1\times1, 128 \\ 3\times3, 128 \\ 1\times1, 512 \end{bmatrix}\times4$	$\begin{bmatrix} 1\times1, 128 \\ 3\times3, 128 \\ 1\times1, 512 \end{bmatrix}\times4$	$\begin{bmatrix} 1\times1, 128 \\ 3\times3, 128 \\ 1\times1, 512 \end{bmatrix}\times8$
conv4_x	14×14	$\begin{bmatrix} 3\times3, 256 \\ 3\times3, 256 \end{bmatrix}\times2$	$\begin{bmatrix} 3\times3, 256 \\ 3\times3, 256 \end{bmatrix}\times6$	$\begin{bmatrix} 1\times1, 256 \\ 3\times3, 256 \\ 1\times1, 1024 \end{bmatrix}\times6$	$\begin{bmatrix} 1\times1, 256 \\ 3\times3, 256 \\ 1\times1, 1024 \end{bmatrix}\times23$	$\begin{bmatrix} 1\times1, 256 \\ 3\times3, 256 \\ 1\times1, 1024 \end{bmatrix}\times36$
conv5_x	7×7	$\begin{bmatrix} 3\times3, 512 \\ 3\times3, 512 \end{bmatrix}\times2$	$\begin{bmatrix} 3\times3, 512 \\ 3\times3, 512 \end{bmatrix}\times3$	$\begin{bmatrix} 1\times1, 512 \\ 3\times3, 512 \\ 1\times1, 2048 \end{bmatrix}\times3$	$\begin{bmatrix} 1\times1, 512 \\ 3\times3, 512 \\ 1\times1, 2048 \end{bmatrix}\times3$	$\begin{bmatrix} 1\times1, 512 \\ 3\times3, 512 \\ 1\times1, 2048 \end{bmatrix}\times3$
	1×1	average pool, 1000-d fc, softmax				
FLOPs		1.8×10^9	3.6×10^9	3.8×10^9	7.6×10^9	11.3×10^9

Figure 3.15 : The ResNet architectures [6].

3 x 3 and 1 x 1 filters in order, come. That is, there exist 48 convolutional layers inside of residual blocks. After the residual blocks, there is an average pooling following with a fully-connected layer with 1000 neurons, which represents the class number.

3.6.3 VGG

Simonyan and Zisserman [25] proposed a very profound architecture for the problem of image recognition. It is aimed to achieve higher classification performance by using a small size filter and increasing the depth of the model. This model was trained with the ILSVRC 2012 ImageNet [17] dataset and achieved high success results. This study has proven the importance of depth in image description models.

VGG16

The input layer of the model architecture starts with a 24 × 24 color image, and there are 12 convolution layers using 3 × 3 filters. There are a total of 5 maximum pooling layers used after some convolution layers. In maximum pooling, 2 x 2 windows were used with stride as 2. After the convolution layers, there are three fully-connected layers such that the first two of which are 4096 neurons and the last one is 1000 neurons, which represents the class number. The ReLU activation function was used after all the hidden layers.

VGG19

[8]Retrieved from: `http://datahacker.rs/deep-learning-vgg-16-vs-vgg-19/` on April 4, 2021.

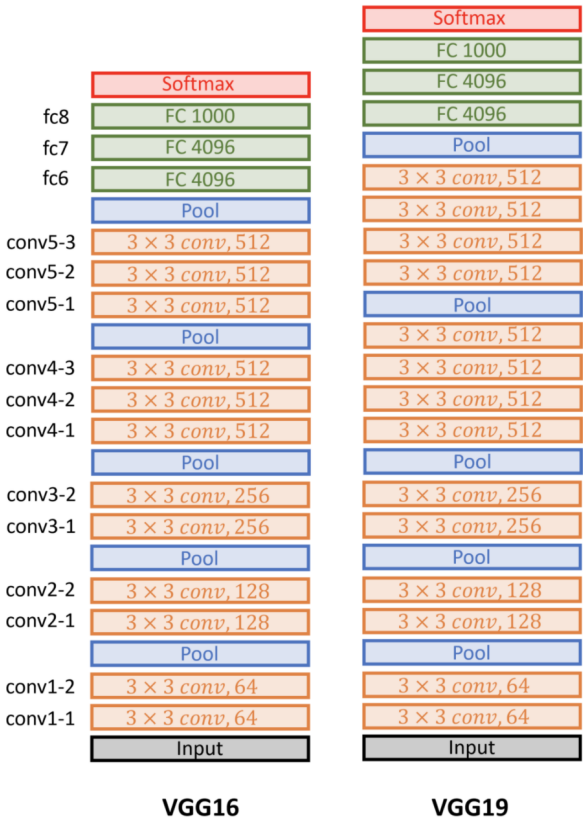

Figure 3.16 : An illustration of VGG architectures.[8]

The input layer of the model architecture starts with a 24 × 24 color image, and there are 14 convolution layers using 3 × 3 filters. There are a total of 5 maximum pooling layers used after some convolution layers. In maximum pooling, 2 x 2 windows were used with stride as 2. After the convolution layers, there are three fully-connected layers such that the first two of which are 4096 neurons and the last one is 1000 neurons, which represents the class number. The ReLU activation function was used after all the hidden layers.

4. INTRODUCTION TO MACHINE LEARNING

In this chapter, we start with the basics of machine learning. Then we mention cross-validation approach, which is a model evaluation technique, and the regularization concept. Finally, we end the section with the ML algorithms used in the thesis.

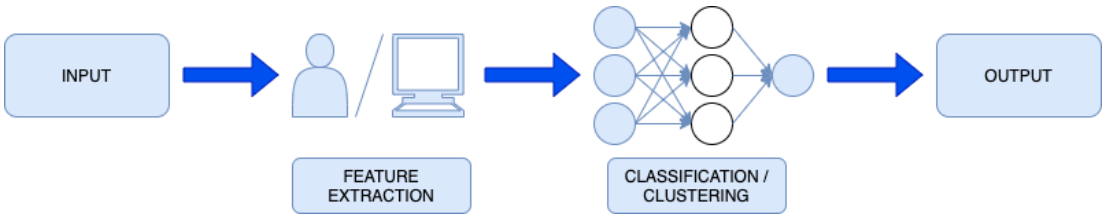

Figure 4.1 : Sample Machine Learning Road Map.

4.1 The Basics of Machine Learning (ML)

The goal of machine learning (Ml) is to learn from available data or experiences to solve a given problem. The pipeline may be listed as:

- defining the problem to solve,
- collecting the data for training and testing,
- designing or extracting the features describing data,
- training the model to tune the parameters by experiments and optimization on the appropriate loss function, and
- testing the model to evaluate the performance of trained model on unseen test data.

The majority of the problems in ML are fall into supervised and unsupervised learning approaches.

4.1.1 Supervised Learning

Supervised learning is a ML method that establishes a relationship between the each attribute of data feature map and its target value. Estimating the output value for

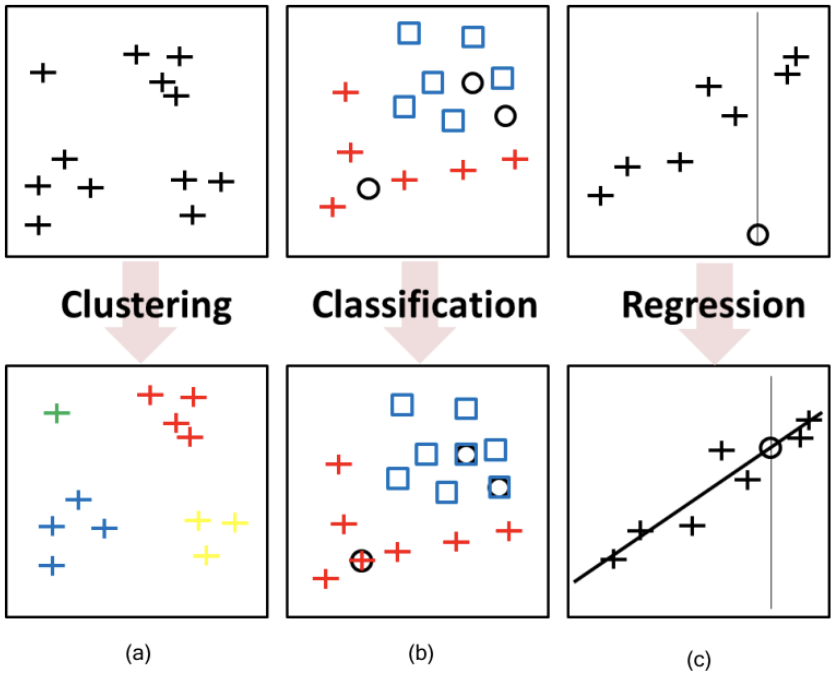

Figure 4.2 : (a) Clustering Problem, (b) Classification Problem, and (c) Regression Problem [7].

each new datum is the main goal. All true target values are known during training and testing. These known true values are used to construct the trained model, and to evaluate the testing performance. Regression and classification problems are solved by supervised learning.

The task in this thesis includes dataset in that each datum has its true label value. Thus, all ML models used in this thesis are from supervised learning algorithms.

4.1.2 Unsupervised Learning

The problems having data with unknown true values are solved by unsupervised learning. While there are hard or impossible to labeling data sets, some data sets can be deliberately left unlabeled since it requires too much time, expert people and special devices to label. Clustering tasks are constructed on these kind of data sets and solved by unsupervised learning.

4.2 Cross-Validation (CV)

As in deep learning, overfitting and underfitting are also big troubles in machine leaning. Cross-validation (CV) methods can be used to overcome these problems. In the CV method, all data is divided into train and test sets. Here, it should not be

forgotten that the train and test sets must be strictly separated from each other, and any sample on test set should not be seen during training process.

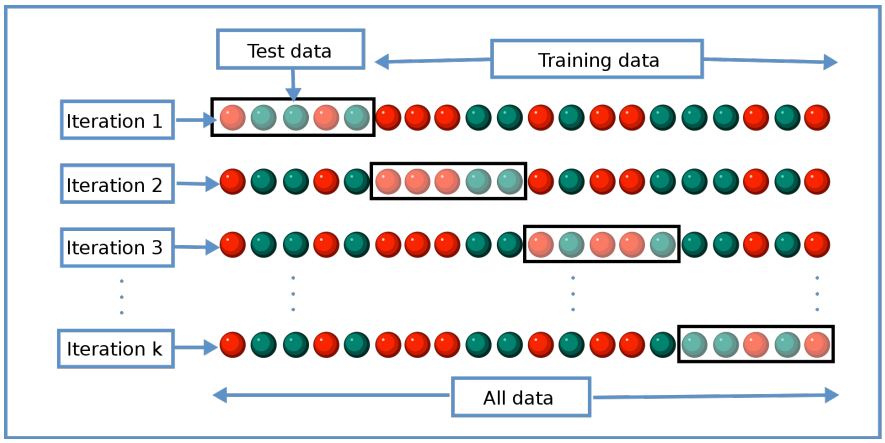

Figure 4.3 : K-Fold Cross-Validation.[1]

4.2.1 K-Fold CV

On K-Fold CV, K is the hyper-parameter to tune that defines the number of folds during partitioning. The choice of K must be greater than 1 and less than the number of data. All data is divided into K folds of the same (if possible) or different sizes. The folds are enumerated from 1 to K. Here, the model is evaluated and tested $(K-1)$ times. On each iteration i, where i is an integer from 1 to K, the i^{th} fold is chosen as the test set and rest as the train set, and model forgets what it learned previously and starts from zero. Otherwise, the test data on the $(i+1)^{th}$ iteration takes place in the train set on the i^{th} iteration and is learned by the model.

4.2.2 Leave-One-Out (LOO)

If the K of K-Fold CV is chosen as the number of data, say N, it is a special case of CV and called as leave-one-out (LOO) method. As a convenience, all data are enumerated from 1 to N. Thus, model is evaluated and tested for N times. On each iteration i, where i is an integer from 1 to N, the i^{th} datum is chosen as the test sample and rest as the train set, and model forgets what it learned previously and starts from zero. Otherwise, the test sample on the current iteration takes place in the train set on the previous iteration and is learned by the model.

[1]Retrieved from: `https://towardsdatascience.com/cross-validation-c4fae714f1c5` on April 10, 2021.

Briefly, LOO is the K-Fold CV where the number of folds is chosen as the number of data.

4.3 Regularization

As discussed in Section 3.3, the training process includes the optimization of corresponding loss function in machine learning. To minimize the loss and obtain the more optimized results, the regularization term is applied to the objective loss function. In general, the regularized loss function for supervised learning can be motivated as:

$$\sum_{(x^i,y^i \in D)} \left(\frac{Error(f_w(x^i), y^i)}{n} \right) + \lambda R(f_w), \tag{4.1}$$

where n is the number of training samples, D is the training feature set with x^i as training input and y^i as the corresponding target output, f_w is the mapping function between feature map and target values, λ is a real number hyper-parameter greater than or equal to zero controlling the effect of regularization term, and R is the regularization term.

Notice that, if λ is chosen as too high, the regularizer drowns out the loss function; and, if λ is chosen as zero, there is no regularization. λ is usually chosen between 0 and 0.1; however, it must be tuned for the corresponding task.

In addition, the regularization term R has a constraint such that $R(f_w) \leq \mu$ for an appropriate real valued constant μ.

The regularization is also called as penalty to the objective function. In this section, we focus on LASSO penalty and Ridge regression concepts which are used in this thesis.

4.3.1 L1 Regularization (LASSO)

L1 regularization term, which is known as LASSO, only penalizes the high coefficients. The LASSO penalty is in the form of:

$$\lambda \left\| w \right\|_1, \tag{4.2}$$

where w is the weight coefficients to optimize, and $\|.\|_1$ is the L1 norm such that:

$$\|x\| = \sum_{i=1}^{p} |x_i|, \tag{4.3}$$

for a vector x in the size of p.

LASSO penalty may produce non-unique solutions [26].

4.3.2 L2 Regularization (Ridge)

L2 regularization term is known as Ridge regression. The penalty term in Ridge regression is in the form of:

$$\lambda \|w\|_2^2, \tag{4.4}$$

where w is the weight coefficients to optimize, and $\|.\|_2^2$ is the squared L2 norm such that:

$$\|x\|_2^2 = \sum_{i=1}^{p} x_i^2, \tag{4.5}$$

for a vector x in the size of p.

4.4 ML Models

In this section, the state-of-the-art ML algorithms used in the thesis are introduced and detailed.

4.4.1 Support-Vector Machines (SVM)

The current support-vector machines algorithm is published by Corinna Cortes and Vladimir Vapnik at 1995 [27]. While it is used for supervised learning problems, the form of it for clustering, which is stated as support-vector clustering [28], can be used for unsupervised learning problems.

A SVM constructs a set of hyper-planes in a high-dimensional or infinite-dimensional space. Usually, it is desired to have samples far away from hyper-planes to achieve a good separation result. The parallel hyper-plane to a SVM hyper-plane including the nearest samples of a class, which are the support-vectors, is called as the margin

of that class to the corresponding hyper-plane, and larger margins provides lower generalization errors for the classifier.

In the task the thesis has, we have binary classification problem; thus, our space is two-dimensional and we have one hyper-plane that has two margins in total. The hyper-planes and so margins differ depending on the used kernel function. The original hyper-plane algorithm proposed by Vapnik is the linear classifier whose kernel function is clearly called as linear kernel. However, to create nonlinear hyper-planes, Bernhard Boser, Isabelle Guyon and Vladimir Vapnik suggest to replace the linear function with another nonlinear kernel functions. This technique is called as kernel trick.

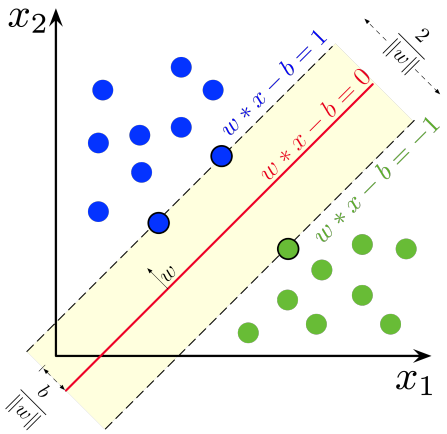

Figure 4.4 : A Hyper-plane and its margins for an SVM to a binary classification problem.[2]

The linear SVM hyper-plane is defined as:

$$\mathbf{w}^T\mathbf{x} - b = 0, \tag{4.6}$$

where x is a p-dimensional real vector, w is a weight vector normal to the hyper-plane, and b is a real valued bias parameter. Thus the distance between margins can be computed as $\frac{2}{\|\mathbf{w}\|_2}$, and we want to maximize it.

Loss Functions

First, let us name the hyper-plane and margins in Figure 4.4 as:

- **hyper-plane:**

$$H_0 = \mathbf{w}^T\mathbf{x} - b = 0\,, \tag{4.7}$$

[2]Retrieved from: `https://en.wikipedia.org/wiki/Support-vector_machine` on April 11, 2021.

- **margin for label +1:**

$$H_{+1} = \mathbf{w}^T \mathbf{x} - b = +1 \text{ , and} \tag{4.8}$$

- **margin for label -1:**

$$H_{-1} = \mathbf{w}^T \mathbf{x} - b = -1 \,. \tag{4.9}$$

Thus, we have the following condition and result relationships for a sample $\mathbf{x}^i$ p-dimensional real vector with its estimated label y^i where y^i is either -1 or +1:

- if $\mathbf{w}^T \mathbf{x}^i - b \geq +1$ and $y^i = +1$, then the prediction is correct and the sample belongs to class +1;
- else, if $\mathbf{w}^T \mathbf{x}^i - b \leq -1$ and $y^i = -1$, then the prediction is correct and the sample belongs to class -1;
- else, the prediction is incorrect and the sample belongs to opposite of predicted label.

When we compound the above conditions, we yield the common condition as:

$$1 - (\mathbf{w}^T \mathbf{x}^i - b) y^i \leq 0 \,. \tag{4.10}$$

And finally, the margin perception loss function, called as hinge loss, is written as:

$$loss_{hinge}(\mathbf{w}, b) = \sum_{i=1}^{n} \max(0, 1 - (\mathbf{w}^T \mathbf{x}^i - b) y^i). \tag{4.11}$$

Besides, the squared hinge loss is defined as:

$$loss_{squaredHinge}(\mathbf{w}, b) = \sum_{i=1}^{n} (\max(0, 1 - (\mathbf{w}^T \mathbf{x}^i - b) y^i))^2. \tag{4.12}$$

The constrained optimization problem of SVM is derived as:

$$\min_{w} \ell(\mathbf{w}) = \min_{w} \frac{\|\mathbf{w}\|_2^2}{2} \quad \text{such that } (\mathbf{w}^T \mathbf{x}^i - b) y^i - 1 \geq 0 \,, \forall i \in \{1, ..., n\} \tag{4.13}$$

The equation (4.13) is called as the primal problem.

By using the Lagrange Function with real valued lagrange multipliers α_i greater than or equal to 0, the dual problem to solve is constructed as:

$$\max_{\alpha} \mathscr{L}(\alpha) = \max_{\alpha} \sum_{i=1}^{n} \alpha_i - \frac{1}{2} \sum_{i=1}^{n} \sum_{j=1}^{n} \alpha_i \alpha_j \, y^i y^i \, \mathbf{x}^{iT} \mathbf{x}^j \quad \text{such that } \sum_{i=1}^{n} \alpha_i y^i = 0, \quad (4.14)$$

where x_i and y_i are a p-dimensional real valued feature vector and its label, that is -1 or +1, respectively, w is a weight vector normal to the hyper-plane, b is a real valued bias parameter, and n is the number of samples.

Further details on constraint optimization of SVM, primal and dual problems, and their solutions can be found at [29, pg. 13-19].

Penalty Terms

Here λ always refers to the regularization parameter during this subsection.

- **L2 Regularizer:** According to [30, pg. 2054-2059], let first recall the primal form of SVM optimization problem in equation (4.13). We can modify the problem as:

$$\min_{\mathbf{w},b} \Big\{ \sum_{i=1}^{n} [1 - (\mathbf{w}^T \mathbf{x}^i - b) y^i]_+ + \lambda \frac{\|\mathbf{w}\|_2^2}{2} \Big\}, \quad (4.15)$$

  where $[1 - (\mathbf{w}^T \mathbf{x}^i - b) y^i]_+$ is the hinge loss term $\max(0, 1 - (\mathbf{w}^T \mathbf{x}^i - b) y^i)$. Yet, the squared hinge loss can be placed as well.

  Then, the corresponding dual problem can be obtained as:

$$\max_{\alpha} \sum_{i=1}^{n} \alpha_i - \frac{1}{2} \sum_{i=1}^{n} \sum_{j=1}^{n} \alpha_i \alpha_j \, y^i y^i \big(\mathbf{x}^{iT} \mathbf{x}^j + \lambda \delta_{ij} \big) \quad \text{such that } \sum_{i=1}^{n} \alpha_i y^i = 0 \,, \quad (4.16)$$

  where α is the lagrange multiplier given in the equation (4.14) and δ_{ij} is the Kronecker's delta function such that it returns 1 for $i = j$, and 0 otherwise.

- **L1 Regularizer:** As stated in [30, pg. 2054-2059], L1 regularization is only applicable for the linear SVM problem. The L1 penalized SVM optimization problem is given by the following equation where the $loss(\mathbf{w}, b)$ is either hinge or squared hinge loss function:

$$\min_{\mathbf{w},b} \sum_{i=1}^{n} loss(\mathbf{w}, b) + \lambda \, \|\mathbf{w}\|_1 \,. \quad (4.17)$$

  Then, the corresponding dual problem can be obtained as:

$$\max_{\alpha} \mathscr{L}(\alpha) \quad \text{such that } \sum_{i=1}^{n} \alpha_i y^i = 0 \text{ and } 0 \leq \alpha_i \leq \frac{1}{\lambda} \,, \quad (4.18)$$

  where $\mathscr{L}$ and α_i are lagrange function and lagrange multipliers given in the equation (4.14).

Kernel Trick

Kernel trick is using a feature transformation ϕ to map samples into a new space where samples become linearly separable. Then all appearances of samples are replaced with the transformation ϕ. Now, the kernel function for p-dimensional feature vectors $\mathbf{x}_i$ and $\mathbf{x}_i$ is defined as:

$$K(\mathbf{x}_i, \mathbf{x}_j) = < \phi(\mathbf{x}_i), \phi(\mathbf{x}_j) > = \phi(\mathbf{x}_i)^T \phi(\mathbf{x}_j). \tag{4.19}$$

This replacement affects to the whole structure of SVM optimization problem.

The most used kernel functions, that are also experienced in this thesis, are:

- **Linear function:**

$$K(\mathbf{x}_i, \mathbf{x}_j) = \mathbf{x}_i^T \mathbf{x}_j. \tag{4.20}$$

- **Gaussian radial basis function (RBF):**

$$K(\mathbf{x}_i, \mathbf{x}_j) = \exp(-\gamma \left\| \mathbf{x}_i - \mathbf{x}_j \right\|_2^2), \tag{4.21}$$

  for $\gamma > 0$. It is common to choose $\gamma = \frac{1}{2\sigma^2}$ where σ represents the standard deviation of original feature map.

- **Sigmoid function:**

$$K(\mathbf{x}_i, \mathbf{x}_j) = \tanh(\alpha \mathbf{x}_i^T \mathbf{x}_j + c), \tag{4.22}$$

  for some $\alpha > 0$ and $c < 0$, and $\tanh(.)$ refers the hyperbolic tangent function.

4.4.2 Logistic Regression (LR)

Logistic regression (LR) aims to solve binary classification problems. If the problem contains more than 2 classes, the model named as Multinomial LR can be used. In the logistic model, each sample $\mathbf{x} \in \mathbb{R}^d$ has a predicted value $0 \leq Pr(\mathbf{x}) \leq 1$ referring if the sample belongs to its actual label y or not. If $0.5 < Pr(\mathbf{x})$, then the prediction is true. By using the logistic sigmoid function, the model is obtained as:

$$Pr(\mathbf{x}) = \frac{1}{1 + e^{-(\mathbf{w}^T \mathbf{x} + b)}}, \tag{4.23}$$

where $\mathbf{w} \in \mathbb{R}^d$ is the weight parameter tuning the scaling, and $b \in \mathbb{R}$ is the bias term tuning the shifting in logistic sigmoid function.

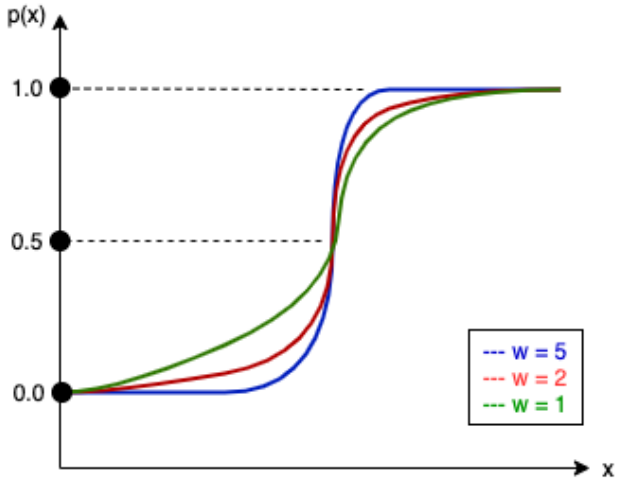

Figure 4.5 : Logistic sigmoid function with different scaling w values.

The sharpness of logistic curve increases with higher **w** values, and vice versa.

Simply, the hypothesis function can be obtained from sigmoid function as:

$$\ln\left(\frac{Pr(\mathbf{x})}{1-Pr(\mathbf{x})}\right) = \mathbf{w}^T\mathbf{x}+b\,. \tag{4.24}$$

Here, $\frac{Pr(\mathbf{x})}{1-Pr(\mathbf{x})}$ is called as odd, and $\log\left(\frac{Pr(\mathbf{x})}{1-Pr(\mathbf{x})}\right)$ as logit.

For simplicity, let define $z = \mathbf{w}^T\mathbf{x}+b$. Then, we have following constraints:

- if $y = 1$, we want $Pr(z) \approx 1$, i.e $z >> 0$, and
- if $y = 0$, we want $Pr(z) \approx 0$, i.e $z << 0$.

Now, we can construct the log-loss function for a sample pair $(\mathbf{x}^i, y^i)$ for $i \in \{1,...,n\}$ as:

$$loss^i(\mathbf{w},b) = -y\ln(Pr(z^i)) + (1-y)\ln(1-Pr(z^i)). \tag{4.25}$$

Consequently, the optimization problem is yielded as:

$$\max_{\mathbf{w},b} \ell(\mathbf{w},b) = \max_{\mathbf{w},b} \sum_{i=1}^{n} loss^i(\mathbf{w},b). \tag{4.26}$$

Penalty Terms

Here λ always refers to the regularization parameter during this subsection.

- **L2 Regularizer:**

$$\max_{\mathbf{w},b} \ell(\mathbf{w},b) + \lambda \|w\|_2^2 . \tag{4.27}$$

- **L1 Regularizer:**

$$\max_{\mathbf{w},b} \ell(\mathbf{w},b) + \lambda \|w\|_1 . \tag{4.28}$$

Optimizers

In this thesis, to solve the optimization problem on LR problem, we use the following the solvers presented by scikit-learn package [31] in Python programming language:

- Newton's Method (newton-cg) [32],
- Limited-Memory Broyden–Fletcher–Goldfarb–Shanno Algorithm (lbfgs) [33],
- A Library for Large Linear Classification (liblinear) [34],
- Stochastic Average Gradient (sag) [35], and
- SAGA [36].

Different types of optimizers were used for a better approximation to the loss function, and to find the best minimization on this loss function.

Table 4.1 shows the solvers eligibility to regularizers.

Table 4.1 : Logistic Regression optimization problem solvers.

Solver	Optimization Problem		
	No Penalty	L1 Penalty	L2 Penalty
newton-cg	X		X
lbfgs	X		X
liblinear		X	X
sag	X		X
saga	X	X	X

4.4.3 K-Nearest Neighbor (KNN)

K-Nearest Neighbor (KNN) algorithm is a classification algorithm developed by Fix, E. and Hodges, L. in 1951 [37]. KNN can be used for regression as well; however, at this time the, the output for an object is not a class label, but the property value which

is the average of the values of its k nearest neighbors. For both usage cases, KNN is a supervised learning algorithm.

Algorithm

Below, the basic algorithm for KNN is explained for n samples $\mathbf{x}^i \in \mathbb{R}^d$ and their corresponding class labels $c^i \in \{-1,+1\}$. Let the target pair is referred by $(\mathbf{x}^*, c^*)$.

1. The K nearest neighbors of $\mathbf{x}^*$ is found with respect to distance between target $\mathbf{x}^*$ and all other samples. To calculate the distance, different metric functions may be used. The used metrics in this thesis are:

   - **Euclidean Distance:**

   $$d(\mathbf{x}^*, \mathbf{x}^i) = \sqrt{\sum_{j=1}^{p} (\mathbf{x}^*{}_j - \mathbf{x}^i{}_j)^2}\,, \tag{4.29}$$

   - **Manhattan Distance:**

   $$d(\mathbf{x}^*, \mathbf{x}^i) = \sum_{j=1}^{p} |\mathbf{x}^*{}_j - \mathbf{x}^i{}_j|\,, \text{and} \tag{4.30}$$

   - **Chebyshev Distance:**

   $$d(\mathbf{x}^*, \mathbf{x}^i) = \max(|\mathbf{x}^*{}_1 - \mathbf{x}^i{}_1|, |\mathbf{x}^*{}_2 - \mathbf{x}^i{}_2|, \ldots, |\mathbf{x}^*{}_p - \mathbf{x}^i{}_p|)\,. \tag{4.31}$$

2. The class label for $\mathbf{x}^*$ is estimated by majority voting around K nearest neighbors of target sample found in step 1. Majority voting makes its decision by looking for which class label has the majority in appearance around K nearest neighbors. Hence, K is preferred as an odd number. For example, if the K is chosen as 3 and 3 nearest neighbors has class labels as $\{+1,-1,+1\}$, then majority voting predicts the target label as +1 since it appears more than label -1. Besides, it can be considered that all of the voters may not have the same effect. In this scenario, one can use weighted majority voting which allows the closer neighbor in K nears neighbors to have the higher effect. That is, the weight of a voter is the multiplicative inverse of its distance to the target sample. For example, assume that the K is chosen as 3 and 3 nearest neighbors has class labels as $\{+1,-1,+1\}$ with their distances to the target sample as $\{3,1,2\}$ respectively. Then the weights of the neighbors are considered as $\{\frac{1}{3},1,\frac{1}{2}\}$ or $\{2,6,3\}$ respectively. Here, the label -1 has the majority; thus, the target label is predicted as -1.

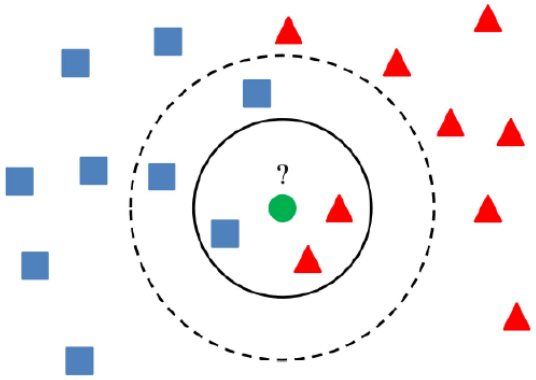

Figure 4.6 : KNN example illustration to detect the class for the green sample in the middle.[3]

At Figure 4.6, when K = 3, it is labeled as red both by majority voting and weighted majority voting. However, when K = 5, it may change whether to use majority voting or weighted majority voting. It is labeled as blue by majority voting; but, it may be labeled as red by the weighted majority voting.

Finding Neighborhood

In this thesis, three algorithms presented by scikit-learn package [31] in Python programming language are used.

- **Brute Force:** Distances between all pairs of samples are computed. Brute force may be quite efficient for small sized dataset.
- **K-Dimensional Tree:** Since brute force becomes inefficient by the increase of dataset size, K-Dimensional (K-D) tree may be used to reduce the required number of computations. If samples x_0 and x_1 are very distant, and x_1 and x_2 are very close, then we can conclude that x_0 and x_2 are very distant too. To create a K-D tree structure, the data space partitioned along the Cartesian axes. Because of the curse of dimensionality, the construction of K-D tree may be inefficient for large dimensions. Further information can be found at [38].
- **Ball Tree:** Ball tree algorithm was developed to solve the size and dimensionality problems. The data space are partitioned along the Spherical axes to construct the tree structure; hence it is more costly than K-D tree. However the structure itself

[3]Retrieved from: `https://ai.plainenglish.io/k-nearest-neighbors-from-scratch-633dfbeac740` on April 17, 2021.

is more effective, especially in high dimensions. Further information can be found at [39].

4.4.4 Linear Discriminant Analysis (LDA)

The linear discriminant analysis (LDA) is a supervised learning algorithm that is generalized from discriminant analysis developed by Sir Ronald Fisher, who was an statistician, geneticist, and academic, in 1936.

Derivation

A discriminant function $g(\mathbf{x})$ from $\mathbb{R}^d$ to $\mathbb{R}$ is, generally, a monotonically increasing function defining a boundary between two groups or classes. Here $\mathbf{x} \in \mathbb{R}^d$ is a sample with d features. $g_i(\mathbf{x})$ is the probability of x belonging to class c_i as given below:

$$g_i(\mathbf{x}) = Pr(c_i|\mathbf{x}) = \frac{Pr(\mathbf{x}|c_i)Pr(c_i)}{Pr(\mathbf{x})}, \tag{4.32}$$

where $Pr(c_i|\mathbf{x})$ is the likelihood of observing $\mathbf{x}$ given class c_i, $Pr(c_i)$ is the prior probability of belonging to class c_i, and $Pr(x)$ is the marginal likelihood of observing $\mathbf{x}$. Here, we discard the $Pr(x)$ since observing $\mathbf{x}$ is independent of class.

For normal data distribution, we can take the logarithm of $g(\mathbf{x})$ since it is monotonically increasing:

$$g_i(\mathbf{x}) = \ln(Pr(c_i|\mathbf{x})) = \ln(Pr(\mathbf{x}|c_i)) + \ln(Pr(c_i))\,. \tag{4.33}$$

Here, we suppose that the class density $Pr(x|c_i)$ is normal distribution with mean μ_i and variance Σ_i where Σ describes the covariance matrix considered as $\sigma^2 I$.

$$Pr(\mathbf{x}|c_i) = \frac{1}{(2\pi)^{d/2}|\Sigma_i|^{1/2}} \exp\Big[-\frac{1}{2}(\mathbf{x}-\mu_i)^T {\Sigma_i}^{-1}(\mathbf{x}-\mu_i)\Big]. \tag{4.34}$$

By inserting equation (4.34) into equation (4.33), we yield:

$$g_i(\mathbf{x}) = -\frac{1}{2}(\mathbf{x}-\mu_i)^T {\Sigma_i}^{-1}(\mathbf{x}-\mu_i) - \frac{d}{2}\ln(\frac{\pi}{2}) - \frac{1}{2}\ln|\Sigma_i| + \ln(Pr(c_i))\,. \tag{4.35}$$

Finally, since $\frac{d}{2}\ln(\frac{\pi}{2})$ is constant, we obtain the linear discriminant function for class i as:

$$g_i(\mathbf{x}) = -\frac{1}{2}(\mathbf{x}-\mu_i)^T{\Sigma_i}^{-1}(\mathbf{x}-\mu_i) - \frac{1}{2}\ln|\Sigma_i| + \ln(Pr(c_i))\,. \tag{4.36}$$

This linear discriminant function outputs the likelihood of $\mathbf{x}$ to be in the class i.

There are two presumptive cases on the linear discriminant function.

- $\Sigma_i = \sigma^2 I$**:** All features have different means, but the same variants.

  $$\begin{aligned}
  g_i(\mathbf{x}) &= -\frac{1}{2\sigma^2}(\mathbf{x}-\mu_i)^T(\mathbf{x}-\mu_i) - \frac{1}{2}\ln(\sigma^{2d}) + \ln(Pr(c_i))\,,\\
  g_i(\mathbf{x}) &= -\frac{1}{2\sigma^2}(\mathbf{x}-\mu_i)^T(\mathbf{x}-\mu_i) + \ln(Pr(c_i)) \quad \text{since } \frac{1}{2}\ln(\sigma^{2d}) \text{ is constant,}\\
  g_i(\mathbf{x}) &= -\frac{1}{2\sigma^2}\big(\mathbf{x}^T\mathbf{x} - \mathbf{x}^T\mu_i - \mu_i^T\mathbf{x} - \mu_i^T\mu_i\big) + \ln(Pr(c_i))\,,\\
  g_i(\mathbf{x}) &= -\frac{1}{2\sigma^2}\big(-2\mathbf{x}^T\mu_i - \mu_i^T\mu_i\big) + \ln(Pr(c_i)) \quad \text{since } \mathbf{x}^T\mathbf{x} \text{ is constant and } \mathbf{x}^T\mu_i = \mu_i^T\mathbf{x}\,,\\
  g_i(\mathbf{x}) &= \frac{\mu_i^T}{\sigma^2}\mathbf{x} + \Big(\ln(Pr(c_i)) - \frac{\mu_i^T\mu_i}{2\sigma^2}\Big).
  \end{aligned} \tag{4.37}$$

  It can be seen that, the final discriminant function in equation (4.37) is a linear function.

- $\Sigma_i = \Sigma$**:** Covariance matrices are all arbitrary, but equal across classes.

  $$\begin{aligned}
  g_i(\mathbf{x}) &= -\frac{1}{2}(\mathbf{x}-\mu_i)^T\Sigma^{-1}(\mathbf{x}-\mu_i) - \frac{1}{2}\ln|\Sigma| + \ln(Pr(c_i))\,,\\
  g_i(\mathbf{x}) &= -\frac{1}{2}(\mathbf{x}-\mu_i)^T\Sigma^{-1}(\mathbf{x}-\mu_i) + \ln(Pr(c_i)) \quad \text{since } \ln|\Sigma| \text{ is constant,}\\
  g_i(\mathbf{x}) &= \frac{-1}{2}\big(\mathbf{x}^T\Sigma^{-1}\mathbf{x} - \mu_i\Sigma^{-1}\mathbf{x}\mathbf{x}^T\Sigma^{-1}\mu_i + \mu_i^T\Sigma^{-1}\mu_i\big) + \ln(Pr(c_i))\,,\\
  g_i(\mathbf{x}) &= \frac{-1}{2}\big(-2\mathbf{x}^T\Sigma^{-1}\mu_i + \mu_i^T\Sigma^{-1}\mu_i\big) + \ln(Pr(c_i)) \quad \text{since } \mathbf{x}^T\Sigma^{-1}\mathbf{x} \text{ is constant}\\
  &\text{and } \mathbf{x}^T\Sigma^{-1}\mathbf{x} = \mu_i\Sigma^{-1}\mathbf{x}\,,\\
  g_i(\mathbf{x}) &= \big(\mu_i^T\Sigma^{-1}\big)\mathbf{x} + \Big(\ln(Pr(c_i)) - \frac{1}{2}\mu_i^T\Sigma^{-1}\mu_i\Big)\,.
  \end{aligned} \tag{4.38}$$

  It can be seen that, the final discriminant function in equation (4.38) is a linear function.

Penalty Terms

[4]Retrieved from: `https://scikit-learn.org/stable/modules/lda_qda.html` on April 18, 2021.

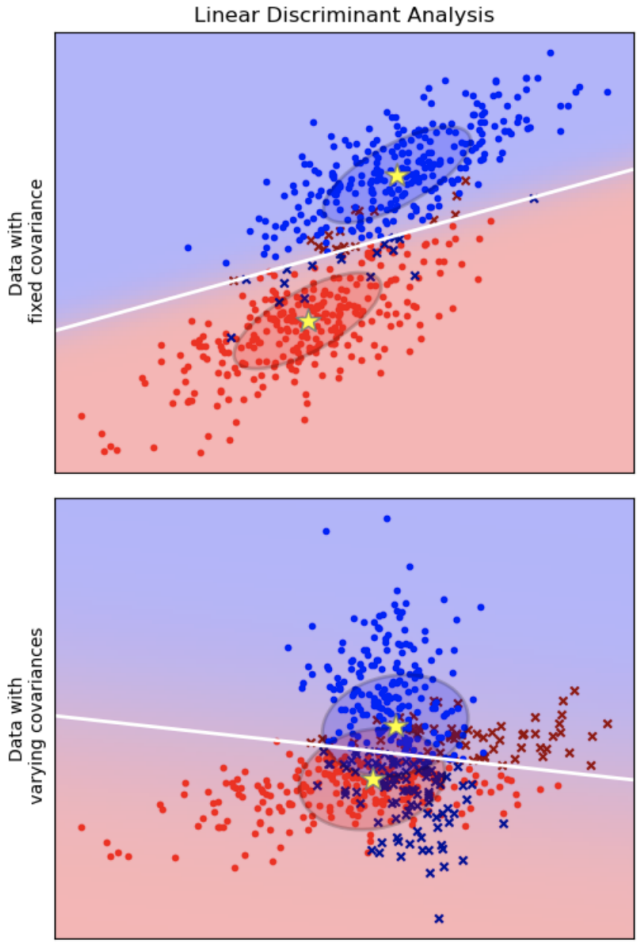

Figure 4.7 : LDA process for fixed and varying covariances.[4]

Since high dimensionality may cause LDA not to be optimal and hard to operate over matrices. That is why, a simple modification on covariance matrix is made as [40]:

$$\widehat{\Sigma} = \alpha\Sigma + (1-\alpha)I, \tag{4.39}$$

for some real valued α in between the range of $[0,1]$. We can consider this regularization as what we are used to use in Section 4.3:

$$\widehat{\Sigma} = \lambda\Sigma + I \quad \text{, or} \tag{4.40}$$

$$\widehat{\Sigma} = \Sigma + \lambda I\,, \tag{4.41}$$

for positive real valued regularization parameter λ. Consequently, the regularized LDA is formulated as:

$$g_i(\mathbf{x}) = -\frac{1}{2}(\mathbf{x}-\mu_i)^T\widehat{\Sigma}_i^{-1}(\mathbf{x}-\mu_i) - \frac{1}{2}\ln|\widehat{\Sigma}_i| + \ln(Pr(c_i))\,. \tag{4.42}$$

Solvers

In this thesis, to solve the LDA functions, we use the solvers presented by scikit-learn package [31] in Python programming language.

Further information about estimators provided by scikit-learn package can be found at [41].

5. EXPERIMENTS

All the code used for the experiments explained in this chapter can be found on master branch of the GitHub public repository:
`https://github.com/ozanguldali/modelsWithLASSO`.

Python programming language in version of 3.7.6 combining with Clang 4.0.1 was used to train, test and classify on our environment. PyTorch module with the torch version of 1.5.0, the torchsummary version of 1.5.1 and the torchvision version of 0.6.0, and Scikit-learn library with the version of 0.23.2 were used for CNN and ML coding respectively. All experiments were performed on the Google Colaboratory using its GPU with the number of workers as four.

5.1 Dataset

The basis data was obtained from GitHub platform repository which can be reached via link `https://github.com/ieee8023/covid-chestxray-dataset/`. On the GitHub repository, the data are placed in "images" folder and the information file about data is in 'metadata.csv' file.

To constuct the dataset, the metedata.csv file was parsed and data were filtered depending on whether it has age and sex info or not, the its finding includes "COVID-19" term or not, its modality is "X-ray" or not, and its view is "PA" or not. First, data having sex and age info, modality as "X-ray", and view as "PA" were chosen. Then two main classes were constructed by separating the chosen data whether its finding includes "COVID-19" or not. The data including "COVID-19" in its finding were labeled as "COVID-19" and the others were labeled as "non-COVID-19". Finally, in the ratio of 0.8, the labeled data were divided into train and test sets. At the end, 131 "COVID-19" and 123 "non-COVID-19" labeled data were obtained and splitted into train and test sets. Train set includes 105 "COVID-19" and 98 "non-COVID-19" labeled data, while test set includes 26 "COVID-19" and 25 "non-COVID-19".

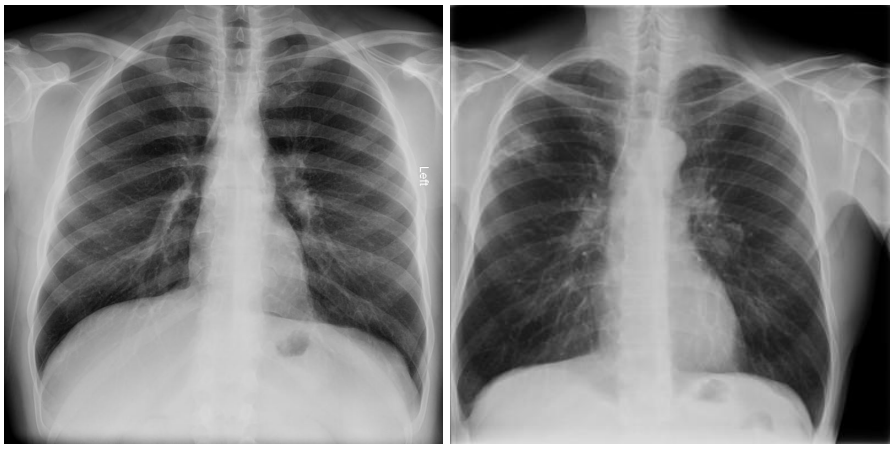

(a) Train COVID-19 Data (b) Test non-COVID-19 Data

Figure 5.1 : Dataset Samples.

Data are appeared in different formats such that .png, .jpg, .jpeg, in different aspect rations and dimensions such as 384×384, 462×450, etc, and in different sizes such as 606 KB, 69 KB, 1 KB, etc. Thus, before using the data, each datum was resized to 224x224, center cropped, gray scaled and normalized by the mean of (0.485, 0.456, 0.406) and the standard deviation of (0.229, 0.224, 0.225) for red, blue and green channels respectively.

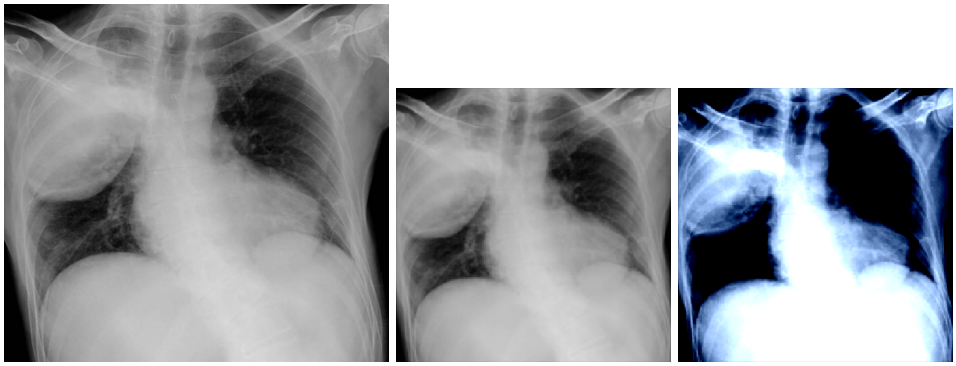

(a) Original (826×768) (b) Resized, Square Cropped and Gray-Scaled (c) Normalized

Figure 5.2 : Image Transformation Steps - Test COVID-19 Sample.

5.2 Data Augmentation

While data sizes on classes are unbalanced, one or more data augmentation techniques are used on train data to balance them. Furthermore, for a balanced dataset, one can use data augmentation to increase the train data size.

Data augmentation techniques on visual data can be classified in 2 groups such that position augmentation and color augmentation. Position augmentation takes the

original data and applies the desired operations from followings: flipping, rotation, translation and scaling. On the other hand, during the color augmentation, the augmented datum is obtained by changing one or more of followings: hue, saturation, brightness and contrast. If n kind augmentation choice is used to m number of data, at the end m*(n+1) data are obtained. That is the summation of n augmented datum for each sample of m data, and the original m samples.

In the thesis, position augmentation with horizontal flip, vertical flip, 90 degrees of rotation, 180 degrees of rotation and 270 degrees of rotation is used on the whole train data. These augmented data are not physical, i.e. not saved as files, and only used on CNN training process. Data augmentation is not used on ML processes.

The number of data on train and test sets for each class after augmentation can be seen on Table 5.1.

Table 5.1 : The detailed number of data.

Class	**Original Set**	**Train Set**		**Test Set**
		Chosen	**After Augmentation**	
COVID-19	131	105	630	26
non-COVID-19	123	98	588	25
TOTAL	254	203	1218	51

5.3 Training and Testing on Convolutional Neural Network Models

All CNN experiments was made on pre-trained CNN models. That is, the corresponding model weights was used with different strategies to feed the models.

Since our dataset is obviously small and the data content is different from ImageNet dataset [17], we experimented to train the entire model, and to freeze the first few layers and train others. The frozen layers for each experiment model are:

- the first convolution layer, and its following ReLU and maximum pooling layers for AlexNet architecture,
- the first convolution layer, and its following batch normalization, ReLU and maximum pooling layers for ResNet architectures, and

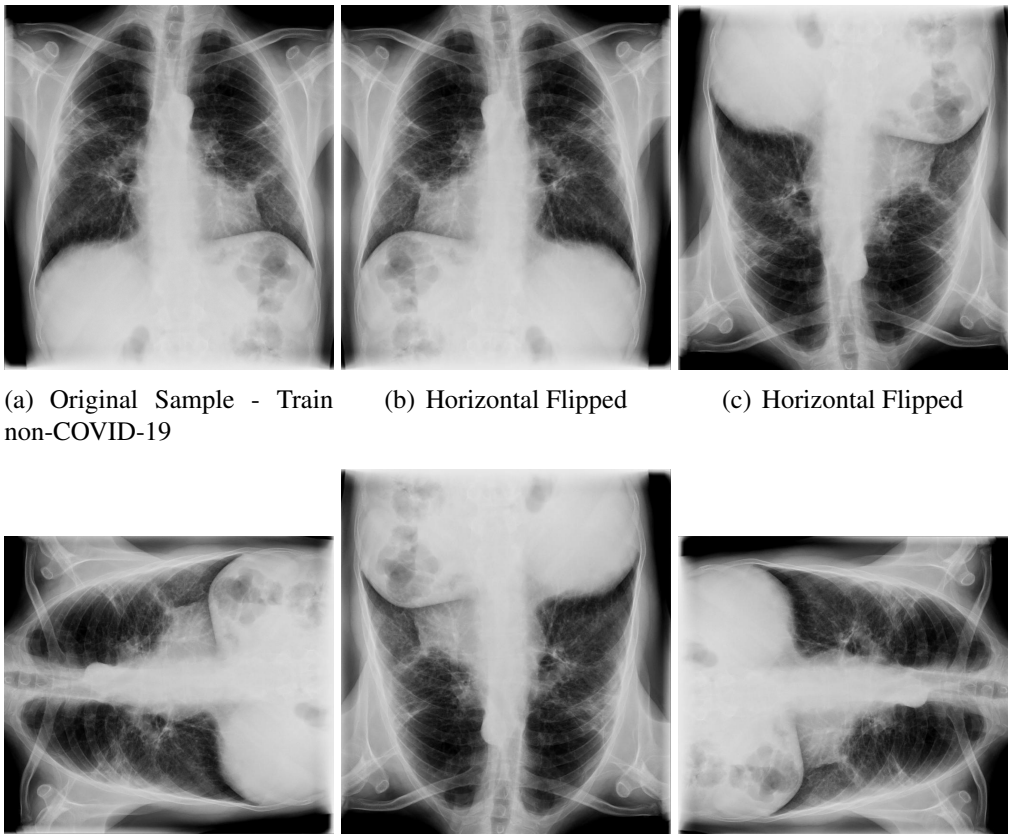

(a) Original Sample - Train non-COVID-19 (b) Horizontal Flipped (c) Horizontal Flipped

(d) Horizontal Flipped (e) Horizontal Flipped (f) Horizontal Flipped

Figure 5.3 : Original Sample and Augmentation.

- the first six layers which are in order of convolution, batch normalization, ReLU, convolution, batch normalization, ReLU and maximum pooling layers for VGG architectures.

The comparison results have shown that, training the entire model instead of freezing the stated number of layers above gives more minimal losses and more accurate classification results. However, it must be remarked that, even the number of frozen layers are not much, since the number of parameters are less on this technique than entire model training, the computation time of each batch is observably shorter as well.

Train data were set to be shuffled on each epoch and the batch size was experimentally set from 2^4 to 2^6. The number of epoch was set to 50, and the validation period was set as $1/50$. That is, before the first training epoch and after each training epoch, validation process was applied on test set. On each validation, the saved model weights files for corresponding configurations were checked. If there exists no saved file having greater accuracy percentage than the current state, the current model weights are saved

as a new model weight *.pth file with the name including the validation result and training configurations. The saved CNN model weights files can be found under the */cnn/saved_models* directory of project repository at `https://github.com/ozanguldali/modelsWithLASSO`. After the last training epoch, test process is applied rather than validation, and the same accuracy comparison over saved *.pth files is executed. That is why, the number of validation accuracy results are 50 whereas the number of validation losses are 49. The reason why we limited the epoch size as 50 is that, the models were overfitting after this number, and even before sometimes.

By our weights file comparison rule, there may be multiple *.pth weights files for the same configuration and accuracy value. This time, the train loss values, before the validation or test result obtained, and the validation loss values, if available, are considered. Here, the less loss is better to choose.

The cross-entropy loss function, explained in Section 3.2, was used for all CNN models. To optimize it, Adam, SGD Momentum and Adam with decoupled weight decay optimizers were experimented with various learning rate, momentum and weight decay parameter values. Moreover, the learning rate was experimentally scheduled by the reducing rate as 0.1 for each quarter of total epoch size. However, the scheduler approach drove the models to overfitting.

Final hyper-parameters experienced as the best for each model and each optimizer differ. The best ones for ResNet-50 model can be seen in Table 5.2. Furthermore, on our experiments, we encountered the optimal batch size, in terms of computational time and obtained losses, as 2^4. Hence, the number of iteration on each epoch was 77 for augmented train data, and 4 for test data which was used on both test and validation processes.

Table 5.2 : CNN models final hyper-parameters.

Optimizer	**Learning Rate**	**Momentum**	**Weight Decay**
SGD Momentum	1e-4	0.9	-
Adam	1e-5	-	1e-3
AdamW	1e-5	-	1e-4

All pre-trained CNN models were experimented by setting the final layer out feature size as the class size, i.e. 2. Furthermore, for all architectures experienced in this

thesis, a modification is applied on the classification section as adding a block of ReLU, dropout and fully-connected layers in order after the last fully-connected layer.

For ResNet-50 model, the total parameters, so the total trainable parameters on full-training, is 25,559,034 for one sample. For an input image in the size of 0.59 MB, forward and backward pass size is 309.48 MB and parameters size is 97.50 MB. Hence, the estimated total size of one iteration on this image is 407.57 MB according to PyTorch.

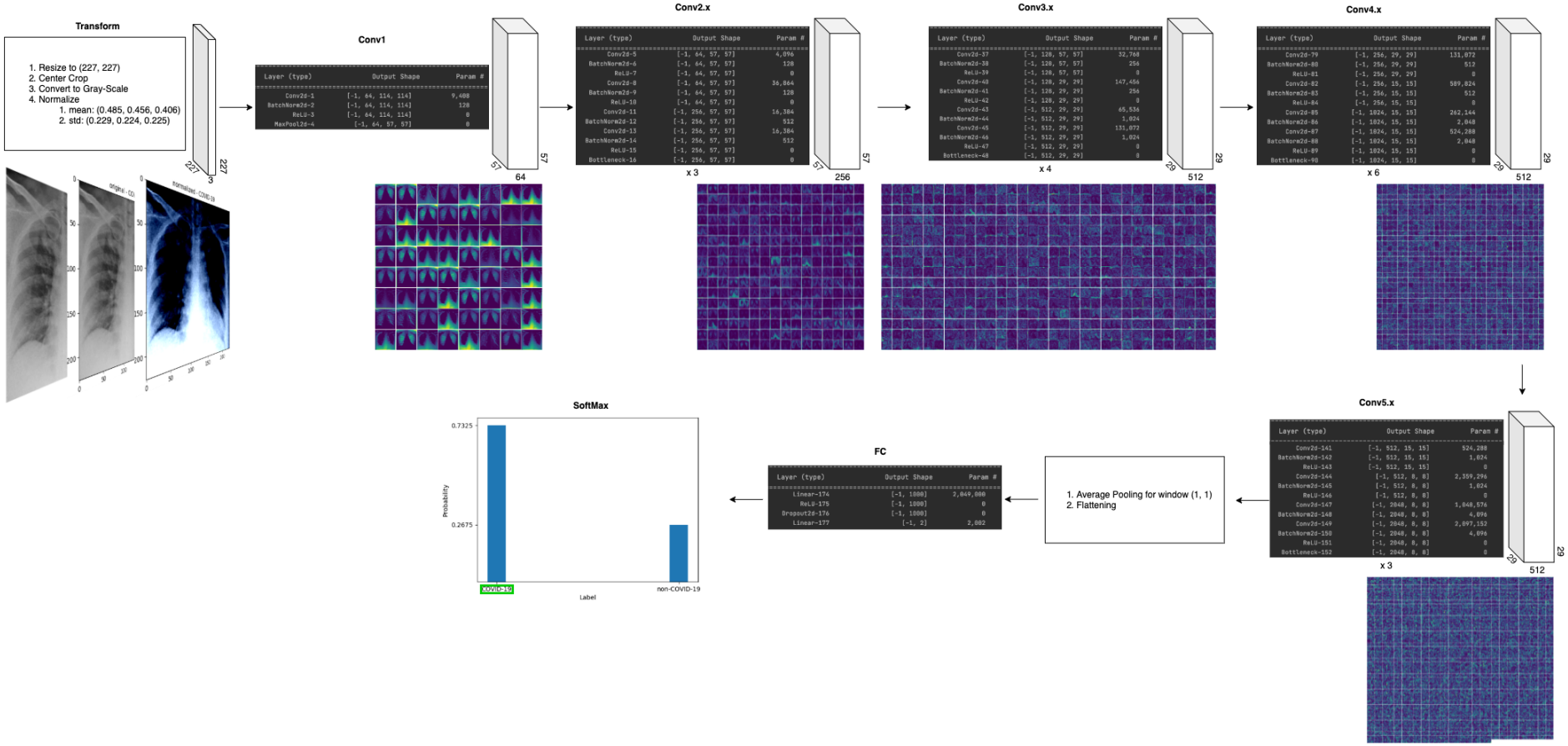

Figure 5.4 : The sample visualization representing one iteration on ResNet-50 architecture and class probability result for COVID-19 labeled data from our dataset. The higher resolution version of image is available at `https://github.com/ozanguldali/modelsWithLASSO/blob/master/figures/resnet50_visual.png`

The higher resolution version of images in Figure 5.4, such as the visualizations of convolution blocks, is available at directory `https://github.com/ozanguldali/modelsWithLASSO/blob/master/figures`.

5.4 Deep Feature Extraction

After training, validating and testing the dataset on pre-trained CNN models, the deep feature extraction progress was started. Since the best results according to accuracy are stored, these model weights files are used to extract deep features from their corresponding CNN architectures.

Here, the modifications on CNN models stated at previous section show its another purpose. The deep feature are extracted from these added or replaced fully-connected layers as:

- using the third fully-connected layer for AlexNet architecture,
- using the first fully-connected layer for ResNet architectures, and
- using the third fully-connected layer for VGG architectures.

The deep features extracted from CNN models are used to feed machine learning algorithms to improve the classification success.

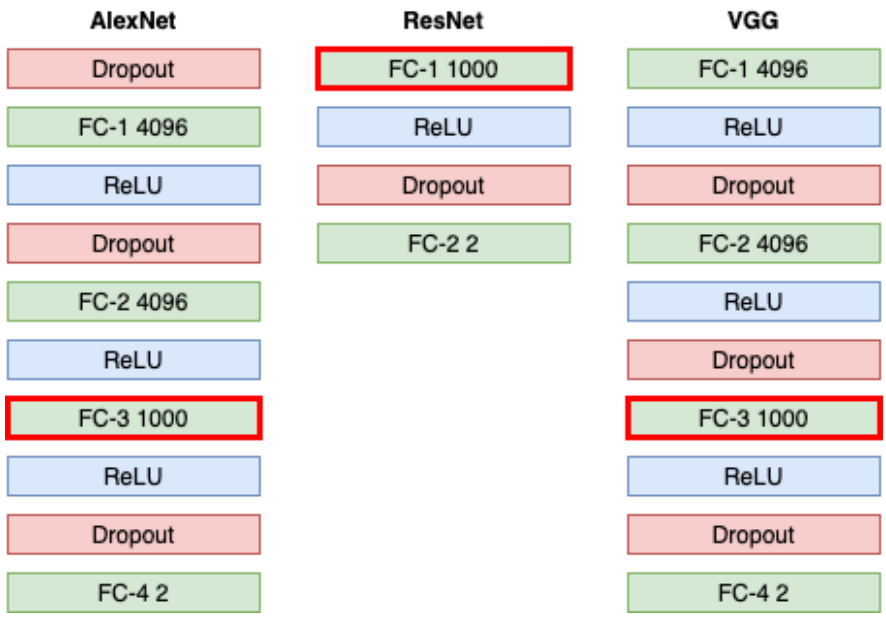

Figure 5.5 : Modified classification blocks where bold red windowed fully-connected layers denotes the deep feature extraction state.

5.5 Forming the Feature Maps

In this study, we have two types of feature matrices and one consisting of their conjunction. The first feature matrix includes the deep features extracted by the help of CNN models. Instead of image segmentation, Red-Green-Blue (RGB) color codes or manual image partition labeling, we use the features derived from deep learning process. The number of features are 1000 for each CNN architecture, because of the output size of used fully-connected layers. We denote the matrix of deep features as X_{cnn} and the feature size as $d_{cnn} = 1000$.

On the other part, we have demographic information for each sample, and that is the why our dataset is restricted. We denote the matrix of demographic information as X_{info} and the feature size as $d_{info} = 2$. Age information was categorized to 5 groups such as under 18, between 18 and 37, between 39 and 59, between 60 and 79, and over 80 ages.

Hence, the merged features matrix denoted by X_{all} has the feature size as $d_{all} = 1002$.

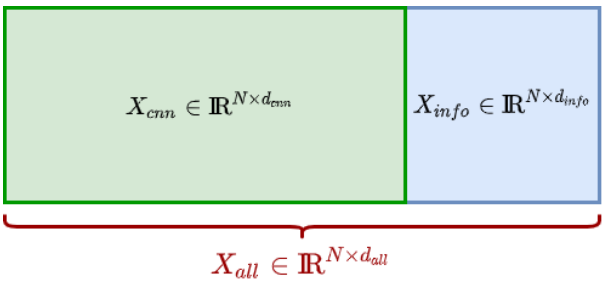

Figure 5.6 : Feature maps where $d_{cnn} = 1000$, $d_{info} = 2$, and $d_{all} = d_{cnn} + d_{info} = 1002$.

5.6 Data Pre-Processing

5.6.1 Data Standardization

Machine learning estimators commonly requires data standardization; because, the data may not be always in the form of standard normal distribution. There are three basic ways to standardize the data such as 1) centering data with the mean, 2) scaling data with the standard deviation, and 3) centering and scaling data with the main and standard deviation. In the experiments, we only centered the data. That is, we set μ as the mean of training samples and σ as 1 in the equation (5.1):

$$Z = (X - \mu * I)/\sigma\,. \tag{5.1}$$

5.6.2 Data Normalization

Data normalization scales each individual sample to have a unit norm in the rational numbers range [0.0, 1.0]. Two ways of normalization was experimented which are least absolute technique, known as L1 normalization, and least squares technique, known as L2 normalization.

- **L1 Norm:** Scales the sum of the absolute differences of each individual feature on a sample to 1. That is, scales the S_{L1} to 1 in the equation (5.2):

$$S_{L1} = \sum_{i=1}^{d} \left| y_k - X_{k,i} \right|, \tag{5.2}$$

  where d is the number of features, X_k is the k^{th} sample and $X_{k,i}$ is the i^{th} feature value of corresponding sample, and y_k is the target value for corresponding sample. Here, the scaling ratio is $1/S_{L1}$; thus, X_k/S_{L1} gives the L1 normalized feature values for this sample.

- **L2 Norm:** Scales the sum of the squares of differences of each individual feature on a sample to 1. That is, scales the S_{L2} to 1 in the equation (5.3):

$$S_{L2} = \sum_{i=1}^{d} \left(y_k - X_{k,i} \right)^2, \tag{5.3}$$

  where d is the number of features, X_k is the k^{th} sample and $X_{k,i}$ is the i^{th} feature value of corresponding sample, and y_k is the target value for corresponding sample. Here, the scaling ratio is $\sqrt{1/S_{L2}}$; thus, $X_k/\sqrt{S_{L2}}$ gives the L2 normalized feature values for this sample.

We used the L2 normalization as the final settings of the data pre-processing pipeline.

5.7 Hyper-Parameter Tuning

For each machine learning algorithm, there exists several hyper-parameters. Since the hyper-parameter settings cannot be generalized, and so differ for each problem and dataset, finding the optimal combination of hyper-parameters is a separate mission.

Which characteristic to look for when choosing the most optimal hyper-parameter combination depends on the problem and the researcher. In this thesis, we decide according to accuracy values. There are three common optimization method such that bayesian optimization, grid search and random search.

- **Grid Search:** all combinations between hyper-parameter options are experimented. For instance, if there exists m number of hyper-parameters and each of them has a_i options where a_i's are positive integers for $i \in \{1, 2, \ldots, m\}$, then the total number of grid search iterations are $\prod_{i=0}^{m} a_i$. Moreover, if K-Fold cross validation is applied, the number of iterations are raised to $K \times \prod_{i=0}^{m} a_i$.
- **Random Search:** randomly chosen hyper-parameter option combinations over all are experienced. The number of combinations to be tried are determined by researcher as less than the total number of combinations.
- **Bayesian Optimization:** this methodology is based on Bayesian Principle. While the combinations of hyper-parameter options are experimented, the previously known results leads to create a new combination space by using bayesian rule. This time, the choice of combinations are not random, but depend on the useful or irrelevant combination estimation.

In thesis, we experimented grid search with 10-Fold cross validation.

5.8 Training and Testing on Machine Learning Models

The partitioning of dataset into train and test sets are preserved on machine learning stage. The only difference is, data augmentation is not applied on train set.

All three types of feature matrices were experienced separately. For each, 10-Fold cross validation was applied on train set only by using grid search to find the generalized optimal combination of hyper-parameter options. To decide the best combination, the first criterion was set as accuracy value, and if there exists multiple same values, the second criterion was determined as the computation time. If there exists combinations such that two of criteria are the same, the last experienced combination was chosen.

For the repeatability of our work, we initialized the Python random number generation with different seeds. In other words, the seed parameter of Python random library is

one of out hyper-parameters, and we chose the best seed among our experiments to achieve final results.

Here, a parenthesis must be open for linear discriminant analysis algorithm. Since there is no library in Python that supports regularization on LDA, we used TULIP package [42] on version 1.0.1 in R programming language with the version of 4.0.3 to implement L1 regularized LDA model. Furthermore, grid search tuning was not applied to this model. Hyper-parameter tuning process was applied only for seed and regularization parameters.

Penalty terms, which are no penalty, Lasso and Ridge, were not considered as hyper-parameters, because they were experienced and compared separately. All hyper-parameter options to be combined can be found in Tables 5.3 - 5.6.

Table 5.3 : SVM algorithm hyper-parameters to tune.

Hyper-Parameter	**Ridge Penalty**	**Lasso Penalty**
Kernel Function	linear, sigmoid, rbf	linear
Regularization Parameter	5e-5, 1e-4, 2e-4, 5e-4, 5e-3, 1e-2, 2e-2, 5e-2, 0.1, 0.5, 1.0, 2.0, 5.0, 10.0, 15.0	5e-5, 1e-4, 2e-4, 5e-4, 5e-3, 1e-2, 2e-2, 5e-2, 0.1, 0.5, 1.0, 2.0, 5.0, 10.0, 15.0

Table 5.4 : LR algorithm hyper-parameters to tune.

Hyper-Parameter	**No Penalty**	**Lasso Penalty**	**Ridge Penalty**
Solver Function	newton-cg, lbfgs, sag, saga	liblinear, saga	newton-cg, lbfgs, sag, saga, liblinear
Regularization Parameter	-	5e-5, 1e-4, 2e-4, 5e-4, 5e-3, 1e-2, 2e-2, 5e-2, 0.1, 0.5, 1.0, 2.0, 5.0, 10.0, 15.0	5e-5, 1e-4, 2e-4, 5e-4, 5e-3, 1e-2, 2e-2, 5e-2, 0.1, 0.5, 1.0, 2.0, 5.0, 10.0, 15.0

Table 5.5 : KNN algorithm hyper-parameters to tune.

Hyper-Parameter	**No Penalty**
Number of Neighbors	3, 5, $\sqrt{\text{the number of samples}}$
Type of Majority Voting	uniform, weighted
Neighborhood Finder	brute force, ball tree, k dimensional tree
Metric Function	euclidean, manhattan, chebyshev

Table 5.6 : LDA algorithm hyper-parameters to tune.

Hyper-Parameter	**No Penalty**	**Lasso Penalty**
Regularization Parameter	-	5e-5, 1e-4, 2e-4, 5e-4, 5e-3, 1e-2, 2e-2, 5e-2, 0.1, 0.5, 1.0, 2.0, 5.0, 10.0, 15.0
Solver Function	svd, lsqr, eigen	-
Computing the Weighted Within-Class Covariance (for svd solver)	Yes, No	-

When the optimal hyper-parameter combination was determined with the aim of generalization, the model weights obtained by training on corresponding machine learning algorithm with these hyper-parameters are used on testing stage. The final results are achieved by testing on this fitted model. Furthermore, another grid search was applied on determined train and test data, and the results were compared by the generalized ones.

6. RESULTS

6.1 Performance Measurement

6.1.1 Confusion Matrix

The confusion matrix is a table that constructed to visualize the performance of classifier. It includes actual and predicted results for each class on the corresponding task. In our study, the rows specifies the actual results while columns specifies predicted ones.

During the performance measurement, the focused class is called as Positive (P), and the others are as Negatives (N). For binary classification problems, which is as in our study, one class can be directly specified as P and the other as N. We indicated the COVID-19 label as Positive class, and the non-COVID-19 label as Negative class.

If a sample in actual P class is predicted as in P class, then it is a True Positive (TP) sample, otherwise it is False Positive (FP). On the other hand, if a sample in actual N class is predicted as in P class, then it is a False Negative (FN) sample, otherwise it is True Negative (TN).

From the definitions, the following equalities can be easily derived: P = TP + FN and N = FP + TN.

Table 6.1 : Sample Confusion Matrix.

CONFUSION MATRIX		Actual	
		P (COVID-19)	N (non-COVID-19)
Predicted	P (COVID-19)	**TP**	FN
	N (non-COVID-19)	FP	**TN**

6.1.2 The Analysis of Confusion Matrix

Various meaningful ratios can be extracted from the confusion matrix. In this section, we study the significant ones which were also used in the thesis to measure the performance on our tasks.

6.1.2.1 Sensitivity (True Positive Rate - TPR)

Sensitivity (TPR) measures the ratio of positive class samples predicted correctly over all samples predicted as positive as given below:

$$TPR = \frac{TP}{P} = \frac{TP}{TP+FN}. \tag{6.1}$$

6.1.2.2 Specificity (True Negative Rate - TNR)

Specificity (TNR) measures the ratio of negative class samples predicted correctly over all samples predicted as negative as given below:

$$TNR = \frac{TN}{N} = \frac{TN}{FP+TN}. \tag{6.2}$$

6.1.2.3 Precision (Positive Predictive Value - PPV)

Precision (PPV) measures the ratio of correctly predicted positive class samples over all samples having actual positive label as given below:

$$PPV = \frac{TP}{TP+FP}. \tag{6.3}$$

6.1.2.4 Accuracy (ACC)

Accuracy (ACC) measures the ratio of correctly predicted samples over all samples as given below:

$$ACC = \frac{TP+TN}{P+N} = \frac{TP+TN}{TP+FP+FN+TN}. \tag{6.4}$$

6.1.2.5 F1 Score

F1 Score is the harmonic mean of sensitivity and precision as given below:

$$F_1 = 2 \times \frac{PPV \times TPR}{PPV+TPR} = \frac{2 \times TP}{2 \times TP+FP+FN}. \tag{6.5}$$

6.1.2.6 Area Under the Curve (AUC Score)

Area Under the Curve (AUC Score) measures the probability of classifier to rank a randomly chosen positive sample higher than a random chosen negative sample (under the assumption that "positive" ranks are higher than "negative" ranks) for normalized samples. The computation of AUC Score value is as given below:

$$
\begin{aligned}
&TPR(t) : t \rightarrow y(x), \\
&FPR(t) : t \rightarrow x, \text{ and} \\
&AUC = \int_0^1 TPR\left(FPR^{-1}(x)\right) dx = \int_{-\infty}^{\infty} TPR(t) \times FPR'(t)\, dt. \qquad (6.6)
\end{aligned}
$$

6.2 Convolutional Neural Network Results

Here, we report the results of convolutional neural network experiments explained in Section 5.3. As stated, AlexNet, ResNet-18, ResNet-34, ResNet-50, VGG-16 and VGG-19 architectures were trained initialized by their pre-trained weights with three different optimizers such that SGD with momentum, Adam and Adam with decoupled weight decay. The accuracy and loss curves for three different optimizers on train and validation processes can be viewed on Figures 6.1 - 6.6 whose x-axis represent the number of epochs. The plots were created by TensorBoard platform prepared with the Python TensorFlow package version 2.3.1. Additional required package versions are as follows: 1) TensorFlow Addons with the version of 0.11.2, 2) TensorFlow Estimator with the version of 2.3.0, 3) TensorFlow Hub with the version of 0.10.0, and 4) TensorFlow Probability with the version of 0.10.0.

The results can be also seen in Table 6.2 including accuracy, sensitivity, specificity, precision and F1 score values, and loss values for last train epoch and test run. We obtained the best result from ResNet-50 model after 9^{th} train epoch in 7 minutes with the accuracy, sensitivity, specificity, precision, F1 score and AUC score of 92.16%, 0.9216, 0.9215, 0.9216, 0.9216, 0.9215 respectively, and the loss of 9^{th} train epoch and validation as 0.0223 and 1.3687.

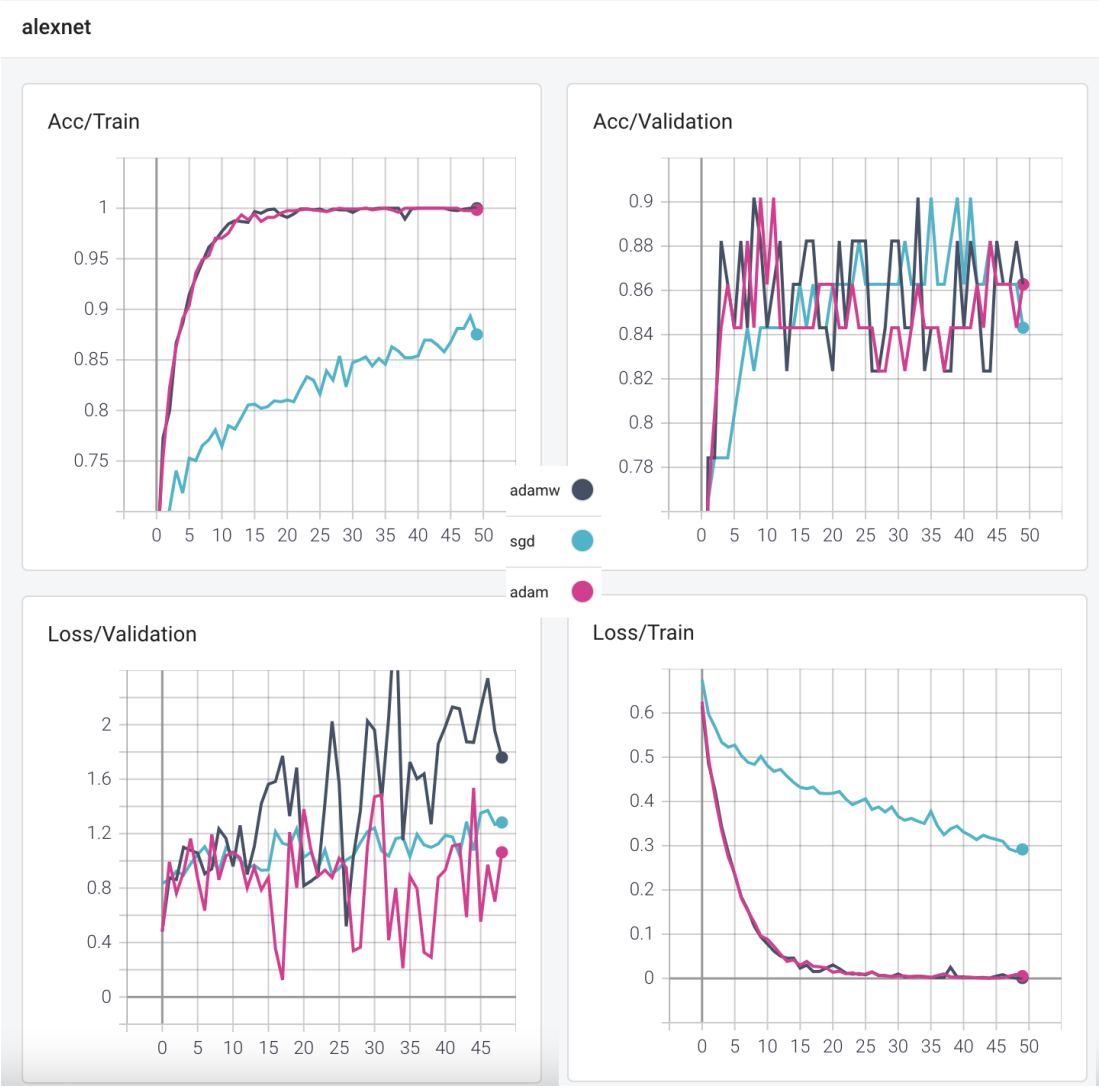

Figure 6.1 : AlexNet model accuracy and loss curves for three different optimizers on train and validation processes.

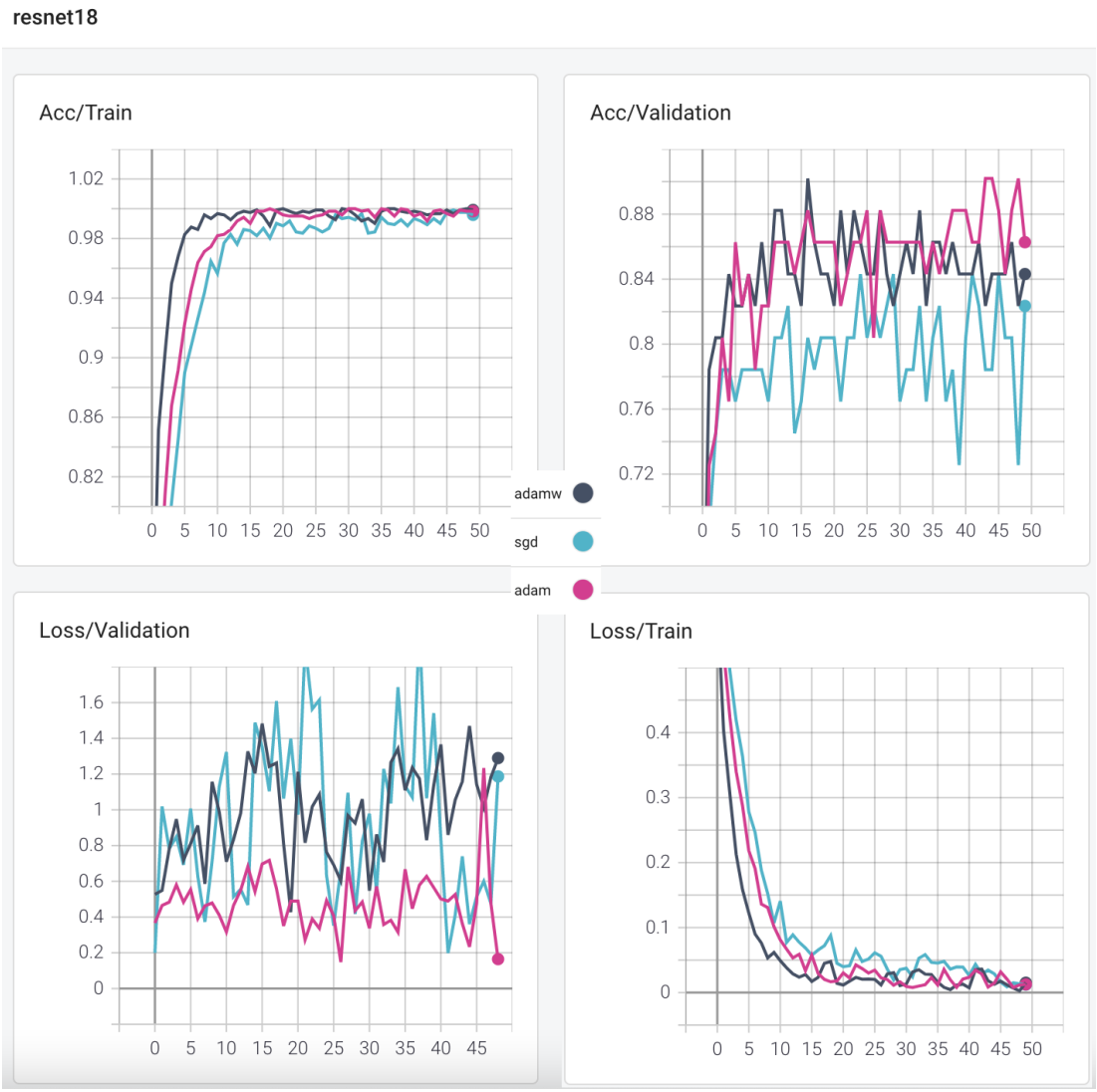

Figure 6.2 : ResNet-18 model accuracy and loss curves for three different optimizers on train and validation processes.

Figure 6.3 : ResNet-34 model accuracy and loss curves for three different optimizers on train and validation processes.

Figure 6.4 : ResNet-50 model accuracy and loss curves for three different optimizers on train and validation processes.

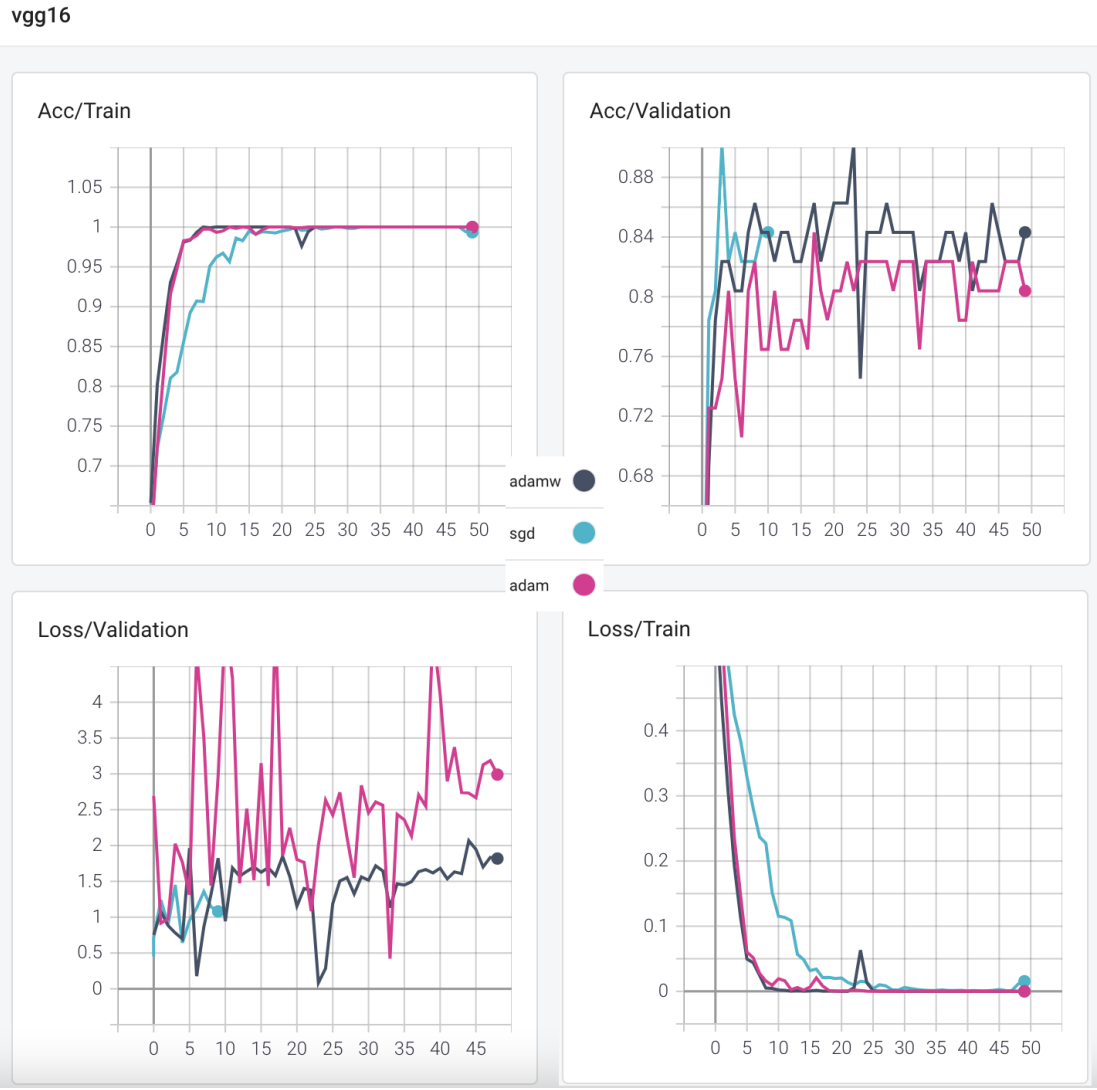

Figure 6.5 : VGG16 model accuracy and loss curves for three different optimizers on train and validation processes.

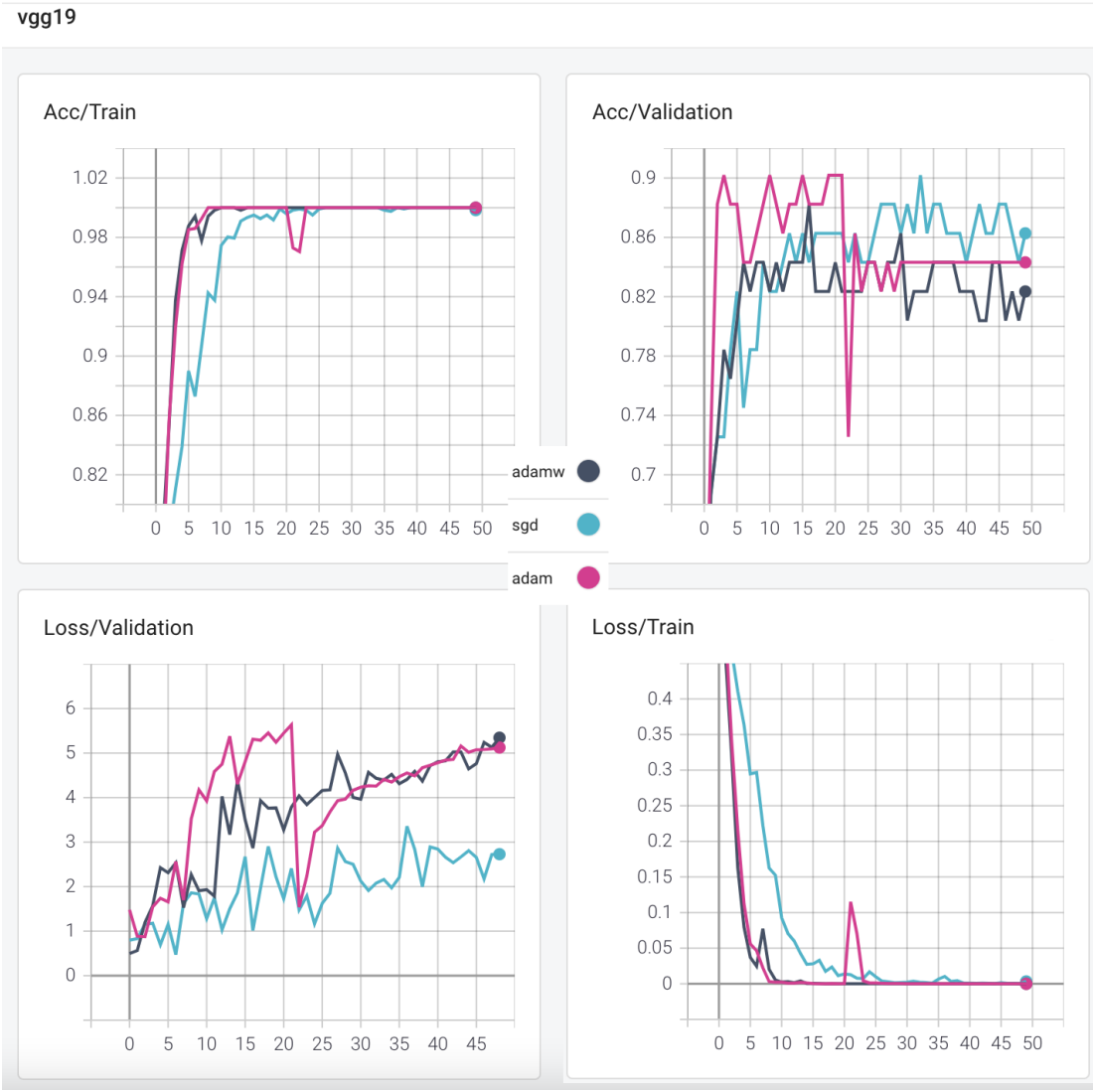

Figure 6.6 : VGG19 model accuracy and loss curves for three different optimizers on train and validation processes.

Table 6.2 : CNN model comparison.

Models and Optimizers		Metrics						Losses		Last Train	Duration
Model	**Optimizer**	**Accuracy (%)**	**Sensitivity**	**Specificity**	**Precision**	**F1 Score**	**AUC Score**	**Last Train**	**Test**	**Epoch**	**(minutes)**
AlexNet	SGD Momentum	90.20	0.9020	0.9026	0.9026	0.9020	0.9019	0.3503	1.0316	35	22
	Adam (no decay)	90.20	0.9020	0.9011	0.9025	0.9019	0.9023	0.1265	1.0373	8	7
	AdamW	90.20	0.9020	0.9042	0.9078	0.9017	0.9018	0.1549	1.2347	9	13
ResNet-18	SGD Momentum	84.31	0.8431	0.8430	0.8431	0.8431	0.8434	0.0194	0.8252	29	20
	Adam (no decay)	90.20	0.9020	0.9026	0.9026	0.9020	0.9022	0.0288	0.3631	43	33
	AdamW	90.20	0.9020	0.9042	0.9078	0.9020	0.9019	0.0171	1.2423	16	12
ResNet-34	SGD Momentum	90.20	0.9020	0.9026	0.9026	0.9020	0.9023	0.0460	1.1830	22	16
	Adam (no decay)	88.24	0.8823	0.8838	0.8849	0.8823	0.8826	0.0136	1.6412	18	10
	AdamW	90.20	0.9020	0.9026	0.9026	0.9020	0.9019	0.0253	1.3553	43	25
ResNet-50	SGD Momentum	88.24	0.8823	0.8823	0.8823	0.8823	0.8821	0.0327	1.2134	29	14
	Adam	**92.16**	**0.9216**	**0.9215**	**0.9216**	**0.9216**	**0.9219**	**0.0223**	**1.3687**	**9**	**7**
	AdamW	88.24	0.8823	0.8823	0.8823	0.8823	0.8827	0.0260	1.4826	50	34
VGG16	SGD Momentum	90.20	0.9020	0.9042	0.9078	0.9017	0.9021	0.0318	1.4500	15	11
	Adam	84.31	0.8431	0.8415	0.8450	0.8428	0.8432	0.0206	5.1689	17	15
	AdamW	90.20	0.9020	0.8996	0.9074	0.9015	0.9023	0.0057	0.0831	23	19
VGG19	SGD Momentum	90.20	0.9020	0.9026	0.9026	0.9020	0.9020	0.0024	2.1594	29	26
	Adam (no decay)	90.20	0.9020	0.9026	0.9026	0.9025	0.9019	0.0344	1.5451	3	2
	AdamW	88.24	0.8823	0.8838	0.8849	0.8823	0.8825	0.0006	2.8652	16	15

One chosen confusion matrix for each CNN architecture according to accuracy and loss values are given in Tables 6.3 - 6.8.

Table 6.3 : The confusion matrix of AlexNet model result with Adam optimizer.

		Actual	
		P	N
Predicted	P	24	3
	N	2	22

Table 6.4 : The confusion matrix of ResNet-18 model result with AdamW optimizer.

		Actual	
		P	N
Predicted	P	22	1
	N	4	24

Table 6.5 : The confusion matrix of ResNet-34 model result with AdamW optimizer.

		Actual	
		P	N
Predicted	P	23	2
	N	3	23

Table 6.6 : The confusion matrix of ResNet-50 model result with Adam optimizer.

		Actual	
		P	N
Predicted	P	23	3
	N	2	23

Table 6.7 : The confusion matrix of VGG16 model result with AdamW optimizer.

		Actual	
		P	N
Predicted	P	25	4
	N	1	21

Table 6.8 : The confusion matrix of VGG19 model result with SGD Momentum optimizer.

		Actual	
		P	N
Predicted	P	23	2
	N	3	23

6.3 Machine Learning Results

After the experiments of CNN models and obtaining the results, the deep feature sets were extracted from exactly the same train and test data. On the other side, the demographic information feature matrices were extracted for the same separation. In this section, we report the results for machine learning experiments on X_{info}, X_{cnn} and X_{all} defined in Section 5.5.

6.3.1 Results for X_{info}

In Table 6.9, the result for experimented machine learning algorithms on X_{info} can be viewed. The reported results can be reproduced with the Python system seed as 4. The best results were obtained with KNN algorithm, and the final hyper-parameters can be seen on Table 6.10. Furthermore, the confusion matrices are on Table 6.11.

Table 6.9 : The result of demographic information experiments with the Python system seed as 4.

Models and Regularizers		**Accuracies (%)**	
Model	**Regularizer**	**Result for Grid Search on Train Data**	**Result for Grid Search on Test Data**
SVM	Ridge	52.94	52.94
	Lasso	52.94	52.94
LR	-	52.94	52.94
	Ridge	52.94	52.94
	Lasso	52.94	52.94
KNN	**-**	**56.86**	**56.86**
LDA	-	52.94	52.94
	Lasso	52.94	52.94

Table 6.10 : KNN algorithm hyper-parameters for X_{info}.

Hyper-Parameter	**Result for Grid Search on Train Data**	**Result for Grid Search on Test Data**
Number of Neighbors	17	17
Type of Majority Voting	uniform	uniform
Neighborhood Finder	brute force	brute force
Metric Function	euclidean	euclidean

6.3.2 Results for X_{cnn}

In Table 6.12, the machine learning experiments on different X_{cnn} feature matrices can be seen for AlexNet model with Adam optimizer, ResNet-18 model AdamW optimizer,

Table 6.11 : Confusion matrices for KNN experiments on demographic information.

		Actual			
		Result for Grid Search on Train Data		**Result for Grid Search on Test Data**	
		P	N	P	N
Predicted	P	5	1	5	1
	N	21	24	21	24

ResNet-34 model AdamW optimizer, ResNet-50 model with Adam optimizer, VGG16 model with AdamW optimizer, and VGG19 model SGD optimizer. The final hyper-parameters for $X_{cnn\_ResNet50}$ feature matrix constructed by the help of ResNet-50 model Adam optimizer can be seen on Tables 6.13 - 6.20. Furthermore, the confusion matrices and all other metrics derived from these confusion matrices are on Tables 6.21 - 6.28.

Table 6.12 : The result of experiments on X_{cnn} with the Python system seed as 4.

Models and Regularizers		**Accuracies (%)**											
Model	**Regularizer**	**Result After Grid Search on Train Data**						**Result After Grid Search on Test Data**					
		AlexNet (Adam)	**ResNet-18 (AdamW)**	**ResNet-34 (AdamW)**	**ResNet-50 (Adam)**	**VGG16 (AdamW)**	**VGG19 (SGD Momentum)**	**AlexNet (Adam)**	**ResNet-18 (AdamW)**	**ResNet-34 (AdamW)**	**ResNet-50 (Adam)**	**VGG16 (AdamW)**	**VGG19 (SGD Momentum)**
SVM	Ridge	88.24	88.24	90.20	92.16	88.24	88.24	90.20	88.24	90.20	92.16	88.24	90.20
	Lasso	90.20	90.20	84.31	86.27	88.24	86.27	90.20	90.20	90.20	92.16	88.24	88.24
LR	-	90.20	88.24	90.20	92.16	90.20	90.20	90.20	88.24	90.20	92.16	90.20	90.20
	Ridge	90.20	88.24	90.20	92.16	88.24	88.24	90.20	88.24	90.20	92.16	88.24	88.24
	Lasso	84.31	86.27	84.31	86.27	86.27	84.31	88.24	86.27	90.20	92.16	86.27	86.27
KNN	-	88.24	88.24	90.20	92.16	86.27	90.20	90.20	88.24	90.20	92.16	86.27	90.20
LDA	-	82.35	82.35	82.35	84.31	82.35	84.31	84.31	84.31	82.35	84.31	84.31	84.31
	Lasso	88.24	88.24	88.24	90.20	88.24	88.24	90.20	90.20	90.20	92.16	88.24	90.20

Table 6.13 : SVM algorithm regularized by Ridge hyper-parameters for $X_{cnn\_ResNet50}$.

Hyper-Parameter	Result for Grid Search on Train Data	Result for Grid Search on Test Data
Kernel Function	linear	linear
Regularization Parameter	5e-5	5e-5

Table 6.14 : SVM algorithm regularized by Lasso hyper-parameters for $X_{cnn\_ResNet50}$.

Hyper-Parameter	Result for Grid Search on Train Data	Result for Grid Search on Test Data
Regularization Parameter	5e-3	5e-2

Table 6.15 : LR algorithm hyper-parameters for $X_{cnn\_ResNet50}$.

Hyper-Parameter	Result for Grid Search on Train Data	Result for Grid Search on Test Data
Solver Function	newton-cg	newton-cg

Table 6.16 : LR algorithm regularized by Ridge hyper-parameters for $X_{cnn\_ResNet50}$.

Hyper-Parameter	Result for Grid Search on Train Data	Result for Grid Search on Test Data
Solver Function	liblinear	liblinear
Regularization Parameter	5e-5	5e-5

Table 6.17 : LR algorithm regularized by Lasso hyper-parameters for $X_{cnn\_ResNet50}$.

Hyper-Parameter	Result for Grid Search on Train Data	Result for Grid Search on Test Data
Solver Function	liblinear	liblinear
Regularization Parameter	2e-2	1.0

Table 6.18 : KNN algorithm hyper-parameters for $X_{cnn\_ResNet50}$.

Hyper-Parameter	Result for Grid Search on Train Data	Result for Grid Search on Test Data
Number of Neighbors	3	3
Type of Majority Voting	uniform	uniform
Neighborhood Finder	ball tree	ball tree
Metric Function	euclidean	euclidean

Table 6.19 : LDA algorithm hyper-parameters for $X_{cnn\_ResNet50}$.

Hyper-Parameter	Result for Grid Search on Train Data	Result for Grid Search on Test Data
Solver Function	svd	svd
Computing the Weighted Within-Class Covariance (for svd solver)	True	True

Table 6.20 : LDA algorithm regularized by Lasso hyper-parameters for $X_{cnn\_ResNet50}$.

Hyper-Parameter	Result for Grid Search on Train Data	Result for Grid Search on Test Data
Regularization Parameter	5e-5	5e-3

Table 6.21 : The confusion matrices and results obtained by SVM algorithm regularized with Ridge for $X_{cnn\_ResNet50}$.

		Result for Grid Search on Train Data							Result for Grid Search on Test Data						
		Actual		**Accuracy (%)**	**Sensitivity**	**Specificity**	**Precision**	**F1 Score**	**AUC Score**	**Actual**		**Accuracy (%)**	**Sensitivity**	**Specificity**	**Precision**	**F1 Score**	**AUC Score**
		P	N	92.16	0.9216	0.9230	0.9243	0.9215	0.9223	P	N	92.16	0.9216	0.9230	0.9243	0.9215	0.9223
Predicted	P	23	1							23	1						
	N	3	24							3	24						

Table 6.22 : The confusion matrices and results obtained by SVM algorithm regularized with Lasso for $X_{cnn\_ResNet50}$.

		Result for Grid Search on Train Data							Result for Grid Search on Test Data						
		Actual		**Accuracy (%)**	**Sensitivity**	**Specificity**	**Precision**	**F1 Score**	**AUC Score**	**Actual**		**Accuracy (%)**	**Sensitivity**	**Specificity**	**Precision**	**F1 Score**	**AUC Score**
		P	N	86.27	0.8627	0.8665	0.8777	0.8617	0.8646	P	N	92.16	0.9216	0.9230	0.9243	0.9215	0.9223
Predicted	P	20	1							23	1						
	N	6	24							3	24						

Table 6.23 : The confusion matrices and results obtained by LR algorithm for $X_{cnn\_ResNet50}$.

		Result for Grid Search on Train Data							Result for Grid Search on Test Data						
		Actual		**Accuracy (%)**	**Sensitivity**	**Specificity**	**Precision**	**F1 Score**	**AUC Score**	**Actual**		**Accuracy (%)**	**Sensitivity**	**Specificity**	**Precision**	**F1 Score**	**AUC Score**
		P	N	92.16	0.9216	0.9230	0.9243	0.9215	0.9223	P	N	92.16	0.9216	0.9230	0.9243	0.9215	0.9223
Predicted	P	23	1							23	1						
	N	3	24							3	24						

Table 6.24 : The confusion matrices and results obtained by LR algorithm regularized with Ridge for $X_{cnn\_ResNet50}$.

		Result for Grid Search on Train Data							Result for Grid Search on Test Data						
		Actual		**Accuracy (%)**	**Sensitivity**	**Specificity**	**Precision**	**F1 Score**	**AUC Score**	**Actual**		**Accuracy (%)**	**Sensitivity**	**Specificity**	**Precision**	**F1 Score**	**AUC Score**
		P	N	92.16	0.9216	0.9230	0.9243	0.9215	0.9223	P	N	92.16	0.9216	0.9230	0.9243	0.9215	0.9223
Predicted	P	23	1							23	1						
	N	3	24							3	24						

Table 6.25 : The confusion matrices and results obtained by LR algorithm regularized with Lasso for $X_{cnn\_ResNet50}$.

		Result for Grid Search on Train Data							Result for Grid Search on Test Data						
		Actual		**Accuracy (%)**	**Sensitivity**	**Specificity**	**Precision**	**F1 Score**	**AUC Score**	**Actual**		**Accuracy (%)**	**Sensitivity**	**Specificity**	**Precision**	**F1 Score**	**AUC Score**
		P	N	86.27	0.8627	0.8665	0.8777	0.8617	0.8646	P	N	92.16	0.9216	0.9230	0.9243	0.9215	0.9223
Predicted	P	20	1							23	1						
	N	6	24							3	24						

Table 6.26 : The confusion matrices and results obtained by KNN algorithm for $X_{cnn\_ResNet50}$.

		Result for Grid Search on Train Data							Result for Grid Search on Test Data						
		Actual		**Accuracy (%)**	**Sensitivity**	**Specificity**	**Precision**	**F1 Score**	**AUC Score**	**Actual**		**Accuracy (%)**	**Sensitivity**	**Specificity**	**Precision**	**F1 Score**	**AUC Score**
		P	N	92.16	0.9216	0.9230	0.9243	0.9215	0.9223	P	N	92.16	0.9216	0.9230	0.9243	0.9215	0.9223
Predicted	P	23	1							23	1						
	N	3	24							3	24						

Table 6.27 : The confusion matrices and results obtained by LDA algorithm for $X_{cnn\_ResNet50}$.

		Result for Grid Search on Train Data							Result for Grid Search on Test Data						
		Actual		**Accuracy (%)**	**Sensitivity**	**Specificity**	**Precision**	**F1 Score**	**AUC Score**	**Actual**		**Accuracy (%)**	**Sensitivity**	**Specificity**	**Precision**	**F1 Score**	**AUC Score**
		P	N	84.31	0.8431	0.8476	0.8638	0.8413	0.8454	P	N	84.31	0.8431	0.8476	0.8638	0.8413	0.8454
Predicted	P	19	1							19	1						
	N	7	24							7	24						

Table 6.28 : The confusion matrices and results obtained by LDA algorithm regularized with Lasso for $X_{cnn\_ResNet50}$.

		Result for Grid Search on Train Data							Result for Grid Search on Test Data						
		Actual		**Accuracy (%)**	**Sensitivity**	**Specificity**	**Precision**	**F1 Score**	**AUC Score**	**Actual**		**Accuracy (%)**	**Sensitivity**	**Specificity**	**Precision**	**F1 Score**	**AUC Score**
		P	N	90.20	0.9020	0.9042	0.9078	0.9017	0.9045	P	N	92.16	0.9216	0.9230	0.9243	0.9215	0.9223
Predicted	P	22	1							23	1						
	N	4	24							3	24						

6.3.3 Results for X_{all}

In Table 6.29, the machine learning experiments on different X_{all} feature matrices can be seen for AlexNet model with Adam optimizer, ResNet-18 model AdamW optimizer, ResNet-34 model AdamW optimizer, ResNet-50 model with Adam optimizer, VGG16 model with AdamW optimizer, and VGG19 model SGD optimizer. The final hyper-parameters for $X_{all\_ResNet50}$ feature matrix constructed by the help of ResNet-50 model Adam optimizer can be seen on Tables 6.30 - 6.37. Furthermore, the confusion matrices and all other metrics derived from these confusion matrices are on Tables 6.38 - 6.45.

Table 6.29 : The result of experiments on X_{all} with the Python system seed as 4.

Models and Regularizers		**Accuracies (%)**											
Model	**Regularizer**	**Result for Grid Search on Train Data**						**Result for Grid Search on Test Data**					
		AlexNet (Adam)	**ResNet-18 (AdamW)**	**ResNet-34 (AdamW)**	**ResNet-50 (Adam)**	**VGG16 (AdamW)**	**VGG19 (SGD Momentum)**	**AlexNet (Adam)**	**ResNet-18 (AdamW)**	**ResNet-34 (AdamW)**	**ResNet-50 (Adam)**	**VGG16 (AdamW)**	**VGG19 (SGD Momentum)**
SVM	Ridge	88.24	90.20	90.20	92.16	88.24	88.24	90.20	88.24	90.20	92.16	88.24	90.20
	Lasso	90.20	90.20	84.31	86.27	88.24	86.27	90.20	90.20	90.20	92.16	88.24	88.24
LR	-	90.20	88.24	90.20	92.16	90.20	90.20	90.20	88.24	90.20	92.16	90.20	90.20
	Ridge	90.20	88.24	90.20	92.16	88.24	88.24	90.20	88.24	90.20	92.16	88.24	88.24
	Lasso	84.31	86.27	84.31	88.24	86.27	86.27	88.24	86.27	90.20	92.16	86.27	88.24
KNN	-	90.20	88.24	90.20	92.16	86.27	90.20	90.20	88.24	90.20	92.16	86.27	90.20
LDA	-	82.35	82.35	82.35	84.31	82.35	84.31	84.31	84.31	82.35	84.31	84.31	84.31
	Lasso	88.24	88.24	88.24	90.20	88.24	88.24	90.20	90.20	90.20	92.16	88.24	90.20

Table 6.30 : SVM algorithm regularized by Ridge hyper-parameters for $X_{all\_ResNet50}$.

Hyper-Parameter	Result for Grid Search on Train Data	Result for Grid Search on Test Data
Kernel Function	linear	linear
Regularization Parameter	5e-5	5e-5

Table 6.31 : SVM algorithm regularized by Lasso hyper-parameters for $X_{all\_ResNet50}$.

Hyper-Parameter	Result for Grid Search on Train Data	Result for Grid Search on Test Data
Regularization Parameter	5e-3	5e-2

Table 6.32 : LR algorithm hyper-parameters for $X_{all\_ResNet50}$.

Hyper-Parameter	Result for Grid Search on Train Data	Result for Grid Search on Test Data
Solver Function	newton-cg	newton-cg

Table 6.33 : LR algorithm regularized by Ridge hyper-parameters for $X_{all\_ResNet50}$.

Hyper-Parameter	Result for Grid Search on Train Data	Result for Grid Search on Test Data
Solver Function	liblinear	liblinear
Regularization Parameter	5e-5	5e-5

Table 6.34 : LR algorithm regularized by Lasso hyper-parameters for $X_{all\_ResNet50}$.

Hyper-Parameter	Result for Grid Search on Train Data	Result for Grid Search on Test Data
Solver Function	liblinear	liblinear
Regularization Parameter	2e-2	2.0

Table 6.35 : KNN algorithm hyper-parameters for $X_{all\_ResNet50}$.

Hyper-Parameter	Result for Grid Search on Train Data	Result for Grid Search on Test Data
Number of Neighbors	3	3
Type of Majority Voting	uniform	uniform
Neighborhood Finder	ball tree	ball tree
Metric Function	euclidean	euclidean

Table 6.36 : LDA algorithm hyper-parameters for $X_{all\_ResNet50}$.

Hyper-Parameter	Result for Grid Search on Train Data	Result for Grid Search on Test Data
Solver Function	svd	svd
Computing the Weighted Within-Class Covariance (for svd solver)	True	True

Table 6.37 : LDA algorithm regularized by Lasso hyper-parameters for $X_{all\_ResNet50}$.

Hyper-Parameter	Result for Grid Search on Train Data	Result for Grid Search on Test Data
Regularization Parameter	5e-5	5e-3

Table 6.38 : The confusion matrices and results obtained by SVM algorithm regularized with Ridge for $X_{all\_ResNet50}$.

		Result for Grid Search on Train Data							Result for Grid Search on Test Data						
		Actual		**Accuracy (%)**	**Sensitivity**	**Specificity**	**Precision**	**F1 Score**	**AUC Score**	**Actual**		**Accuracy (%)**	**Sensitivity**	**Specificity**	**Precision**	**F1 Score**	**AUC Score**
		P	N	92.16	0.9216	0.9230	0.9243	0.9215	0.9223	P	N	92.16	0.9216	0.9230	0.9243	0.9215	0.9223
Predicted	P	23	1							23	1						
	N	3	24							3	24						

Table 6.39 : The confusion matrices and results obtained by SVM algorithm regularized with Lasso for $X_{all\_ResNet50}$.

		Result for Grid Search on Train Data							Result for Grid Search on Test Data						
		Actual		**Accuracy (%)**	**Sensitivity**	**Specificity**	**Precision**	**F1 Score**	**AUC Score**	**Actual**		**Accuracy (%)**	**Sensitivity**	**Specificity**	**Precision**	**F1 Score**	**AUC Score**
		P	N	86.27	0.8627	0.8665	0.8777	0.8617	0.8646	P	N	92.16	0.9216	0.9230	0.9243	0.9215	0.9223
Predicted	P	20	1							23	1						
	N	6	24							3	24						

Table 6.40 : The confusion matrices and results obtained by LR algorithm for $X_{all\_ResNet50}$.

		Result for Grid Search on Train Data							Result for Grid Search on Test Data						
		Actual		**Accuracy (%)**	**Sensitivity**	**Specificity**	**Precision**	**F1 Score**	**AUC Score**	**Actual**		**Accuracy (%)**	**Sensitivity**	**Specificity**	**Precision**	**F1 Score**	**AUC Score**
		P	N	92.16	0.9216	0.9230	0.9243	0.9215	0.9223	P	N	92.16	0.9216	0.9230	0.9243	0.9215	0.9223
Predicted	P	23	1							23	1						
	N	3	24							3	24						

Table 6.41 : The confusion matrices and results obtained by LR algorithm regularized with Ridge for $X_{all\_ResNet50}$.

		Result for Grid Search on Train Data							Result for Grid Search on Test Data						
		Actual		Accuracy (%)	Sensitivity	Specificity	Precision	F1 Score	AUC Score	Actual		Accuracy (%)	Sensitivity	Specificity	Precision	F1 Score	AUC Score
		P	N	92.16	0.9216	0.9230	0.9243	0.9215	0.9223	P	N	92.16	0.9216	0.9230	0.9243	0.9215	0.9223
Predicted	P	23	1							23	1						
	N	3	24							3	24						

Table 6.42 : The confusion matrices and results obtained by LR algorithm regularized with Lasso for $X_{all\_ResNet50}$.

		Result for Grid Search on Train Data							Result for Grid Search on Test Data						
		Actual		Accuracy (%)	Sensitivity	Specificity	Precision	F1 Score	AUC Score	Actual		Accuracy (%)	Sensitivity	Specificity	Precision	F1 Score	AUC Score
		P	N	88.23	0.8824	0.8853	0.8923	0.8818	0.8838	P	N	92.16	0.9216	0.9230	0.9243	0.9215	0.9223
Predicted	P	21	1							23	1						
	N	5	24							3	24						

Table 6.43 : The confusion matrices and results obtained by KNN algorithm for $X_{all\_ResNet50}$.

		Result for Grid Search on Train Data							Result for Grid Search on Test Data						
		Actual		Accuracy (%)	Sensitivity	Specificity	Precision	F1 Score	AUC Score	Actual		Accuracy (%)	Sensitivity	Specificity	Precision	F1 Score	AUC Score
		P	N	92.16	0.9216	0.9230	0.9243	0.9215	0.9223	P	N	92.16	0.9216	0.9230	0.9243	0.9215	0.9223
Predicted	P	23	1							23	1						
	N	3	24							3	24						

Table 6.44 : The confusion matrices and results obtained by LDA algorithm for $X_{all\_ResNet50}$.

		Result for Grid Search on Train Data							Result for Grid Search on Test Data						
		Actual		Accuracy (%)	Sensitivity	Specificity	Precision	F1 Score	AUC Score	Actual		Accuracy (%)	Sensitivity	Specificity	Precision	F1 Score	AUC Score
		P	N	84.31	0.8431	0.8476	0.8638	0.8413	0.8454	P	N	84.31	0.8431	0.8476	0.8638	0.8413	0.8454
Predicted	P	19	1							19	1						
	N	7	24							7	24						

Table 6.45 : The confusion matrices and results obtained by LDA algorithm regularized with Lasso for $X_{all\_ResNet50}$.

		Result for Grid Search on Train Data							Result for Grid Search on Test Data						
		Actual		**Accuracy (%)**	**Sensitivity**	**Specificity**	**Precision**	**F1 Score**	**AUC Score**	**Actual**		**Accuracy (%)**	**Sensitivity**	**Specificity**	**Precision**	**F1 Score**	**AUC Score**
		P	N	90.20	0.9020	0.9042	0.9078	0.9017	0.9045	P	N	92.16	0.9216	0.9230	0.9243	0.9215	0.9223
Predicted	P	22	1							23	1						
	N	4	24							3	24						

We can brief all these results about our experiments on our dataset such as:

- generalized optimal hyper-parameters may not be best combination for our initially determined test data,
- demographic information support only boosts the performance on logistic regression algorithm regularized by Lasso, and
- penalty approach only increases the success on linear discriminant analysis algorithm.

7. CONCLUSIONS AND RECOMMENDATIONS

The main scope of this thesis was to show a method to use image data without segmenting or manually extracting features from them on machine learning algorithms, and how to use it on a continuing global public health problem. One recommendation here can be given as to use data eliminated by professionals. In the studies like ours, getting support from specialist radiologists provides to have more qualified chest X-Ray images, and through this better classifiers may be yielded.

The reason why applying cross validation on train data and yielding optimized hyper-parameters from these experiments is that to find the most generalized hyper-parameter settings. If the grid search was applied to the experiment including training on train data and testing on test data, the yielding parameters indeed would be only optimized for our test data. This would be enough for this work, if we only cared about the mathematical results and out success. However, we aimed to find more generalized optimal parameters. Thus, we used 10-Fold cross validation which means we experimented on 10 different validation sets. Then we tested these hyper-parameters on test data and reported the final results. In addition to that, we also experimented grid search only on the initially determined test set and reported the results. In this way, the comparison on metrics and optimized parameters can be performed between generalized and specific to our test data.

After the experiments, we encountered the benefits of obtaining parameters by using grid search on train set. We have seen that the parameters in this way are not always the best parameters for our test set. Thanks to this way, we provided the method for how to obtain results not specific to a group of data but more suitable for random grouped data.

Although this study mainly focused on chest X-Rays and image data, the one of aim was to show non-image data can be combined with image data. Our non-image data is the demographic information of patients for corresponding chest X-Rays. Since the data size was not enough for a good classification and the non-image data types

was restricted to two features, desired result may not be seen. To see the results of the singular use of demographic information, we also experimented only on these two features with machine learning algorithms. We expect a visible effect of non-image data, if more information from patient such as doctors report, tobacco product use, associated genetic diseases, etc. is used. Moreover, the singular use results of non-image information would be better with more effective and numerically superior features.

Another main comparison was about the effect of regularization on machine learning algorithms. We wanted to see the performance of Lasso and Ridge, and obtained an improvement on linear discriminant analysis with Lasso.

The final best results are as follows:

- **CNN:** the best result was obtained from ResNet-50 model after 9th train epoch in 7 minutes with the accuracy, sensitivity, specificity, precision, F1 score and AUC score of 92.16%, 0.9216, 0.9215, 0.9216, 0.9216, 0.9215 respectively, and the loss of 9th train epoch and validation as 0.0223 and 1.3687, and
- **ML:** since the best model on CNN experiments was ResNet-50 model, the feature matrices of deep features providing the best results were also the ones transferred from ResNet-50 model. The results for three feature matrices X_{info}, $X_{cnn\_ResNet50}$ and $X_{all\_ResNet50}$ are as follows:
  - the best result obtained from demographic information features was on KNN algorithm as the accuracy of 56.86%, the sensitivity of 0.56863, the specificity of 0.58368 the precision of 0.6863, the F1 score of 0.49545, and the AUC score of 0.5745. The hyper-parameters were the number of neighbors as 17, the type of majority voting as uniform, the neighbor finder as brute force, and the metric function as euclidean,
  - the best result obtained from deep transferred features was not singular. According the generalized hyper-parameters, SVM with Ridge regularizer, LR, LR with Ridge, and KNN algorithms had the same results with the accuracy, sensitivity, specificity, precision, F1 score and AUC score of 92.16%, 0.9216, 0.9230, 0.9243, 0.9215, 0.9223 respectively, and

- the best result obtained from the combined features of demographic information and deep features was not singular. According the generalized hyper-parameters, SVM with Ridge regularizer, LR, LR with Ridge, and KNN algorithms had the same results with the accuracy, sensitivity, specificity, precision, F1 score and AUC score of 92.16%, 0.9216, 0.9230, 0.9243, 0.9215, 0.9223 respectively.

As it can be seen on confusion matrices of convolutional neural network results and machine learning results, the performance of classification for non-COVID labeled data was improved by machine learning algorithms. Moreover, the sensitivity, specificity, precision and F1 score was 0.9216, 0.9215, 0.9216 and 0.9216 respectively for ResNet-50 model, the result for machine learning algorithms was 0.9216, 0.9230, 0.9242, and 0.9216 for the sensitivity, specificity, precision and F1 score respectively. Briefly, even though the accuracy, sensitivity and F1 score did not improve, the specificity and precision improved. This can be interpreted as the answers of two questions could be given better: 1) how many of data estimated as infected were actually infected, and 2) how many of non-COVID-19 data over all patients correctly predicted.

7.1 Future Work

The contribution of this thesis is to understand how to use deep features extracted from convolutional neural network models on machine learning algorithms, and how to combine the image data features with non-image data to use in machine learning algorithms. To research on this topic, a global health problem COVID-19 disease and chest X-Rays images data including demographic information were used. However, any other image classification problem can be studied for future work. If a dataset consisting of images also includes non-image information, this thesis can be used as a guide for corresponding classification problem.

For instance, this study can be applied on multi-class classification problem on various respiratory diseases by chest computed tomography images of patients together with the demographic, doctors report, tobacco product use, associated genetic diseases, and respiratory test information. We also recommend to get help from one or more

specialist radiologists and chest disease specialists on eliminating the data, for the given study example.

This study can be improved by using more qualified dataset with more data in number, and extended by using chest computer tomography and more information of the patients in terms of variety. On the other hand, optimizers on convolutional neural networks such as Adagrad [43] and Padam [44], and elastic net regularization method [45] on machine learning algorithms can be used to extend this study. Moreover, ensemble learning [46] on convolutional neural network process and machine learning process separately can be used to extend the scope and results of this study.

REFERENCES

[1] **Kevles, B.** (1997). Naked to the bone : medical imaging in the twentieth century.

[2] **Loshchilov, I. and Hutter, F.** (2017). Fixing Weight Decay Regularization in Adam, *CoRR*.

[3] **Srivastava, N.**, **Hinton, G.**, **Krizhevsky, A.**, **Sutskever, I. and Salakhutdinov, R.** (2014). Dropout: A Simple Way to Prevent Neural Networks from Overfitting, *Journal of Machine Learning Research*, *15*(56), 1929–1958, http://jmlr.org/papers/v15/srivastava14a.html.

[4] **Nour, M.**, **Cömert, Z. and Polat, K.** (2020). A Novel Medical Diagnosis model for COVID-19 infection detection based on Deep Features and Bayesian Optimization, *Applied Soft Computing*, *97*, 106580, https://www.sciencedirect.com/science/article/pii/S1568494620305184.

[5] **Krizhevsky, A.**, **Sutskever, I. and Hinton, G.E.** (2012). ImageNet Classification with Deep Convolutional Neural Networks, *Proceedings of the 25th International Conference on Neural Information Processing Systems - Volume 1*, Curran Associates Inc., Red Hook, NY, USA.

[6] **He, K.**, **Zhang, X.**, **Ren, S. and Sun, J.**, (2015), Deep Residual Learning for Image Recognition, 1512.03385.

[7] **Nielsen, F.**, (2016). Parallel Linear Algebra, p.140.

[8] **Kahn, J.S. and McIntosh, K.** (2005). History and Recent Advances in Coronavirus Discovery, *The Pediatric Infectious Disease Journal*, *24*(11), https://journals.lww.com/pidj/Fulltext/2005/11001/History_and_Recent_Advances_in_Coronavirus.12.aspx.

[9] **Gorbalenya, A.E.**, **Baker, S.C.**, **Baric, R.S.**, **de Groot, R.J.**, **Drosten, C.**, **Gulyaeva, A.A.**, **Haagmans, B.L.**, **Lauber, C.**, **Leontovich, A.M.**, **Neuman, B.W.**, **Penzar, D.**, **Perlman, S.**, **Poon, L.L.M.**, **Samborskiy, D.V.**, **Sidorov, I.A.**, **Sola, I.**, **Ziebuhr, J. and of Viruses, C.S.G.o.t.I.C.o.T.** (2020). The species Severe acute respiratory syndrome-related coronavirus: classifying 2019-nCoV and naming it SARS-CoV-2, *Nature Microbiology*, *5*(4), 536–544, https://doi.org/10.1038/s41564-020-0695-z.

[10] (2020), WHO Director-General's opening remarks at the media briefing on COVID-19 - 11 March 2020, https://www.who.int/director-general/speeches/detail/who-director-general-s-opening-remarks-at-the-media-briefing-on-covid-19---11-march-2020.

[11] (2020), Coronavirus disease (COVID-19), https://www.who.int/emergencies/diseases/novel-coronavirus-2019/question-and-answers-hub/q-a-detail/coronavirus-disease-covid-19.

[12] (2021), Coronavirus (COVID-19), https://news.google.com/covid19/map?hl=tr&gl=TR&ceid=TR%3Atr&state=1.

[13] (2020), PCR Test for COVID-19: What it Is, How its Done, What the Results Mean, https://my.clevelandclinic.org/health/diagnostics/21462-covid-19-and-pcr-testing.

[14] **Villines, Z. and Martinez, K.** (2020). *Medical News Today*, https://www.medicalnewstoday.com/articles/pneumonia-and-covid-19.

[15] **Ardakani, A.A.**, **Kanafi, A.R.**, **Acharya, U.R.**, **Khadem, N. and Mohammadi, A.** (2020). Application of deep learning technique to manage COVID-19 in routine clinical practice using CT images: Results of 10 convolutional neural networks, *Computers in Biology and Medicine*, *121*, 103795, https://www.sciencedirect.com/science/article/pii/S0010482520301645.

[16] **Pathak, Y.**, **Shukla, P.K.**, **Tiwari, A.**, **Stalin, S. and Singh, S.** (2020). Deep Transfer Learning Based Classification Model for COVID-19 Disease, *Ingenierie et recherche biomedicale : IRBM = Biomedical engineering and research*, 10.1016/j.irbm.2020.05.003, https://pubmed.ncbi.nlm.nih.gov/32837678, 32837678[pmid].

[17] **Deng, J.**, **Dong, W.**, **Socher, R.**, **Li, L.**, **Kai Li and Li Fei-Fei** (2009). ImageNet: A large-scale hierarchical image database, *2009 IEEE Conference on Computer Vision and Pattern Recognition*, pp.248–255.

[18] **Ozturk, T.**, **Talo, M.**, **Yildirim, E.A.**, **Baloglu, U.B.**, **Yildirim, O. and Rajendra Acharya, U.** (2020). Automated detection of COVID-19 cases using deep neural networks with X-ray images, *Computers in Biology and Medicine*, *121*, 103792, https://www.sciencedirect.com/science/article/pii/S0010482520301621.

[19] **Redmon, J. and Farhadi, A.**, (2016), YOLO9000: Better, Faster, Stronger, 1612.08242.

[20] **Oh, Y.**, **Park, S. and Ye, J.C.**, (2020), Deep Learning COVID-19 Features on CXR using Limited Training Data Sets, 2004.05758.

[21] **Elshennawy, N.M. and Ibrahim, D.M.** (2020). Deep-Pneumonia Framework Using Deep Learning Models Based on Chest X-Ray Images, *Diagnostics*, *10*(9), https://www.mdpi.com/2075-4418/10/9/649.

[22] **Ruaa A. Al-Falluji, Zainab Dalaf Katheeth, B.A.** (2021). Automatic Detection of COVID-19 Using Chest X-Ray Images and Modified ResNet18-Based Convolution Neural Networks, *Computers, Materials & Continua*, *66*(2), 1301–1313, http://www.techscience.com/cmc/v66n2/40667.

[23] **Sutskever, I.**, **Martens, J.**, **Dahl, G. and Hinton, G.E.** (2013). On the importance

of initialization and momentum in deep learning, *ICML*, *28*, 1139—1147.

[24] **Graetz, F.M. and Matters, W.A.**, (2018), Why AdamW matters, https://towardsdatascience.com/why-adamw-matters-736223f31b5d.

[25] **Simonyan, K. and Zisserman, A.**, (2015), Very Deep Convolutional Networks for Large-Scale Image Recognition, 1409.1556.

[26] **Chang, M.**, (2020). Artificial Intelligence for Drug Development, Precision Medicine, and Healthcare, p. 38.

[27] **Cortes, C. and Vapnik, V.** (1995). Support-Vector Networks, *Mach. Learn.*, *20*(3), 273–297, https://doi.org/10.1023/A:1022627411411.

[28] **Ben-Hur, A.**, **Horn, D.**, **Siegelmann, H. and Vapnik, V.** (2001). Support Vector Clustering, *Journal of Machine Learning Research*, *2*, 125–137.

[29] **Christmann, A. and Steinwart, I.** (2008). *Support Vector Machines*.

[30] **Koshiba, Y. and Abe, S.** (2003). Comparison of L1 and L2 Support Vector Machines, volume 3, pp.2054 – 2059 vol.3.

[31] **Pedregosa, F.**, **Varoquaux, G.**, **Gramfort, A.**, **Michel, V.**, **Thirion, B.**, **Grisel, O.**, **Blondel, M.**, **Prettenhofer, P.**, **Weiss, R.**, **Dubourg, V.**, **Vanderplas, J.**, **Passos, A.**, **Cournapeau, D.**, **Brucher, M.**, **Perrot, M. and Duchesnay, E.** (2011). Scikit-learn: Machine Learning in Python, *Journal of Machine Learning Research*, *12*, 2825–2830.

[32] **Yu, H.F.**, **Huang, F.L. and Lin, C.J.** (2011). Dual coordinate descent methods for logistic regression and maximum entropy models, *Machine Learning*, *85*(1), 41–75, https://doi.org/10.1007/s10994-010-5221-8.

[33] **Zhu, C.**, **Byrd, R.H.**, **Lu, P. and Nocedal, J.** (1997). Algorithm 778: L-BFGS-B: Fortran Subroutines for Large-Scale Bound-Constrained Optimization, *ACM Trans. Math. Softw.*, *23*(4), 550–560, https://doi.org/10.1145/279232.279236.

[34] **Fan, R.E.**, **Chang, K.W.**, **Hsieh, C.J.**, **Wang, X.R. and Lin, C.J.** (2008). LIBLINEAR: A Library for Large Linear Classification, *J. Mach. Learn. Res.*, *9*, 1871–1874.

[35] **Schmidt, M.**, **Roux, N.L. and Bach, F.**, (2016), Minimizing Finite Sums with the Stochastic Average Gradient, 1309.2388.

[36] **Defazio, A.**, **Bach, F. and Lacoste-Julien, S.**, (2014), SAGA: A Fast Incremental Gradient Method With Support for Non-Strongly Convex Composite Objectives, 1407.0202.

[37] **Fix, E. and Hodges, J.L.** (1989). Discriminatory Analysis. Nonparametric Discrimination: Consistency Properties, *International Statistical Review / Revue Internationale de Statistique*, *57*(3), 238–247, http://www.jstor.org/stable/1403797.

[38] **Bentley, J.L.** (1975). Multidimensional Binary Search Trees Used for Associative Searching, *Commun. ACM*, *18*(9), 509–517, https://doi.org/10.1145/361002.361007.

[39] **Omohundro, S.M.** (1989). Five Balltree Construction Algorithms, **Technical Report**.

[40] **Guo, Y.**, **Hastie, T. and Tibshirani, R.** (2006). Regularized linear discriminant analysis and its application in microarrays, *Biostatistics*, *8*(1), 86–100, https://doi.org/10.1093/biostatistics/kxj035, https://academic.oup.com/biostatistics/article-pdf/8/1/86/698312/kxj035.pdf.

[41] **scikit-learn developers**, Linear and Quadratic Discriminant Analysis, https://scikit-learn.org/stable/modules/lda_qda.html#estimation-algorithms.

[42] **Pan, Y.**, **Mai, Q. and Zhang, X.** (2021). TULIP: A Toolbox for Linear Discriminant Analysis with Penalties, *The R Journal*, *12*(2), 61–81, https://doi.org/10.32614/RJ-2021-025.

[43] **Duchi, J.**, **Hazan, E. and Singer, Y.** (2011). Adaptive Subgradient Methods for Online Learning and Stochastic Optimization, *J. Mach. Learn. Res.*, *12*(null), 2121–2159.

[44] **Chen, J. and Gu, Q.** (2018). Closing the Generalization Gap of Adaptive Gradient Methods in Training Deep Neural Networks, *CoRR*, *abs/1806.06763*, http://arxiv.org/abs/1806.06763, 1806.06763.

[45] **Zou, H. and Hastie, T.** (2005). Regularization and variable selection via the Elastic Net, *Journal of the Royal Statistical Society, Series B*, *67*, 301–320.

[46] **Darıcı, M.B.**, (2020), Göğüs kafesi röntgen görüntülerinde derin öğrenme metoduyla zatürre hastalığının tanısı, https://tez.yok.gov.tr/UlusalTezMerkezi/tezDetay.jsp?id=YSoGULG5Nf-WfjvJZXgxQQ&no=VhZc08s4-L5HmRYXK4bwIA.

APPENDICES

APPENDIX A.1 : ReadMe File
APPENDIX A.2 : Python Notebook File

APPENDIX A.1 ReadMe File

The ReadMe.md file is available at https://github.com/ozanguldali/modelsWithLASSO/blob/master/ReadMe.md.

ISTANBUL TECHNICAL UNIVERSITY - Institute of Science and Technology

Ozan GÜLDALİ

Department of Mathematical Engineering - Mathematical Engineering Program

M.Sc. THESIS

DEEP FEATURE TRANSFER FROM DEEP LEARNING MODELS INTO MACHINE LEARNING ALGORITHMS TO CLASSIFY COVID-19 FROM CHEST X-RAY IMAGES

- dataset may be a must for some run-configurations
  - Link to dataset: https://github.com/ozanguldali/modelsWithLASSO/blob/master/dataset

- dataset_constructor.py was used to create the dataset from https://github.com/ieee8023/covid-chestxray-dataset source
- image_operations.py was used to investigate the augmentations of image data
- visualize_layers was used to visualize the layers of cnn models
- To run only ML, only CNN or both as transfer learning, app.py file can be run with corresponding function parameters.

How to Run

- **transfer_learning:** True if wanted to transfer deep features from CNN model
- **save_numpy:** True if wanted to save computed features. Default is False.
- **load_numpy:** True if wanted to use previously computed features. Default is False.
- **numpy_prefix:** Prefix for numpy feature files. Default is empty string.
- **method:** "ML" or "CNN". Required if transfer_learning is False.
- **ml_model_name:** Model name for ML. "svm", "lr", "knn", "lda", or "all". Default is empty string. Required if method is not CNN.

- **ml_features:** Type of features. “info”, “cnn”, or “all”. Default is empty “all”.
- **validate_cv:** True if wanted to apply cross-validation on train set. Default is False.
- **save_ml:** True if wanted to save ML weights. Default is False.
- **save_cnn:** True if wanted to save CNN weights. Default is False.
- **cv:** Type of cross-validation. Any positive integer or “LOO”. Default is 10.
- **lasso:** Type of regularization. True, False, “l2”, or None. None is used for all choices. Default is False.
- **dataset_folder:** Folder name of dataset. Default is “dataset”.
- **pretrain_file:** CNN pretrained pth file name without “pth” extension. Default is None.
- **batch_size:** Size of each batch. Default is 16.
- **img_size:** Size of image dimension. Default is 227.
- **num_workers:** Number of parallel workers. Default is 2.
- **augmented:** True if wanted to augment data. Default is False.
- **cnn_model_name:** Name of CNN model. “alexnet”, “resnet18”, “resnet34”, “resnet50”, “vgg16”, or “vgg19”. Default is empty string. Required if method is not ML.
- **optimizer_name:** Name of optimizer on CNN process. “Adam”, “AdamW” or “SGD”. Default is “Adam”.
- **validation_freq:** Validation frequency ratio on CNN process. Any positive rational number. Default is 0.02.
- **lr:** Learning rate for CNN optimizers. Any positive rational number. Default is 0.00001.
- **momentum:** Momentum ratio for SGD optimizer. Any positive rational number. Default is 0.9.
- **weight_decay:** Weight decay ratio for Adam and AdamW. Any positive rational number. Default is 0.0001.

- **update_lr:** True if wanted to periodically decrease the learning rate on CNN process. Default is False.

- **is_pre_trained:** True if the CNN model wanted to use is pretrained. Default is True.

- **fine_tune:** True if wanted to freeze first convolution block on CNN models. Default is False.

- **num_epochs:** Number of epochs for CNN process. Any positive integer. Default is 50.

- **normalize:** True if wanted to normalize the data. Default is True.

- **lambdas:** Lambda values for regularization on ML process. Single positive real number, or a list of positive real numbers. Default is None. List of [0.00005, 0.0001, 0.0002, 0.0005, 0.005, 0.01, 0.02, 0.05, 0.1, 0.5, 1.0, 2.0, 5.0, 10.0, 15.0] is used, if it is None.

- **seed:** System seed value for ML process. Any positive integer. Default is 4.

Example of Transfer Leaning:

1. (Dataset folder is required: `https://github.com/ozanguldali/modelsWithLASSO/blob/master/dataset`)

    - Unless exists, 92.16_resnet50_Adam_out.pth file must be downloaded and inserted into "cnn/saved_models" directory.

    - Link to file:

        - `https://github.com/ozanguldali/modelsWithLASSO/blob/master/cnn/saved_models/92.16_resnet50_Adam_out.pth`

```
app.main(transfer_learning=True, ml_model_name="all",
ml_features="all", cnn_model_name="resnet50",
is_pre_trained=True, cv=10, dataset_folder="dataset",
pretrain_file="92.16_resnet50_Adam_out", seed=4)
```

2. (Dataset folder is not needed)
    - Unless exists, 92.16_resnet50_Adam_final_X_cnn_train.npy, 92.16_resnet50_Adam_final_X_cnn_test.npy, X_info_train.npy, X_info_test.npy, y_train.npy, and y_test.npy files must be downloaded and inserted into project root directory.

    - Link to files:

        - `https://github.com/ozanguldali/modelsWithLASSO/blob/master/92.16_resnet50_Adam_final_X_cnn_t`

```
        rain.npy

      - https://github.com/ozanguldali/modelsWithLASSO
        /blob/master/92.16_resnet50_Adam_final_X_cnn_t
        est.npy

      - https://github.com/ozanguldali/modelsWithLASSO
        /blob/master/X_info_train.npy

      - https://github.com/ozanguldali/modelsWithLASSO
        /blob/master/X_info_test.npy

      - https://github.com/ozanguldali/modelsWithLASSO
        /blob/master/y_train.npy

      - https://github.com/ozanguldali/modelsWithLASSO
        /blob/master/y_test.npy
app.main(transfer_learning=True, ml_model_name="all",
ml_features="all", load_numpy=True, validate_cv=True,
cv=10, numpy_prefix="92.16_resnet50_Adam_final",
seed=4)
```

Package Versions

- Python Language: 3.7.6
- Clang: 4.0.1
- pip: 20.1.1

- PyTorch: 1.5.0
- TorchSummary: 1.5.1
- TorchVision 0.6.0
- Scikit-Learn: 0.23.2

- R Language: 4.0.3
- TULIP: 1.0.1
- TensorFlow: 2.3.1

- TensorFlow-Addons: 0.11.2
- TensorFlow-Estimator: 2.3.0
- TensorFlow-Hub: 0.10.0
- TensorFlow-Probability: 0.10.0

- log4p: 2019.7.13.3

- log4python: 0.2.31

APPENDIX A.2 Python Notebook File

The Python Notebook app_run.ipynb file is available at https://github.com/ozanguldali/modelsWithLASSO/blob/master/app_run.ipynb.

[ ]:
```
# To run on Google Colaboratory
%cd
%cd ..
%cd content
%ls
# User must see sample_data/ folder
```

[ ]:
```
import os.path
```

[ ]:
```
project_exists = False
if os.path.exists("modelsWithLASSO"):
  print("project directory is already exist, pulling␣
 ↪last changes")
  %cd modelsWithLASSO
  ! git fetch --all
  ! git reset --hard origin/method-in-paper
  ! git pull origin method-in-paper
else:
  print("project directory is NOT exist, checkouting␣
 ↪the project")
  ! git clone https://github.com/ozanguldali/
 ↪modelsWithLASSO.git
  %cd modelsWithLASSO
  ! git pull origin method-in-paper
```

[ ]:
```
%ls
# User must see project inner folder and files
```

[ ]:
```
import os.path
```

[ ]:
```
! pip install log4p
```

[ ]:
```
import run_CNN
from importlib import reload
run_CNN = reload(run_CNN)
```

[ ]:
```
run_CNN.main(save=True, model_name="resnet50",␣
 ↪optimizer_name="Adam", is_pre_trained=True,␣
 ↪batch_size=16, lr=0.00001, num_epochs=50,␣
 ↪validation_freq=1/50, augmented=True, num_workers=2)
```

[ ]:
```
```

```
# To run CNN process
run_CNN.main(test_without_train=True,␣
 ↪model_name="resnet50", is_pre_trained=True,␣
 ↪pretrain_file="92.16_resnet50_Adam_out")
```

[ ]:
```
import app
from importlib import reload
app = reload(app)
```

[ ]:
```
# To run deep feature transfer from saved CNN model␣
 ↪weights to ML algorithms
app.main(transfer_learning=True, ml_model_name="all",␣
 ↪ml_features="all", cnn_model_name="resnet50",␣
 ↪is_pre_trained=True, cv=10, dataset_folder="dataset",␣
 ↪pretrain_file="92.16_resnet50_Adam_out", seed=4)
```

CURRICULUM VITAE

Name Surname: Ozan GÜLDALİ

Place and Date of Birth: İstanbul, 16 August 1994

E-Mail: ozan.guldali@hotmail.com

EDUCATION:

- **B.Sc.:** 2018, Istanbul Technical University, Faculty of Science and Letters, Mathematics Engineering
- **M.Sc.:** Present, Istanbul Technical University, Graduate School, Mathematics Engineering

PROFESSIONAL EXPERIENCE AND REWARDS:

- 2018 Completed Undergraduate Education at Istanbul Technical University.
- 2017-2019 Software Test and Automation Engineer at Finartz Information Technologies Inc.
- 2019-Current Software Test and Automation Engineer at AVCR Information Technologies Inc.